

**INVESTIGATION AND CHARACTERIZATION  
OF ORGANIC SOLAR CELLS BASED ON LOW  
BAND GAP POLYMERS FOR OPTIMAL DEVICE  
EFFICIENCY**

by

***NEERAJ CHAUDHARY***

**(2K13/PhD/ME/05)**

**Department of Mechanical Engineering**

**Submitted**

**in fulfilment of the requirements of the degree of**

***Doctor of Philosophy***

**to the**



**Delhi Technological University**

**Bawana Road, Delhi-110042 (India)**

**December-2017**

## DECLARATION

---

I hereby declare that the thesis entitled “Investigation and characterization of organic solar cells based on low band gap polymers for optimal device efficiency” is an original work carried out by me under the supervision of Dr. Rajiv Chaudhary, Associate Professor, Dr. J. P. Kesari, Associate Professor, Department of Mechanical Engineering, Delhi Technological University, Delhi and Dr. Asit Patra, Senior Scientist, CSIR-National Physical Laboratory, New Delhi. This thesis has been prepared in conformity with the policy and system of the Delhi Technological University, Delhi. The research work reported and results presented in the thesis have not been submitted either in part or full to any other university or institute for the award of any other degree or diploma.

**(Neeraj Chaudhary)**

(2K13/PhD/ME/05)

Research Scholar

Mechanical Engineering Department

Delhi Technological University,

Delhi-110042

## CERTIFICATE

---

This is to certify that the thesis entitled “Investigation and characterization of organic solar cells based on low band gap polymers for optimal device efficiency”, being submitted by **Neeraj Chaudhary** is creditable of consideration for the award of the degree of “Doctor of Philosophy” and is a record of the original bonafide research work carried out by him under our guidance and supervision, in the Department of Mechanical Engineering, Delhi Technological University, Delhi and CSIR-National Physical Laboratory, New Delhi. The results contained in the present dissertation have not been submitted to any other university or institute for the award of any degree.

**Dr. Rajiv Chaudhary**

Associate Professor,  
Department of Mechanical Engg.  
Delhi Technological University  
Delhi-110042

**Dr. J. P. Kesari**

Associate Professor,  
Department of Mechanical Engg.  
Delhi Technological University  
Delhi-110042

**Dr. Asit Patra**

Senior Scientist,  
Advance Materials and Devices Division  
(Flexible Organic Energy devices section)  
CSIR-National Physical Laboratory  
New Delhi - 110012

***DEDICATED***

***TO***

***MY PARENTS***

## ACKNOWLEDGEMENTS

---

First and foremost, I acknowledge my University supervisors **Dr. Rajiv Chaudhary** and **Dr. J. P. Kesari** for the opportunity to do PhD at Delhi Technological University (DTU). I am thankful to both for purpose, censure, passion and commitment without which it would have been impossible for this work to reach its recognition. I am very thankful to **Dr. Chaudhary** for his enormous and constant support throughout the residence of PhD work. He encourages me like a friend for work hard without taking any stress. I would like to propose my most sincere gratitude to **Dr. Kesari**, who during the course of my PhD work has constantly provided insightful direction and advice for my personal enhancement.

Regarding the work in this thesis, I would like to acknowledge the priceless contribution of **Dr. Asit Patra**, Senior Scientist, Advance Materials and Devices Division, CSIR-National Physical Laboratory, New Delhi, in this thesis which is really beyond expression in words. Basically, the wave of bliss originating from him has provided the guiding brightness and nourishing force for me during the movement of PhD work. It is due to his support and energetic guidance that this thesis has approached to the present stage of exactness. From the bottom of my heart, My sincere gratitude to **Dr. Patra** for showering his stable grace and blessings on me till the finishing point of my PhD work.

I am most grateful to **Prof. R.S. Mishra**, Head of Mechanical Engineering department (DTU) for encouragement and support that he has provided to me for completion of my research work. I would also like to thank all Faculties and staffs of Mechanical Engineering department for their kind support through my research work.

I also wish my sincere thank to **Dr. Suresh Chand** and **Dr. Ajay Dhar** CSIR-National Physical Laboratory, for their motivation and encouragement during the course of my PhD work.

I am highly thankful to **Dr. Shailesh N. Sharma, Dr. Ritu Srivastava, Dr. Vinay Gupta, Dr. Pankaj Kumar, Dr. Rajiv Kumar Singh** and **Dr. Rachana Kumar**, Advance Materials and Devices Division, CSIR-National Physical Laboratory for his time to time guidance and constant support during my work. The interesting and productive discussions with them are also appreciatively acknowledged.

A huge thank you to **Dr. G. D. Sharma** (Principal Technical Officer), **Dr. Ramil Kumar Bhardwaj** (Technical Officer) and **Mr. Hawa Singh** (Senior Technician) from CSIR-National Physical laboratory for giving me easy access to all the resources required for the successful completion of the project as well as refreshing me during exhausted situation.

I express my truthful credit to my PhD colleagues **Mr. Amrik Singh** and **Ms. Deepanjali Nimker** for their help and co-operation in University during my research work.

I acknowledge the involvement to all the lab members of Flexible Organic Energy devices section for teamwork and suitable help. Apart from all, I would like thanks especially to **Dr. Sweety Rathi**, who help me during thesis writing and suggest me various ideas for presenting my thesis attractive and precious.

I am very thankful to CSIR-TAPSUN (NWP-54) and DST Indo-UK energy initiative project entitled “Advancing the efficiency and production potential of excitonic solar cells (APEX Phase-II)” for financially support.

I would also like to acknowledge the contribution of my colleagues and friends **Mr. Jasveer Singh, Mr. Naval Kishor Upadhyay, Mr. Dinesh Singh Chauhan** and **Mr. Jai Tawale** for their help and corporation throughout the entire period of my PhD work.

Finally, I would like to express my sincere thank my mother **Mrs. Rajendri**, my father **Mr. Satya Bir Chaudhary** and my wife **Mrs. Gunjan** who provided me marvellous support, encouragement and lot of love during entire PhD work. The entertainment by playing games with my elder son, master **Yash (Ansh)** and funny activities with my younger son, master **Kavya** is heartedly acknowledged. Above all I am thankful to the ‘Almighty’ for showering his blessings upon me to complete my work successfully.

NEERAJ CHAUDHARY

## ABSTRACT

---

The invention of solar cells remains the breakthrough towards clean energy alternatives since its discovery. Organic solar cells may be the replacement to inorganic ones, because of their excellent properties and solution processability leading to low financial and ecological cost, ultra-light weight, good efficiencies and improved stability. Conventional organic solar cells have been fabricated from a blend of active layers of a conjugated material (donor material) and a fullerene derivative (acceptor material) sandwiched between the hole transport layer (HTL) on an indium tin oxide (ITO) positive electrode and the electron transport layer (ETL) on a low-work-function metal negative electrode. The HTL in a photovoltaic device plays a pivotal role in device performance.

The aim of the thesis is to investigate the low band gap polymeric solar cells based on inexpensive and solution-processable HTL and optimization of device efficiency. The thesis is mainly directed towards:

1. Fabrication of organic solar cells based on low band gap polymer as core problem of the thesis using solution-processable CuSCN as hole transporting layer.
2. Development of low band gap polymeric solar cells using solution-processable CuI as hole transport material.
3. Optimization of composition ratio of P3HT:PC<sub>61</sub>BM in organic solar cells for optimal device efficiency.

The present thesis deals with the fabrication of efficient organic solar cells using different buffer layers as HTL/ETL. Focus was on using inexpensive and solution



processable Cu(I) salt as HTL in organic solar cells. The optical property, physical property and morphology of the deposited HTLs were studied using UV-Vis-NIR spectroscopy, X-ray diffraction (XRD), scanning electron microscope (SEM), transmission electron microscopy (TEM) and atomic force microscope (AFM) characterizations. The current density voltage (J-V) characteristics and PCEs were measured with a computer controlled Keithley 2400 source meter.

The present thesis consists of six chapters, which are briefly described below.

*Chapter 1* This chapter of the thesis is devoted towards the extensive literature survey on past and present research work done on organic solar cells including working mechanism, various geometry, buffer layers, both hole and electron transport layers (HTL and ETL) which are used in organic solar cells, are discussed keeping focus on various HTL. It summarizes the general review on various methods for the enhancement in the performance (both stability and efficiency) of organic solar cells by using different HTL, ETL and conducting polymers.

*Chapter 2* This chapter details the various characterization techniques performed to characterize the parameters of organic solar cells e.g. morphology, I-V measurement etc. The detailed process for the fabrication of solution processed optoelectronic devices such as solar cell is discussed. Equipments require for fabrication process like Glove Box, thermal evaporation systems and spin coating unit with characterization techniques including UV-vis-NIR, XRD, SEM, TEM and AFM etc. are discussed in brief.

*Chapter 3* describes the utilization of copper (I) thiocyanate (CuSCN) as an efficient and solution processable hole transport layer (HTL) in bulk heterojunction solar cells. The work has been discussed in two subsequent sections.

*Chapter 3A* In this section three different combinations of the most studied active layers of P3HT:PC<sub>61</sub>BM, PCDTBT:PC<sub>71</sub>BM and PTB7:PC<sub>71</sub>BM were used for photovoltaic device fabrication with the simplest device structure of ITO/CuSCN/active layer/Al. The use of CuSCN as an HTL has improved light absorption within the active layer and thereby leads to up to 5.94% and 4.60% power conversion efficiencies (PCEs) for these active layers respectively. These results are slightly better when compared to the devices fabricated using thermal deposition of MoO<sub>3</sub> and solution processed deposition of PEDOT:PSS as an HTL under similar conditions.

*Chapter 3B* During past few years, significant research on solution-processable deposition of copper(I)thiocyanate (CuSCN) as an efficient hole transporting layer (HTL) for excitonic solar cells have been successfully reported. Surprisingly, till now only two solvents diisopropyl sulfide and diethyl sulfide are known which have been used for CuSCN film deposition as a HTL for device fabrication. It is also noticeable that both the solvents are an irritant solvent having very foul smell. In this section we have used eco-friendly and inexpensive solvent dimethyl sulfoxide (DMSO) for solution processed thin film deposition of CuSCN for organic solar cells. The photovoltaic devices were fabricated using two different donor polymers PCDTBT and PTB7 blended with PC<sub>71</sub>BM as an acceptor material with device structure of ITO/CuSCN/active layer/Al. The power conversion efficiency (PCE) based on CuSCN using DMSO as a deposition solvent have been achieved up to 4.20% and 3.64% respectively, with relative higher fill factor (FF) as compared to previously reported values in literature.

In parallel with the above work, investigations were also directed towards development of alternative and universal solvents for copper (I) thiocyanate for

fabrication of low band gap polymeric solar cells to boost the utilization of CuSCN. In this connection, we used five different alternative solvents compactable with CuSCN for fabrication of organic solar cells: *N,N*-dimethylformamide, dioxane, acetonitrile, ethylene glycol, propylene carbonate.

*Chapter 4* In this chapter, we have shown the performance of solution-processable copper iodide (CuI) as an alternative hole transporting layer (HTL) for polymeric solar cells. Optical spectra of the CuI thin film reveal highly transparent and practically no absorption in the range vis-NIR region (450-1110 nm). X-ray diffraction (XRD) patterns of CuI exhibits a *p*-type semiconductor as well as crystalline nature. The power conversion efficiencies (PCEs) based on CuI as an HTL have been achieved to up to 3.04% and 4.48% for PCDTBT and PTB7 based donor materials blended with PC<sub>71</sub>BM as an acceptor material respectively with a configuration based on ITO/CuI(40 nm)/active layer (60 nm)/Al (120 nm). Furthermore, we use a wide range of solvents for solution-processed deposition of copper iodide (CuI) thin films as hole transport layer for efficient polymeric solar cells in general. Three different solvents (dimethyl sulfoxide (DMSO), *N,N*-dimethylformamide (DMF) and diisopropyl sulfide) are used for solution-processable HTL for low band gap solar cells. To examine the feasibility of these deposited solvents for HTL, we used two different combination of active layers based on low band gap polymers (PCDTBT: PC<sub>71</sub>BM and PTB7:PC<sub>71</sub>BM) for fabrication of solar cells with a device configuration based on ITO/CuI(40 nm)/active layer (60 nm)/Al (120 nm).

*In Chapter 5* the effects of different composition ratios of P3HT:PC<sub>61</sub>BM in active layer on photovoltaic parameters were systematically studied in ambient conditions. The P3HT:PC<sub>61</sub>BM composition ratios range from 1.0:0.4 to 1.0:1.2 in

active layer shows relatively good PCE and further decrease or increase of P3HT:PC<sub>61</sub>BM ratio the resulted devices show very poor PCE. The devices with various composition ratios clearly demonstrated that 1.0:0.8 weight ratio of P3HT:PC<sub>61</sub>BM has achieved highest power conversion efficiency.

*Chapter 6* This chapter presents the major conclusions derived from the present work and the scope of the future study in this field has been suggested.

# TABLE OF CONTENTS

---

## LIST OF FIGURES

## LIST OF TABLES

## LIST OF ABBREVIATIONS AND SYMBOLS

## LIST OF PUBLICATIONS

## CHAPTER: 1 INTRODUCTION 1-45

- 1.1 Background and Motivation
- 1.2 Solar cells
  - 1.2.1 First generation photovoltaic cells*
  - 1.2.2 Second generation photovoltaic cells*
  - 1.2.3 Third generation photovoltaic cells*
  - 1.2.4 Fourth generation photovoltaic cells*
- 1.3 Polymer Solar Cells
- 1.4 Advantages of Organic Solar Cells
- 1.5 Solar Cell Parameters
- 1.6 Operating Mechanism of Organic Solar Cells
  - 1.6.1 Exciton generation*
  - 1.6.2 Exciton diffusion*
  - 1.6.3 Exciton dissociation*
  - 1.6.4 Charge separation*
  - 1.6.5 Charge transport*
  - 1.6.6 Charge extraction*

1.7	Device Architecture
1.7.1	<i>Single layer solar cells</i>
1.7.2	<i>Bilayer solar cells</i>
1.7.3	<i>Bulk-heterojunction solar cells</i>
1.7.4	<i>Hybrid planar-mixed heterojunction cells</i>
1.7.5	<i>Tandem solar cells</i>
1.7.6	<i>Inverted solar cells</i>
1.7.7	<i>Perovskite solar cells</i>
1.8	Device Configuration
1.8.1	<i>Electrodes (anode/ cathode)</i>
1.8.2	<i>Interface layers (HTL/ETL)</i>
1.8.3	<i>Active layer (Donor/Acceptor)</i>
1.9	Objectives of this Thesis
1.10	Thesis Outline

## References

## **CHAPTER: 2 EXPERIMENTAL METHODS AND CHARACTERIZATION TECHNIQUES. 47-78**

2.1	Introduction
2.2	Materials Used
2.3	Brief Experimental Detail
2.4	Device Fabrication Process
2.4.1	<i>Patterning of ITO coated glass substrates</i>
2.4.2	<i>Cleaning of patterned ITO glass substrates</i>
2.4.3	<i>UV ozone cleaning of cleaned ITO glass substrates</i>

- 2.4.4 *Deposition of hole transport layer (HTL) on ITO coated substrates*
- 2.4.5 *Deposition of active layer thin film over the hole transport layer*
- 2.4.6 *Deposition of cathode electrode*
- 2.5 Measurement of Solar Cell Characteristics in Dark and under Illumination
- 2.6 Devices Fabrication
- 2.7 Characterization Equipments
  - 2.7.1 *Atomic force microscope (AFM)*
  - 2.7.2 *X-ray diffraction (XRD)*
  - 2.7.3 *UV-Vis absorption spectroscopy*
  - 2.7.4 *Transmission electron microscope (TEM)*
  - 2.7.5 *Scanning electron microscopy (SEM)*

## References

## CHAPTER: 3, PART: A

### **EFFICIENT LOW BAND GAP POLYMER SOLAR CELLS USING COPPER THIOCYANATE (CuSCN) AS SOLUTION PROCESSABLE HOLE TRANSPORTING LAYER.**

**79-96**

- 3.1 Introduction
- 3.2 Results and Discussion
  - 3.2.1 *Photovoltaic properties*
  - 3.2.2 *Absorption and transmission of HTL*
  - 3.2.3 *Morphological studies*
- 3.3 Experimental
  - 3.3.1 *Materials*
  - 3.3.2 *Preparation of CuSCN hole transport layer (HTL)*

- 3.3.3 *Preparation of MoO<sub>3</sub> hole transport layer (HTL)*
- 3.3.4 *Preparation of active materials*
- 3.3.5 *Device fabrication*
- 3.3.6 *Device characterization*
- 3.4 Conclusion

## **CHAPTER: 3, PART: B**

### **AN ECO-FRIENDLY AND INEXPENSIVE SOLVENTS FOR SOLUTION PROCESSABLE CuSCN AS A HOLE TRANSPORTING LAYER IN ORGANIC SOLAR CELLS. 97-119**

- 3.5 Introduction
- 3.6 Results and Discussion
- 3.7 Experimental Section
  - 3.7.1 *Materials*
  - 3.7.2 *Preparation of CuSCN solutions*
  - 3.7.3 *Preparation of active materials*
  - 3.7.4 *Device fabrication*
  - 3.7.5 *Device characterization*
- 3.8 Conclusion
- References

### **CHAPTER: 4 COST EFFECTIVE LOW BAND GAP POLYMERIC SOLAR CELLS USING SOLUTION PROCESSABLE COPPER IODIDE (CuI) AS HOLE TRANSPORTING LAYER. 121-142**



4.1	Introduction
4.2	Results and Discussion
4.3	Experimental Section
4.3.1	<i>Materials</i>
4.3.2	<i>Preparation of CuI thin film as an HTL</i>
4.3.3	<i>Preparation of PEDOT:PSS as an HTL</i>
4.3.4	<i>Preparation of active materials</i>
4.3.5	<i>Device fabrication</i>
4.3.6	<i>Device characterization</i>
4.4	Conclusion

References

**CHAPTER: 5 EFFECT OF COMPOSITION RATIO OF P3HT:PC<sub>61</sub>BM IN ORGANIC SOLAR CELLS: OPTICAL AND MORPHOLOGICAL PROPERTIES. 143-157**

5.1	Introduction
5.2	Results and Discussion
5.2.1	<i>Photovoltaic properties</i>
5.2.2	<i>Absorption and emission spectra</i>
5.2.3	<i>Morphology</i>
5.3	Experimental
5.3.1	<i>Device fabrication</i>
5.3.2	<i>Device characterization</i>
5.4	Conclusion

References

**CHAPTER: 6 CONCLUSIONS AND SCOPE OF FUTURE WORK      159-162**

6.1      Conclusions

6.2      Scope of future work

**CURRICULUM VITA**

## LIST OF FIGURES

---

### CHAPTER: 1

- Figure 1.1**      *World energy consumption 1990-2040.*
- Figure 1.2**      *Evolution of record cell efficiencies of various solar cell technologies. This graph is provided by the NREL.*
- Figure 1.3**      *Schematic diagram of polymer solar cells in which HTL and active material is sandwich in between ITO coated anode and aluminium cathode.*
- Figure 1.4**      *J-V characteristic of a solar cell presenting open-circuit voltage ( $V_{oc}$ ), short-circuit current ( $J_{sc}$ ) and the maximum power ( $P_{max}$ ) with current and voltage at maximum power.*
- Figure 1.5**      *Energy band diagram of organic solar cell based on donor-acceptor concept.*
- Figure 1.6**      *Conversion steps with loss mechanism in organic solar cells architecture.*
- Figure 1.7**      *Schematic diagram of polymer solar cells in which HTL, active material and ETL are sandwich in between ITO coated anode and aluminium cathode.*
- Figure 1.8**      *Schematic diagrams of single layer solar cell device.*
- Figure 1.9**      *Schematic diagrams of bilayer solar cell device.*
- Figure 1.10**      *Bulk heterojunction configuration in organic solar cells along with donor –acceptor.*
- Figure 1.11**      *Schematic diagrams of hybrid planar-mixed heterojunction solar cell device.*

- Figure 1.12**      *Schematic diagrams of tandem solar cell devices.*
- Figure 1.13**      *Schematic diagrams of inverted solar cell devices.*
- Figure 1.14**      *Schematic diagrams of perovskite solar cell devices (A) n-i-p planar, (B) n-i-p mesoscopic, (C) p-i-n planar, (D) p-i-n mesoscopic.*

## **CHAPTER: 2**

- Figure 2.1**      *Schematic diagram of standard structure of conventional organic solar cells.*
- Figure 2.2**      *ITO coated glass substrates before and after patterning the strip of 2 mm width.*
- Figure 2.3**      *Laser scribing system for patterning and etching of ITO substrates as per required design.*
- Figure 2.4**      *(a) Realization of patterned devices, (b) Shadow-mask used for aluminium evaporation.*
- Figure 2.5**      *Photograph of UV ozone cleaner placed in glove box.*
- Figure 2.6**      *Thin layer of PEDOT:PSS coated on the top of ITO coated glass substrate.*
- Figure 2.7**      *Spin coating unit for deposition of HTL in environment.*
- Figure 2.8**      *Boat containing MoO<sub>3</sub> fixed between two electrodes in a thermal evaporating system.*
- Figure 2.9**      *Thin layer of (a) CuSCN, (b) CuI coated on the top of ITO coated glass substrate.*
- Figure 2.10**      *Spin coating unit for deposition of active material(s) in glove box.*
- Figure 2.11**      *Glove Box (MBRAUN) used for deposition of active material(s).*

- Figure 2.12** Thermal evaporation systems (back side on LHS and front side on RHS) along with filament used for deposition of metal cathode (Al).
- Figure 2.13** Schematic diagrams of low band gap OPV devices using (a) CuSCN as HTL (b) CuI as HTL.
- Figure 2.14** Solar simulator showing the experimental set-up for J-V characteristics of solar cell devices under illumination with Keithley 2400 source meter.
- Figure 2.15** AFM setup
- Figure 2.16** Block diagram of atomic force microscope.
- Figure 2.17** XRD setup
- Figure 2.18** UV-vis absorption spectroscopy
- Figure 2.19** Block diagram of UV-vis absorption spectroscopy.
- Figure 2.20** Schematic diagram of the conventional TEM.
- Figure 2.21** Schematic diagram of SEM.

### CHAPTER: 3

- Figure 3.1** Schematic of the conventional BHJ solar cell in which the HTL is sandwiched between an ITO cathode and active layer.
- Figure 3.2** Chemical structures of P3HT, PCDTBT, PTB7, PC<sub>61</sub>BM and PC<sub>71</sub>BM.
- Figure 3.3** Electronic energy levels of the materials used in organic solar cells.
- Figure 3.4** Dark curves for OPV devices for

*ITO/CuSCN/PCDTBT:PC<sub>71</sub>BM/Al geometry.*

**Figure 3.5** *J-V curves for OPV device performance for ITO/CuSCN/PCDTBT:PC<sub>71</sub>BM/Al geometry. (black line) HTL was annealed at 90°C for 20 minutes; (red line) HTL was annealed at 120°C for 20 minutes.*

**Figure 3.6** *J-V curves for OPV device performance for ITO/MoO<sub>3</sub>/PCDTBT:PC<sub>71</sub>BM/Al geometry.*

**Figure 3.7** *Dark and light J-V curves for OPV device for ITO/PEDOT:PSS/PCDTBT:PC<sub>71</sub>BM/Al geometry.*

**Figure 3.8** *Dark curves for OPV devices for ITO/CuSCN/PTB7:PC<sub>71</sub>BM/Al geometry.*

**Figure 3.9** *J-V curves for OPV device performance for ITO/CuSCN/PTB7:PC<sub>71</sub>BM/Al geometry. (black line) HTL was annealed at 90°C for 20 minutes; (red line) HTL was annealed at 120°C for 20 minutes.*

**Figure 3.10** *UV-vis-NIR absorption spectra of CuSCN thin films on quartz substrate. (black) as prepared, (red) annealed at 90°C for 20 min and (blue) annealed at 120°C for 20 min.*

**Figure 3.11** *Transmission spectra of CuSCN thin films on quartz substrate. (black) as prepared, (red) annealed at 90°C for 20 min and (blue) annealed at 120°C for 20 min.*

**Figure 3.12** *SEM image of CuSCN film annealed at (left) 90°C for 20 minutes and (right) 120°C for 20 minutes on ITO.*

**Figure 3.13** *SEM image of (left) MoO<sub>3</sub> film and (right) PEDOT:PSS on ITO.*

- Figure 3.14** AFM surface images of a spin coated of CuSCN film on glass after annealed at 120°C for 20 minutes, (left) 2D image and (right) 3D image.
- Figure 3.15** TEM images of the CuSCN film (left, scale bar 600 nm and right scale bar 5 nm).
- Figure 3.16** Device geometry of organic solar cells in which CuSCN (HTL) thin film was deposited from DMSO solvent.
- Figure 3.17** Chemical structures of PTB7, PCDTBT and PC<sub>71</sub>BM.
- Figure 3.18** Energy level diagram of materials.
- Figure 3.19** Optical spectra of CuSCN thin films were deposited using DMSO solution on glass substrates, a) absorption and b) transmission.
- Figure 3.20** XRD spectra of CuSCN (a) solid power, film on glass deposited from (b) DMSO and (c) diisopropyl sulfide.
- Figure 3.21** Current density versus voltage (J-V) curves of photovoltaic device based PCDTBT:PC<sub>71</sub>BM as active layer.
- Figure 3.22** Current density versus voltage (J-V) curves of photovoltaic device based PTB7:PC<sub>71</sub>BM active layers.
- Figure 3.23** Photograph of CuSCN solution in representative solvents.
- Figure 3.24** J-V curves for OPV device performance for ITO/CuSCN/PCDTBT:PC<sub>71</sub>BM/Al in which CuSCN (HTL) dissolved in five different solvents.
- Figure 3.25** J-V curves for OPV device performance for ITO/CuSCN/PTB7:PC<sub>71</sub>BM/Al in which CuSCN (HTL) dissolved in five different solvents.

**Figure 3.26** *A bar diagram representation of device efficiency of polymer blend (a) PCDTBT:PC<sub>71</sub>BM and (b) PTB7:PC<sub>71</sub>BM in solvents used for the present studies.*

**Figure 3.27** *SEM images of CuSCN thin films deposited from DMSO solution on glass substrate.*

**Figure 3.28** *AFM images of CuSCN thin films deposited from DMSO solution on glass substrate.*

#### **CHAPTER: 4**

**Figure 4.1** *Schematic diagram of the conventional polymeric solar cells in which the CuI layer is sandwiched between an ITO anode and active layer and the thickness.*

**Figure 4.2** *Energy level diagram of the materials used in organic solar cells.*

**Figure 4.3** *Chemical structures of PCDTBT, PTB7 and PC<sub>71</sub>BM.*

**Figure 4.4** *Optical spectra of CuI thin films on quartz substrate, (a) absorption and (b) transmission.*

**Figure 4.5** *XRD pattern of CuI.*

**Figure 4.6** *Current density versus voltage (J-V) curves of photovoltaic device based PCDTBT:PC<sub>71</sub>BM active layer.*

**Figure 4.7** *J-V curves for the devices based on the structure of ITO/PEDOT:PSS/PCDTBT:PC<sub>71</sub>BM/Al geometry.*

**Figure 4.8** *Current density versus voltage (J-V) curves of photovoltaic device based PTB7:PC<sub>71</sub>BM active layer.*

**Figure 4.9** *J-V curves for the devices based on the structure of*



*ITO/PEDOT:PSS/ PTB7:PC<sub>71</sub>BM /Al geometry.*

**Figure 4.10** *Current density versus voltage (J-V) curves for OPV device performance for ITO/CuI/PCDTBT:PC<sub>71</sub>BM/Al in which CuI (HTL) dissolved in three different solvents.*

**Figure 4.11** *Current density versus voltage (J-V) curves for OPV device performance for ITO/CuI/PTB7:PC<sub>71</sub>BM/Al in which CuI (HTL) dissolved in three different solvents.*

**Figure 4.12** *A bar diagram representation of device efficiency of polymer blend (a) PCDTBT:PC<sub>71</sub>BM and (b) PTB7:PC<sub>71</sub>BM in solvents used for the present studies.*

**Figure 4.13** *SEM image of CuI thin films on glass substrate.*

**Figure 4.14** *AFM images of CuI films on glass substrate.*

## **CHAPTER: 5**

**Figure 5.1** *Conventional structure of BHJ solar cells and chemical structures of P3HT and PC<sub>61</sub>BM.*

**Figure 5.2** *Electronic energy levels of the materials used in organic solar cells.*

**Figure 5.3** *Current density vs voltage (J-V) curves using P3HT:PC<sub>61</sub>BM having composition ratios (1.0:0.2; 1.0:0.4; 1.0:0.6; 1.0:0.8; 1.0:1.0)) measured under 100 mW cm<sup>-1</sup> AM 1.5 G illumination with dark curve.*

**Figure 5.4** *Current density vs voltage (J-V) curves using P3HT:PC<sub>61</sub>BM composition ratios (1.0:1.2; 1.0:1.4; 1.0:1.6; 1.0:1.8; 1.0:2.0) measured under 100 mW cm<sup>-1</sup> AM 1.5 G illumination.*

- Figure 5.5** Bar diagram showing OPV cell parameters, PCE, Jsc, FF, and Voc vs the PC<sub>61</sub>BM:P3HT composition ratio used for device fabrication. The Jsc has strong correlation with composition ratio resulting in higher PCE with 1.0:0.8 composition ratio of P3HT:PC<sub>61</sub>BM.
- Figure 5.6** UV-vis absorption spectra of different composition ratio of P3HT:PC<sub>61</sub>BM mixture, P3HT and PCBM. (a-c) in chlorobenzene and (d) in film.
- Figure 5.7** Emission spectra of different weight ratio P3HT:PC<sub>61</sub>BM mixture in chlorobenzene.
- Figure 5.8** 2D AFM image of a spin coated of P3HT:PC<sub>61</sub>BM (composition ratio 1.0:0.8) and 3D AFM surface image on glass.
- Figure 5.9** 2D AFM image of a spin coated of PEDOT:PSS and 3D AFM surface image on glass.

*All the Instruments shown in Photographs are used in Flexible Organic Energy devices section of CSIR- National Physical Laboratory.*

## LIST OF TABLES

---

### CHAPTER: 1

- Table 1.1**      *Laboratory and module power conversion efficiencies (PCEs) of various types of solar cells.*
- Table 1.2**      *Device geometry with performance of various organic solar cells based on bilayer configuration.*
- Table 1.3**      *Device geometry with performance of various organic solar cells based on bulk-heterojunction configuration.*

### CHAPTER: 2

- Table 2.1**      *List of materials required for fabrication of OPV devices.*
- Table 2.2**      *Conjugated polymers and their chemical structure used for fabrication of polymer solar cells.*
- Table 2.3**      *Device configurations used for fabrication of OPV devices in this thesis.*
- Scheme 1.1**      *Flowchart representing the cleaning procedure for cleaning the ITO substrates.*

### CHAPTER: 3

- Table 3.1**      *Solar cells parameters of the devices from the solution-processable HTL of CuSCN and donor materials with PC<sub>71</sub>BM of active area 6.0 mm<sup>2</sup>.*

<b>Table 3.2</b>	<i>Solar cell parameters of the devices from the solution-processable CuSCN as an HTL and donor materials with PC<sub>71</sub>BM of active area 6.0 mm<sup>2</sup> (average of 4 devices).</i>
<b>Table 3.3</b>	<i>Photovoltaic parameters of the OPV device using CuSCN as HTL dissolved in different solvents having ITO/CuSCN/ PCDTBT: PC<sub>71</sub>BM /Al architecture with 0.05 mm<sup>2</sup> of active area.</i>
<b>Table 3.4</b>	<i>Photovoltaic parameters of the OPV device using CuSCN as HTL dissolved in different solvents having ITO/CuSCN/ PTB7:PC<sub>71</sub>BM /Al architecture with 0.05 mm<sup>2</sup> of active area.</i>

#### **CHAPTER: 4**

<b>Table 4.1</b>	<i>Solar cells parameters of the devices from the solution-processable CuI as an HTL and donor materials with PC<sub>71</sub>BM of active area 5.0 mm<sup>2</sup> (average of 8 devices).</i>
<b>Table 4.2</b>	<i>Parameters of the OPV device using CuI as HTL dissolved in 3 different solvents having 5.0 mm<sup>2</sup> active area using PCDTBT (donor) as low band gap polymeric solar cells.</i>
<b>Table 4.3</b>	<i>Parameters of the OPV device using CuI as HTL dissolved in 3 different solvents having 5.0 mm<sup>2</sup> active area using PTB7 (donor) as low band gap polymeric solar cells.</i>

#### **CHAPTER: 5**

<b>Table 5.1</b>	<i>BHJ solar cells parameters using P3HT:PC<sub>61</sub>BM with different</i>
------------------	---

*weight ratio ((1.0:0.2; 1.0:0.4; 1.0:0.6; 1.0:0.8; 1.0:1.0) in chlorobenzene with devices structure ITO/PEDOT:PSS/P3HT:PC<sub>61</sub>BM/Al.*

**Table 5.2** *BHJ solar cells parameters using P3HT:PC<sub>61</sub>BM with different weight ratio ((1.0:1.2; 1.0:1.4; 1.0:1.6; 1.0:1.8; 1.0:2.0) in chlorobenzene with devices structure ITO/PEDOT:PSS/P3HT:PC<sub>61</sub>BM/Al.*

## LIST OF ABBREVIATIONS AND SYMBOLS

---

OPV	Organic Photovoltaics
OSC	Organic Solar Cells
PSC	Polymer Solar Cells
AFM	Atomic Force Microscopy
LUMO	Lowest Unoccupied Molecular Orbital
HOMO	Highest Occupied Molecular Orbital
HTL	Hole Transport Layer
ETL	Electron Transport Layer
XRD	X-ray Diffraction
TEM	Transmission Electron Microscopy
SEM	Scanning Electron Microscope
HRTEM	High Resolution Transmission Electron Microscopy
UV-Vis	Ultraviolet-Visible
PL	Photoluminescence
ITO	Indium Tin Oxide
Al	Aluminium
Au	Gold
Ag	Silver
PEDOT:PSS	Poly(3,4-ethylenedioxythiophene):Poly(styrenesulfonate)
MoO <sub>3</sub>	Molybdenum Oxide
V <sub>2</sub> O <sub>5</sub>	Vanadium Oxide
NiO	Nickel Oxide

WO <sub>3</sub>	Tungsten Oxide
CuSCN	Copper Thiocyanate
CuI	Copper Iodide
P3HT	Poly(3-hexylthiophene)
PC <sub>61</sub> BM	Phenyl-C <sub>61</sub> -butyric Acid Methyl Ester
PC <sub>71</sub> BM	Phenyl-C <sub>71</sub> -butyric Acid Methyl Ester
PCDTBT	Poly[2,6-(4,4-bis-(2-ethylhexyl)-4H-cyclopenta[2,1-b;3,4-b']dithiophene)-alt-4,7-(2,1,3 benzothiadiazole)]
PTB7	Poly[[4,8-bis[(2-ethylhexyl)oxy]benzo[1,2-b:4,5-b']dithiophene-2,6-diyl][3-fluoro-2-[(2-ethylhexyl)carbonyl]thieno[3,4-b]thiophenediyl]]
DIO	1,8-diiodooctane
DMSO	Dimethyl Sulfoxide
BHJ	Bulk Heterojunction
ETM	Electron Transport Material
HTM	Hole Transport Material
HCl	Hydrochloric Acid
LSS	Laser Scribing System
VCU	Vacuum Coating Unit
DMF	<i>N,N</i> -Dimethylformamide
MeCN	Acetonitrile
PC	Propylene Carbonate
EG	Ethylene Glycol
O <sub>2</sub>	Oxygen
H <sub>2</sub> O	Water
ppm	Part Per Million

Mg	Magnesium
Ca	Calcium
AM	Air mass
Jsc	Short-Circuit Current Density
Isc	Short-Circuit Current
Voc	Open Circuit Voltage
FF	Fill Factor
$\eta$	Power Conversion Efficiency
PCE	Power Conversion Efficiency
$\lambda$	Optical Wavelength
$\alpha$	Absorption Coefficient
Eg	Band Gap Energy
h $\nu$	Energy of Photon
PECVD	Plasma Enhanced Chemical Vapour Deposition
CdTe	Cadmium Telluride
CIGS	Copper Indium Gallium Diselenide
CdS	Cadmium Sulfide
CdSe	Cadmium Selenide
TiO <sub>2</sub>	Titanium Dioxide
PbS	Lead Sulfide
ZnO	Zinc Oxide
GaAs	Gallium Arsenide
I-V	Current-Voltage
J-V	Current Density-Voltage
D-A	Donor-Acceptor



CNT	Carbon Nanotubes
InP	Indium Phosphide
CPV	Concentrator Photovoltaic Technologies
PV	Photo Voltaic
$P_{\max}$	Maximum Power
$J_{\max}$	Maximum Current Density
$V_{\max}$	Maximum Voltage
$V_{bi}$	Built-in-Potential
TCO	Transparent Conductive Oxide
CuPc	Copper Phthalocyanine
PTCBI	Perylene derivative 3,4,9,10-perylene Tetracarboxylicbis-Benzimidazole
ZnPc	Zinc Phthalocyanine
BCP	Bathocuproine
MEH-PPV	Poly[2-methoxy-5-(2-ethylhexyloxy)-1,4-phenylenevinylene]
MDMO-PPV	Poly[2-methoxy-5-(3',7'-dimethyloctyloxy)-1,4-phenylenevinylene]
PFDTBT	Poly{[2,7-(9,9-bis-(2-octyl)-fluorene)]-alt-[5,5-(4,7-di-2-thienyl-2,1,3-benzothiadiazole)]}
LiF	Lithium Fluoride
PCPDTBT	Poly[2,6-(4,4-bis-(2-ethylhexyl)-4H-cyclopenta[2,1-b;3,4-b']dithiophene)- alt-4,7- (2,1,3 benzothiadiazole)]
$C_{60}$	Buckminsterfullerene
PFN	[(9,9-bis(3'-(N,N-dimethylamino)propyl)-2,7-fluorene)-alt-2,7-(9,9-dioctylfluorene)]
FTO	Fluorine Doped Tin Oxide

NP	Nanoparticle
$\text{Cs}_2\text{CO}_3$	Caesium Carbonate
$\text{Nb}_2\text{O}_5$	Niobium Pentoxide
ISC	Inverted Solar Cell
D-A	Donor-Acceptor

## LIST OF PUBLICATIONS

---

### Publications from Thesis

1. **Neeraj Chaudhary**, Rajiv Chaudhary, J. P. Kesari, AsitPatra, and Suresh Chand, Copper Thiocyanate (CuSCN): An Efficiency Solution-Processable Anode Interfacial Layer In Organic Solar Cells, *Journal of Materials Chemistry C*, 3 (2015) 11886.
2. **Neeraj Chaudhary**, J. P. Kesari, Rajiv Chaudhary, and Asit Patra, Low Band Gap Polymeric Solar Cells using Solution-Processable Copper Iodide as Hole Transporting Layer, *Optical Materials*, 58 (2016) 116.
3. **Neeraj Chaudhary**, Rajiv Chaudhary, J. P. Kesari, and Asit Patra, Effect of Composition Ratio of P3HT:PC<sub>61</sub>BM in Organic Solar Cells: Optical and Morphological Properties, *Materials Research Innovations*, DOI: 10.1080/14328917.2017.1317061.
4. **Neeraj Chaudhary**, Rajiv Chaudhary, J. P. Kesari, and Asit Patra, An Eco-Friendly and Inexpensive Solvent for Solution Processable CuSCN as A Hole Transporting Layer in Organic Solar Cells, *Optical Materials*, 69 (2017) 367.

### Publication not included in the Thesis

5. Hemant Kumar, Pankaj Kumar, **Neeraj Chaudhary**, Ramil Bhardwaj, Suresh Chand, S. C. Jain, and Vikram Kumar, Effect of Temperature on the Performance of Cupc/C60 Photovoltaic Device, *Journal of Physics D: Applied Physics*, 42 (2009) 015102.

6. Ramil K. Bhardwaj, Vishal Bharti, Abhishek Sharma, Dibyajyoti Mohanty, Vikash Agrawal, Nakul Vats, Gauri D. Sharma, **Neeraj Chaudhary**, Shilpa Jain, Jitender Gaur, Kamalika Banerjee, and Suresh Chand, Green Approach for In-Situ Growth of CdS Nanorods in Low Band Gap Polymer Network for Hybrid Solar Cell Applications, *Advances in Nanoparticles*, 3 (2014) 106.
7. Hemant Kumar, Pankaj Kumar, **Neeraj Chaudhary**, Ramil Bhardwaj, G. D. Sharma, P. Venkatesu, and Suresh Chand, Temperature Effect on the Performance of Phthalocyanine based Photovoltaic Devices, *Indian Journal of Engineering & Materials Sciences*, 17 (2010) 358.
8. R. K. Bhardwaj, H. S. Kushwaha, J. Gaur, T. Upreti, V. Bharti, V. Gupta, **N. Chaudhary**, G. D. Sharma, K. Banerjee, and S. Chand, A Green Approach for Direct Growth of CdS Nanoparticles Network in poly(3-hexylthiophene-2,5-diyl) Polymer Film for Hybrid Photovoltaic, *Materials Letters*, 89 (2012) 195.
9. Vinay Gupta, **Neeraj Chaudhary**, Ritu Srivastava, Gauri Datt Sharma, Ramil Bhardwaj, and Suresh Chand, Luminescent Graphene Quantum Dots for Organic Photovoltaic Devices, *Journal of the American Chemical Society*, 133 (2011) 9960.

#### **International Patent (not included in the thesis)**

10. Improved Bulk Heterojunction Solar Cells Based on Modified PTB7-PC<sub>60</sub>BM  
 Inventors: Vinay Gupta, Vishal Bharti, **Neeraj Chaudhary**, Suresh Chand  
 Publication date: 06-03-2014  
 Patent number: WO2014033755 A1  
 Application number: PCT/IN2013/000519



# ***Chapter:1***

### Introduction

---

#### 1.1 Background and Motivation

Energy plays a significant role in the economic growth of a country and its demand is increasing day by day. Conventionally, major portion of energy is being drawn from petroleum and coal. Due to large consumption of these sources the available amount is continuously decreasing and may not be able to meet the demand in near future. The combustion of these sources causes harmful effects on the environment, for example, global warming which has now become an issue of global concern. Therefore, efforts are being made to develop new kind of energy sources which could belong lasting and environment friendly.

Renewable energy sources are believed to be one of the best options to handle energy problem. Among many renewable energy sources solar cells are the most important, which convert sunlight directly into electricity and is entirely environment friendly. Solar cells can be made economically competitive with respect to fossil fuels and other emerging renewable energy technologies. Large scale manufacturing of these devices is expected to offer sustainable energy source which shall provide significant portion of our daily energy requirements (1-7).

The main advantage of solar cells involves their graceful procedure: just converting daylight into electricity. No requirement of water and fuels, maintenance requirements is very less, no by-product, no sound pollution or no requirement of transferring from one location to other after installation. Although the initial cost is very high yet operation and maintenance cost is very low (1-6, 8). A lot of research has been carried out in order to reduce initial cost, increase in the efficiency, life time and to simplify the production procedure.

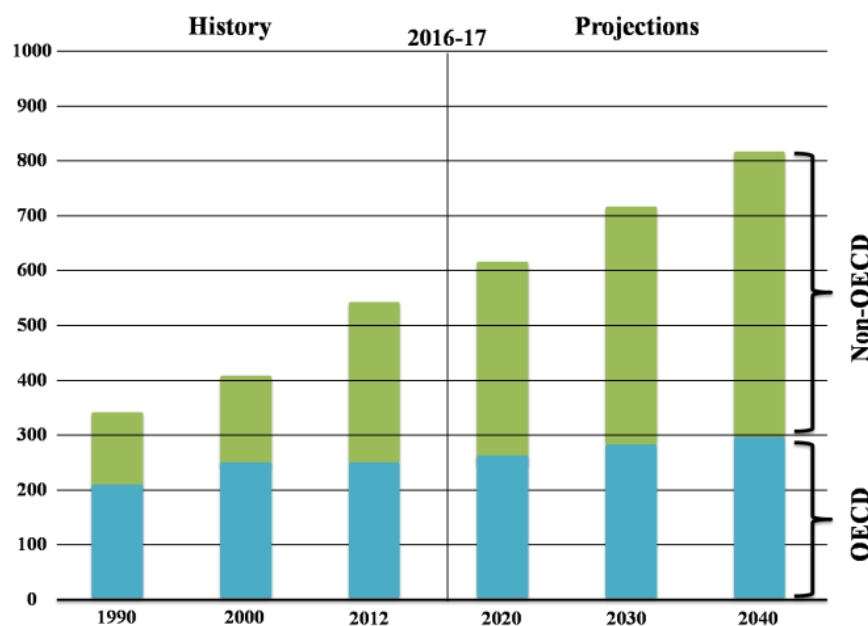


**Figure 1.1** World energy consumption 1990-2040.

First generation solar cells were based on silicon (Si) which possess good efficiency ( $>15\%$ ) and durability ( $>20$  years). Si based solar cells are available in the market but because of their high cost they are away from the reach of a common man of the country. Therefore efforts are being made to reduce the cost and improve further the performance of Si based solar cells or find out new materials to replace Si. Organic semiconductors have evolved as truly revolutionary materials for electronic devices such as light emitting diodes, thin film transistors, biosensors and solar cells. Compared to inorganic counterpart organic based electronic devices will be thin, light weight, easy to process and could be fabricated on large flexible surfaces like plastic, cloth and paper. Along with this, these devices will be very cost effective. Efforts are being made all over the world to develop these materials and devices. Organic light emitting diodes are now well developed and are available in the market. Presently intense work is being done on organic solar cells (OSCs).

## 1.2 Solar Cells

In 1839, Alexander Edmond Becquerel (French physicist) discovered the solar cells effects during analyzing with a solid electrode in an electrolyte solution (9). However, the first solar cell based coating a wide plate of copper with selenium and then topped it with an extremely thin semi-transparent layer of gold leaf; was discovered by an American inventor Charles Edgar Fritts in 1883 (10). Later on in 1954, Chaplin fabricated first inorganic solar cell based on crystalline silicon and achieved power conversion efficiency (PCE) of about 6%, six years after the discovery of the p-n junction by Walther H. Brattain, William B. Shockley, and John Bardeen who have got Nobel Prize for the transistor (11). In the 1970s oil embargoes lead to a rapid attention in different sources of energy, and the first modern solar modules for worldly use were fabricated in 1976 (12). The development of solar cells can be considered to be in four generations.

Year wise development on the power conversion efficiency (PCE) of different solar cells devices is shown in Figure 1.2.

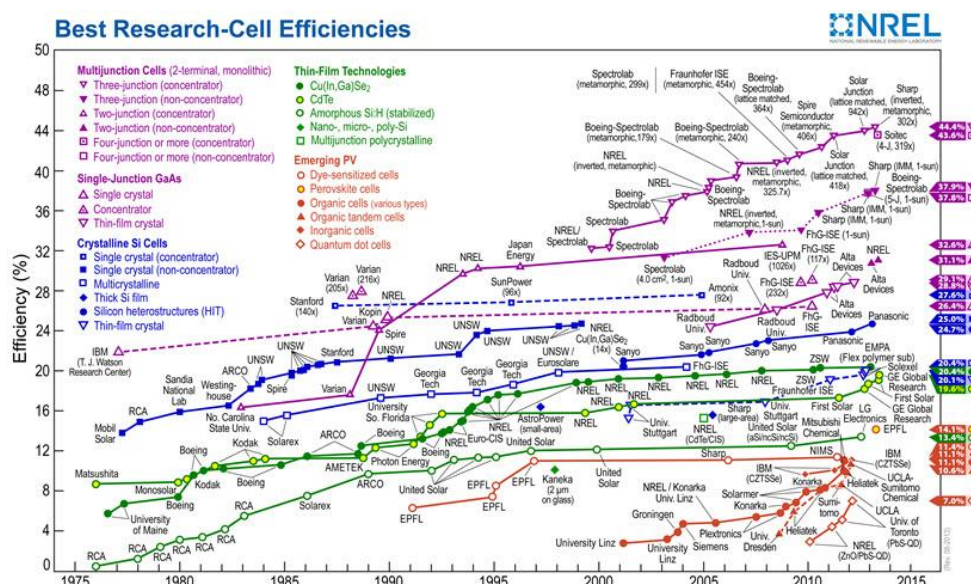


**Figure 1.2** Evolution of record cell efficiencies of various solar cell technologies. This graph is provided by the NREL.



### *1.2.1 First Generation Photovoltaic Cells*

First generation photovoltaic cells which are also known as silicon wafer based solar cells are fabricated by crystalline silicon wafer. This is most advanced technology for the production of solar cells at industrial scale and has a share of more than 90% in solar energy market (13).

These cells are single layer p-n junction diode with large-area and are capable of generating functional electricity from light sources with the wavelengths of sunlight. The power conversion efficiency of commercially available silicon based photovoltaic module is about 20% (14). Although the efficiency achieved at laboratory is 25% which is just closer to the theoretical efficiency of about 33% (15). The main advantages of c-Si solar cells are high carrier mobility, broad spectral absorption range, and high efficiency (16, 17). The main drawback of this generation of solar cell is expensive production cost (18). The cost of electricity generation is normally 10 times higher than that of the fossil fuel.

### *1.2.2 Second Generation Photovoltaic Cells*

The second-generation solar cells include thin films semiconductors, which are much efficient compared to crystalline silicon based first generation solar cells. In this generation four types of solar cells were introduced: amorphous silicon, polycrystalline silicon, cadmium telluride, copper indium gallium diselenide. These cells were also known as Plasma Enhanced Chemical Vapour Deposition (PECVD). Amorphous silicon cells are the non-crystalline form of silicon which can be deposited over large areas with help of PECVD including the large variety of techniques. Optical band gap of unhydrogenated amorphous silicon is reported to vary in a range from 1.1-1.5 eV and its function similar to crystalline silicon (c-Si) solar cells. Polycrystalline silicon are made of pure silicon grains, they work better than

previous designs because of their mobility feature. We can easily move them over large magnitude. Cadmium telluride (CdTe) cells are formed with cadmium and tellurium mixed with zinc cubic crystal structure. This material is cheaper than silicon but not as efficient as silicon. Copper indium gallium diselenide (CIGS) alloy cells having band gap about 1.38 eV are deposited on glass or stainless steel and are complex in model. This generation includes all types of thin film technology of solar cell and has 10% share of solar cells production. Photovoltaic devices based on these materials have achieved efficiency of about 15-20% (19-22).

### *1.2.3 Third Generation Photovoltaic Cells*

To boost the performance of second generation solar cells and to reduce the cost of production third generation solar cells were introduced. A lot of research has been approved internationally to develop organic materials based solar cells which come under this generation of solar cells (23-38). The main advantages of such technology are low production cost, flexible devices, light weight, large area devices, and easy fabrication process which can be done either by spin coating or by printing technology of solution processable polymers. The limitations of third generation solar cells are: unable to commercialise in market due to sensitive nature of organic materials to environment which lead to fast degradation and reduced efficiency with time; the PCE of such cells are less compared to first and second generations of solar cells.

### *1.2.4 Fourth Generation Photovoltaic Cells*

The main objective for development of fourth generation solar cells is to defeat the limitation like low efficiency and fast degradation of polymer based solar cells. For that, a lot of research has been done based on hybrid solar cells in which organic and inorganic materials are used to enhance the solar cells efficiency due to

utilization of broad solar spectrum band of inorganic materials and easy fabrication of polymers. Hybrid solar cells consists of conductive polymers and inorganic semiconductor nanocrystals (38-45) such as cadmium sulfide (CdS) (46, 47), cadmium selenide (CdSe) (48-54), titanium dioxide (TiO<sub>2</sub>) (55-58), cadmium telluride (CdTe) (59, 60), lead sulfide (PbS) (61), zinc oxide (ZnO) (62-64), carbon nanotubes (CNT) (65, 66) etc. Inorganic semiconductors nanoparticles are good electron acceptors have high absorption coefficients and good physical and chemical stabilities.

**Table 1.1** Laboratory and module power conversion efficiencies (PCEs) of various types of solar cells.

Solar Technology	Solar cells devices	Power conversion efficiencies
Silicon	Si (crystalline cell)	Laboratory efficiency: 26.3% (67) Module efficiency: 24.4% (67)
	Si (multi-crystalline cell)	Laboratory efficiency: 21.3% (68) Module efficiency: 19.9% (69)
Thin-Film Technologies	Amorphous silicon (a-Si) solar cells	Laboratory efficiency: 9.5% (70)
	CIGS based solar cells	Laboratory efficiency: 19.9% (71) Module efficiency: 17.5% (72)
	Cadmium telluride solar cells (CdTe)	Laboratory efficiency: 21.0% (73) Module efficiency: 18.6% (74)
III-V Cells	GaAs (thin film cell)	Laboratory efficiency: 28.8% (75) Module efficiency: 24.1% (76)
	GaAs (multicrystalline) InP (crystalline cell)	Laboratory efficiency: 18.4% (77) Laboratory efficiency: 22.1% (78)
Organic-Based Solar Cells	Bulk-heterojunction solar Cells	Laboratory efficiency: 10.2% (79)
	Dye-sensitized solar cells	Laboratory efficiency: 11.9% (80)
	Tandem solar cells	Laboratory efficiency: 10.6% (81)
	Inverted solar cells	Laboratory efficiency: 11.2% (82) Module efficiency: 8.7% (83)
Perovskite	Perovskite cells	Laboratory efficiency: 19.7% (84) Module efficiency: 12.1% (85)
Novel PV Technologies	Quantum wells, quantum wires, quantum dots, nanoparticle inclusion in host semiconductor	Theoretical efficiencies are 50-60% (86, 87).
Concentrator Photovoltaic Technologies (CPV)	Si concentrator cells	Laboratory efficiency: 26.8% @96 suns (88).

### 1.3 Polymer Solar Cells

An alternative progress towards inorganic solar cells is the use of small molecules and polymers as active layers, which can be processed over large areas at relatively low temperatures, either through thermal deposition of small molecules or by spin coating of solution processable polymers. The energy consumption for fabrication of PSCs are very less compared to inorganic solar cells due to high throughput and low temperature process which permits preparation through printing technology (89). Due to inexpensive and high absorption coefficients, these materials are allowed to make thin film of thickness in nanometer order. Along with low cost and easy to process flexibility of polymers raise an attraction toward PSCs (90-92).

The typical diagram of PSCs is illustrated in Figure 1.3, in which active materials, HTL and ETL are sandwiched systematically between indium tin oxide (ITO) acting as an anode and aluminium metal (low work function) that acts as a cathode in conventional structure. A lot of research has been done in polymer based solar cells but these cells are unable to commercialize due to their poor efficiencies and limited life time compared to silicon based solar cells. The main challenges for PSCs: to investigate new donor and acceptor materials, alternative HTL and ETL, modifying device architecture, new method of fabrication and processing and searching of perfect encapsulation materials.

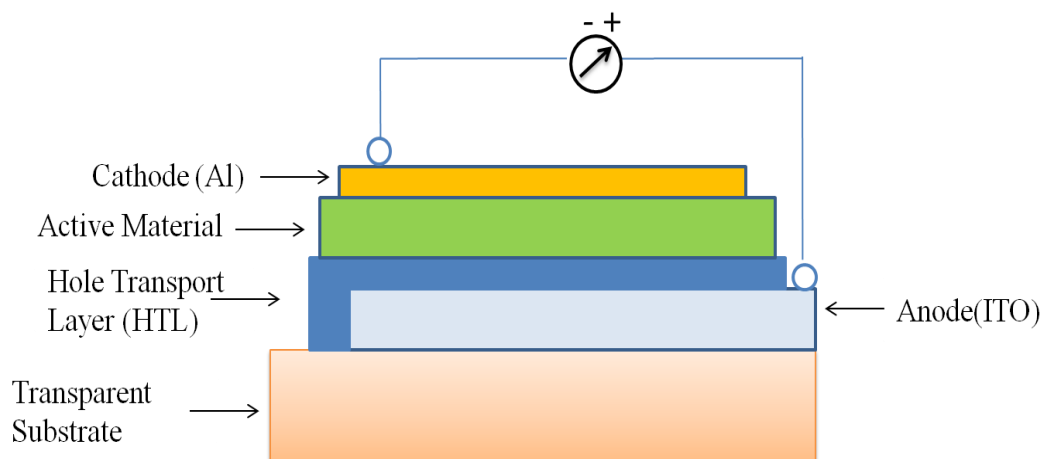


**Figure 1.3** Schematic diagram of polymer solar cells in which HTL and active material is sandwich in between ITO coated anode and aluminium cathode.

#### 1.4 Advantages of Organic Solar Cells

- ❖ Appreciably lower production costs by deposition techniques under low temperature compared to conventional inorganic technologies
- ❖ Modules of OPV devices have low weight and mechanically flexible, that's why these devices can be used in mobile devices.
- ❖ Manufacturing of OPV in a continuous process using state of the art printing tools.
- ❖ New market opportunities, e.g. wearable PV.
- ❖ High energy yield due to a good low-light performance and a positive temperature coefficient of the efficiency.
- ❖ Wide range of applications due to semi-transparent nature of devices.
- ❖ Non-toxicity and low consumption of abundant absorbing materials.
- ❖ Due to light weight, these devices can be easy integrated into other products.
- ❖ Short energy payback times and low environmental impact during manufacturing and operations.

## 1.5 Solar Cell Parameters

The standard parameters used to characterize the performance of an OPV devices are described briefly in this segment. These parameters will be useful to compare the electrical performance of different OPV devices. The characteristics including the electrical behaviour of organic solar cell can be performed by current density-voltage (J-V) measurements in the dark and under illumination exposed to particular light intensity. Figure 1.4 shows the classic J-V curve of a solar cell in the dark (black coloured) and under illumination (red coloured). Four parameters: the short circuit current density ( $J_{sc}$ ), the open circuit voltage ( $V_{oc}$ ), the fill factor (FF) and the power conversion efficiency (PCE) can be determined from this J-V curve. The short-circuit current density ( $J_{sc}$ ) is the current density at zero voltage, there is no power created at this point, but the ( $J_{sc}$ ) does mark the arrival of power generation. Similar to  $J_{sc}$ , the open-circuit voltage ( $V_{oc}$ ) is the voltage across the solar cell when  $J=0$ , which is same as the device being open-circuited. The operating command of a solar cell is the range of bias from 0 to  $V_{oc}$  in which the cell delivers power.

The cell power density is given by:

$$\mathbf{P = J \times V} \quad \text{.....(1)}$$

P reaches a maximum at the device operational point. The maximum of the obtained electrical power  $P_{max}$  is situated in the fourth quadrant in which the product of current density (J) and voltage (V) reaches its maximum value:

$$\mathbf{P_{max} = J_{max} \times V_{max}} \quad \text{.....(2)}$$

Fill factor (FF) is a parameter which determines the maximum power of a solar cell. It is the ratio of maximum obtainable power to the product of short circuit current density ( $J_{sc}$ ) and open circuit voltage ( $V_{oc}$ ); it determines the shape of the J-V curve. FF should be 1, but due to various losses during transport and recombination, it always remains less than 1. Solar cells with high FF shows the convex shape in J-V curve whereas solar cells having low FF show concave shape or linear shape in J-V curve.

$$\boxed{FF = \frac{J_{max} \times V_{max}}{J_{sc} \times V_{oc}}} \quad \text{.....(3)}$$

The performance of one solar cell can be compared with another by using most common parameter referred to efficiency. Efficiency may be defined as the ratio of output power of the devices to input or incident power which depends upon the spectrum and intensity of the incident power and the temperature of the device. In laboratory, most of the devices are measured under AM1.5 conditions and at a temperature of 25°C to compare the performance of one device to another.

$$\boxed{PCE (\eta) = \frac{J_{sc} \times V_{oc} \times FF}{P_{in}}} \quad \text{.....(4)}$$



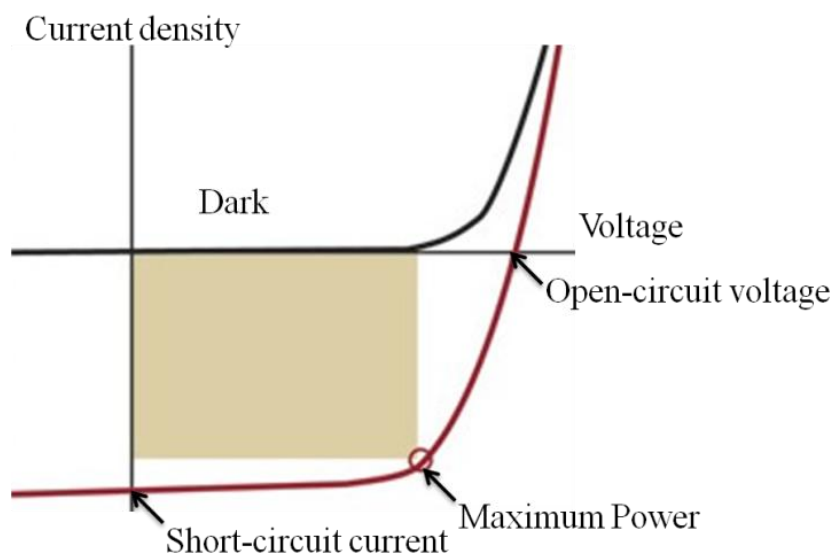


**Figure 1.4** *J-V characteristic of a solar cell presenting open-circuit voltage ( $V_{oc}$ ), short-circuit current ( $J_{sc}$ ) and the maximum power ( $P_{max}$ ) with current and voltage at maximum power.*

## 1.6 Operating Mechanism of Organic Solar Cells

The basic operation mechanism of organic solar cells is shown in Figure 1.5(93). The process of conversion of light into electricity by an organic solar cell can be systematically briefly described by the following steps (93, 94).

1. Light incident on active material of OPV devices, having an energy that exceeds the band gap of active material, excites an electron to an unoccupied state above band gap, to form electron hole pair.
2. The electron hole pair is then separated over a built-in gradient in the electrochemical potential of the OPV devices.
3. After all, the electron and hole is collected at respective electrodes and lead to recombination for external circuit work.

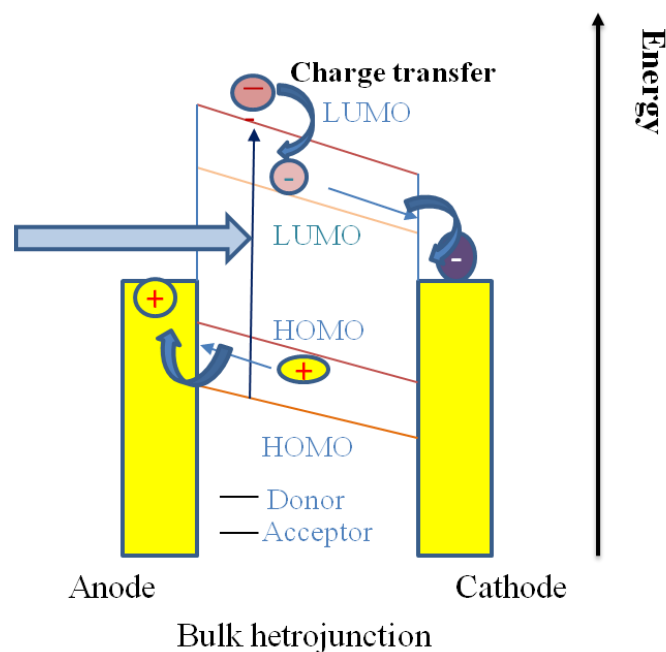


**Figure 1.5** Energy band diagram of organic solar cell based on donor-acceptor concept.

#### 1.6.1 Exciton Generation.

The materials accountable for the absorption of photons in the OPV devices are the organic semiconductors which form the active layer. When incident photons are absorbed by the organic semiconductors, electrons are excited from its HOMO into the LUMO, leaving behind an electron vacancy, which is corresponding to a positively charged carrier termed as a hole. The generated excitons in the organic semiconductors having binding energy, normally in the range of 200-500 meV binds the electron and hole jointly and resist to dissociate due to the low polymeric dielectric constant (95).

#### 1.6.2 Exciton Diffusion

The photo-generated excitons diffuse in the organic semiconductors until reaching the donor-acceptor interface where exciton dissociation occurs or the excitons are unable to recombine. A fundamental problem of the disordered organic

materials is that the diffusion length of the exciton in most of the organic semiconductors is  $\sim 10$  nm so the exciton has to move much distance otherwise the recombination can take place (96, 97). Therefore, the thickness of active layer of OPV devices should be thin to obtain a larger fraction of excitons to reach the interface.

### *1.6.3 Exciton Dissociation*

The excitons dissociation takes place only when the potential drop across donor and acceptor interface is larger than the binding energy of exciton. After photo excitation, an electron can jump from LUMO of the donor to the LUMO of the acceptor and leave the hole in the donor due to its higher HOMO level. The resulting state of the electron and hole is termed as a polaron pair, which is bound by less strong Coulombic force (98, 99).

### *1.6.4 Charge Separation*

The polaron pairs have to be separated in order to expand free charge carriers (electrons and holes). The separation of photogenerated polaron pairs in OPV devices is based on the Braun-Onsager model (100-102). During the process, a fraction of the polaron pairs can recombine geminately. The geminate recombination is a monomolecular process in which the recombination rate is proportional to the concentration of the polaron pairs.

### *1.6.5 Charge Transport*

The transport is driven by the built-in electric field in OPV devices, which is induced by the difference in the intrinsic work functions of anode and cathode before contact (27). During charge transportation, holes and electrons transport toward anode and cathode respectively. Here, the free electrons and holes are independent and recombine by a second order process in non geminate recombination fashion, termed

as bimolecular process which is different from geminate recombination. In geminate recombination, electrons and holes are from the same origin.

### 1.6.6 Charge Extraction

At last, holes are extracted from the anode at the same time as electrons from the cathode of the device to generate the electrical current. During the charge extraction, surface recombination at the organic-metal interface take place which resists the performance of OPV devices (103, 104).

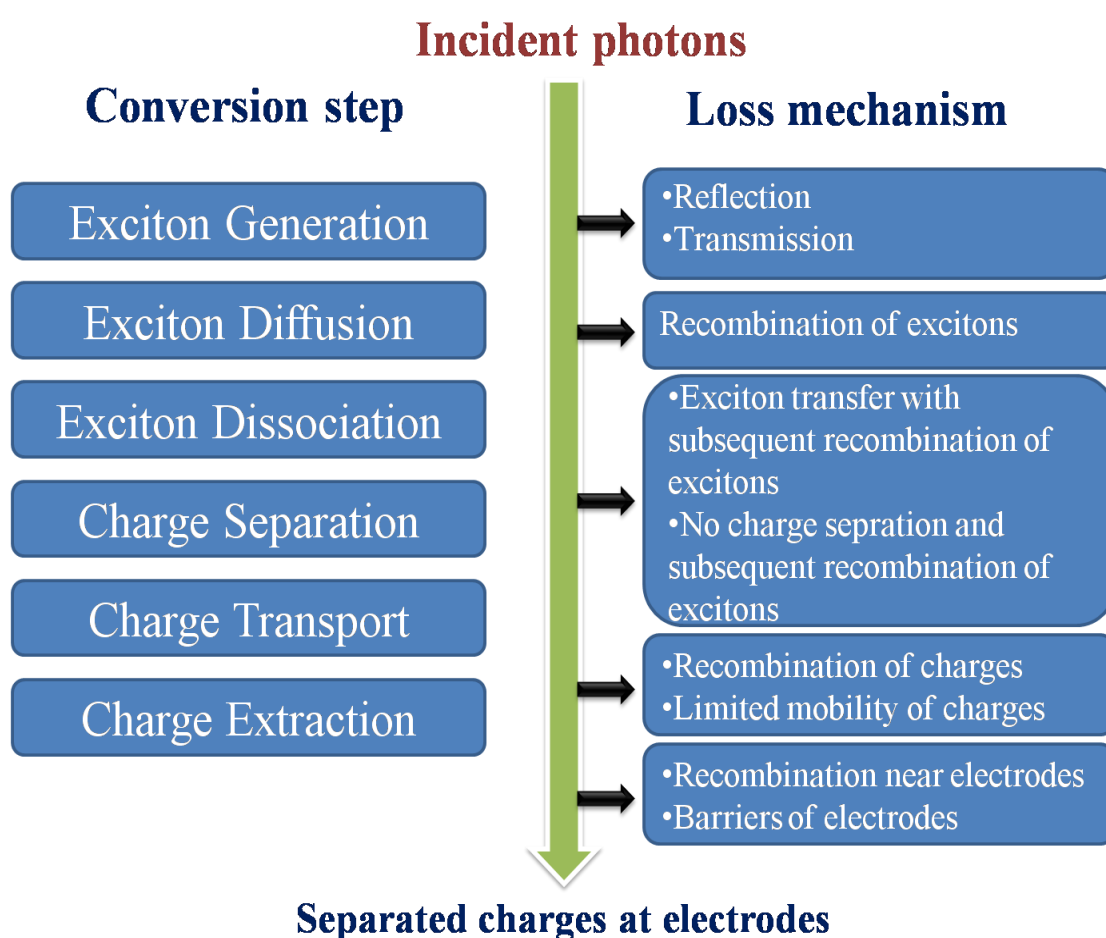


**Figure 1.6** Conversion steps with loss mechanism in organic solar cells architecture.

## 1.7 Device Architecture

The basic design of polymer based organic solar cells is illustrated in Figure 1.7. Polymer based organic solar cells consist of two electrodes having different work functions. One electrode should be optically transparent. Indium tin oxide (ITO) is taken as anode due to its good electrical conductivity and optical transparency, on the other side the low work function metals like aluminium, silver and gold are taken as cathode electrode. The hole transport layer (HTL), active organic layer(s) (donor and acceptor), electron transport layer (ETL) are sandwiched in between these two electrodes in systematic order. These layers are fabricate either by spin coating method or by thermal evaporation process, depending upon the nature of materials. The built-in-potential ( $V_{bi}$ ) is developed due to difference in work functions of these two electrodes which generates an internal potential.  $V_{bi}$  along with active material(s) and interface material (s) plays a very important role to measure various parameters of organic solar cells.

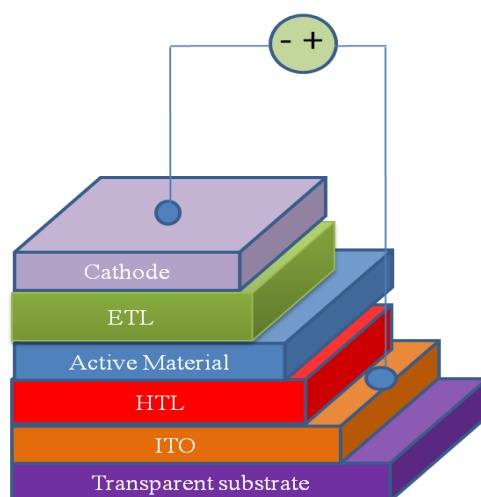


**Figure 1.7** Schematic diagram of polymer solar cells in which HTL, active material and ETL are sandwich in between ITO coated anode and aluminium cathode.

Different device architectures of OSCs are classified based on development to get better efficiencies and improved parameters:

### 1.7.1 Single Layer Solar Cells

The first structure of organic photo-voltaic solar cells (OPV-SCs) was quite simple, consisting of single layer of an organic material between two electrodes, typically a transparent conductive oxide (TCO), as anode, and a metal cathode.

The first polymer solar cells were fabricated by using single layer of an organic material which was sandwiched in between two electrodes, typically an optically transparent conductive oxide as anode and a metal cathode with different work functions. Figure 1.8 illustrates the typical structure of single layer solar cell. For example, a solution of P3HT polymer was inserted in between ITO electrode and aluminium electrode. The efficiency was very less about only 0.1% which is the main limitation of single layer solar cells. The electrical field generated at active material is due to the difference in work function of two electrodes which is very less for efficient exciton dissociation in polymers (105, 106). Moreover, recombination losses are very high due to movement of holes and electrons in the same material (107).

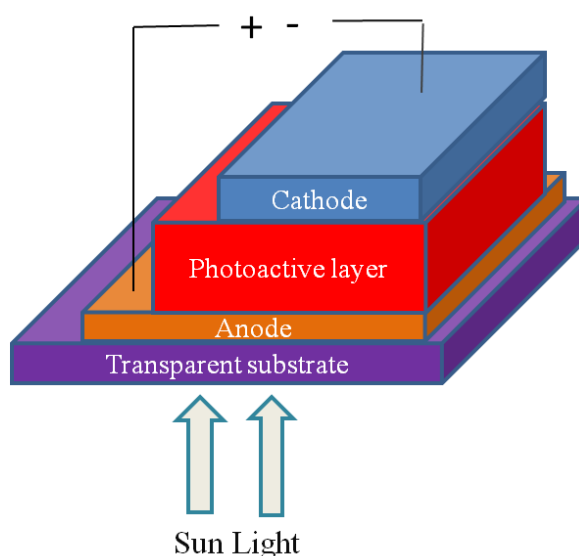


**Figure 1.8** Schematic diagrams of single layer solar cell device.

### 1.7.2 Bilayer Solar Cells

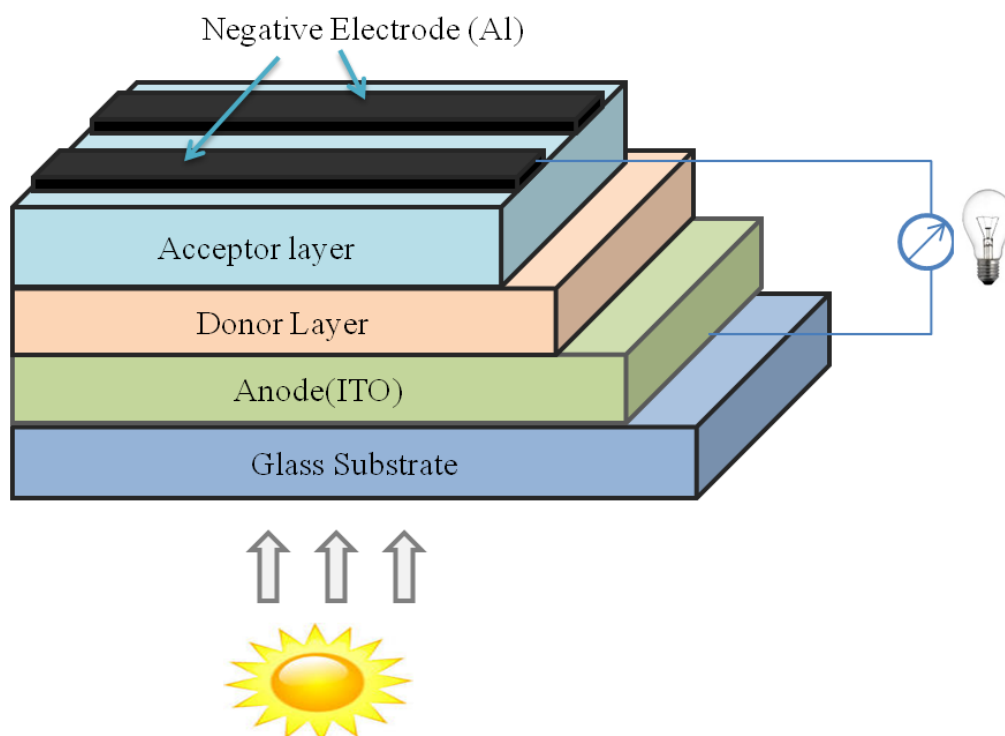


**Figure 1.9** Schematic diagrams of bilayer solar cell devices.

Fundamentally, the bilayer solar cells are composed of two different organic layers (donor and acceptor) deposited sequentially, between two electrodes in systematic order. The basic structure of bilayer solar cell is demonstrated in Figure 1.9. The first OSC based on bilayer configuration was fabricated by Dr. Ching Tang at Kodak Research Laboratories in 1986, by using copper phthalocyanine (CuPc) as a donor material while a perylene derivative 3,4,9,10-perylene tetracarboxylicbis-benzimidazole (PTCBI) as acceptor material and achieved an efficiency of about 1% (108). The efficiency was further improved by Forrest as he replaced perylene tetracarboxylic dianhydride as acceptor and obtained efficiency of 1.8% (109). Bilayer solar cells are generally fabricated by thermal evaporation of small molecules. The thickness of each layer plays a very important role for achieving desired parameters of device. The exciton dissociation occurs far from the collecting

electrodes as a result of which low quantum efficiencies is the main drawback of bilayer solar cells. The other small molecule used are zinc phthalocyanine (ZnPc) (110), metal free phthalocyanine (111), pentacene (112), tin phthalocyanine (113), boron subphthalocyanine (114, 115) bis(2,2-dicyanovinyl)-quinoxaline (116).

**Table 1.2** Device geometry with performance of various organic solar cells based on bilayer configuration.

Device geometry	Voc (V)	Jsc (mA/cm <sup>2</sup> )	FF (%)	PCE (%)	Ref.
ITO/ CuPc/ PTCBI/ Ag	0.45	2.30	0.65	0.95	(108)
ITO/ CuPc/ SubPc/ C <sub>60</sub> / BPhen/ Al	0.42	5.16	0.47	1.29	(115)
ITO/ SubPc /C <sub>60</sub> / BCP/ Al	0.97	3.36	0.57	2.1	(114)
ITO/ PEDOT:PSS/ tetracene/ C <sub>60</sub> / BCP/ Al	0.58	7.00	0.57	2.3	(117)
ITO/ pentacene/ C <sub>60</sub> / BCP/ Al	0.36	15.0	0.50	2.7	(118)
ITO/ PEDOT:PSS/ CuPc/ C <sub>60</sub> / BCP/ Al	0.58	18.8	0.52	3.6	(119)
ITO/ PEDOT:PSS/ P3HT/ PCBM/ Ca/ Al	0.60	8.71	0.73	3.8	(120)

### 1.7.3 Bulk-Heterojunction Solar Cells

In case of bulk-heterojunction solar cells, the donor and acceptor materials are mixed together with suitable solvent(s) to form a blend which is inserted in between two different work function electrodes in a methodical way. First BHJ solar cell was fabricated by American physicist Alan J. Heeger in 1995 and achieved an efficiency of about 1.5 % (121) by using MEH-PPV as a donor while PCBM as acceptor material. After that the same concept was followed by Sir Richard Friend for fabrication of efficient solar cells (122). Later on, the efficiency was further improved to 2.5% by using MDMO-PPV as donor and PCBM as acceptor. The reason behind improved efficiency is due to better morphology of MDMO-PPV and PCBM blend along with better optical and electrical properties of MDMO-PPV (123).



Fabrication of BHJ solar cells based on P3HT (donor): PCBM (accepter) blend was fabricated by Padinger in 2003. In case of P3HT: PCBM blend, post annealing and externally applied voltage of devices plays very important role to improve the efficiency. It was published that PCE of above blend improved from 0.4% to 2.5% post annealing at 70° and after applying external voltage of 2.7 V across the device with post annealing, PCE was enhanced to 3.5%. Improving morphology and better charge carrier mobilities of active layer were the two main reasons for improvement the efficiency values (124).

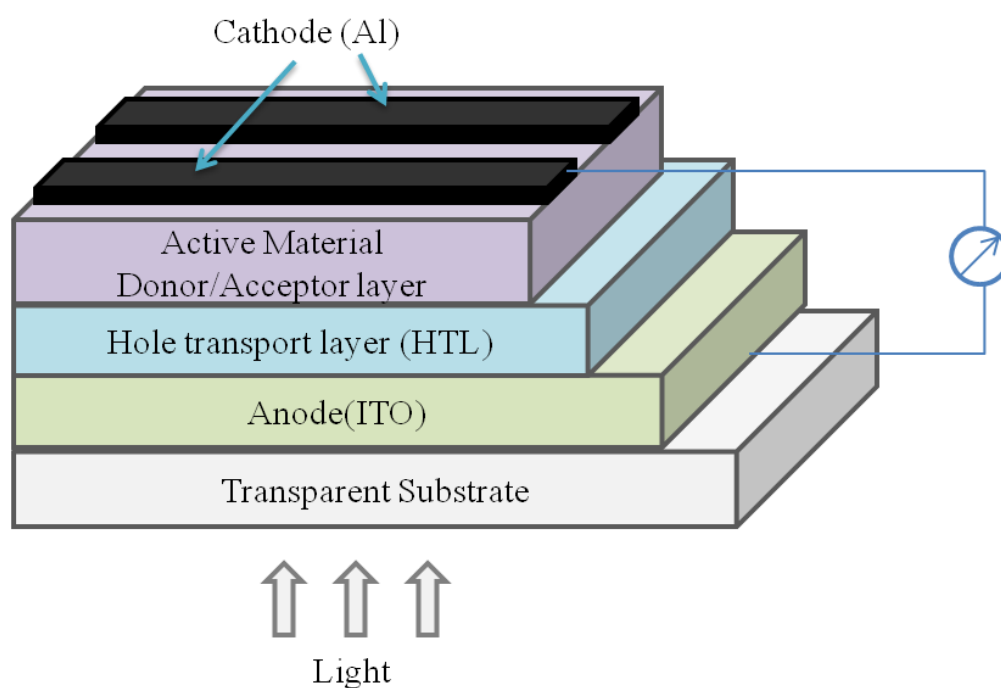


**Figure 1.10** Bulk heterojunction configuration in organic solar cells along with donor-acceptor.

**Table 1.3** Device geometry with performance of various organic solar cells based on bulk-heterojunction configuration.

Device geometry	Voc (V)	Jsc (mA/cm <sup>2</sup> )	FF (%)	PCE (%)	Ref.
ITO/ MEH-PPV:PCBM/Ca	0.8	2.0	0.25	1.5	(121)
ITO/ PEDOT:PSS/ PFDTBT:PCBM/ LiF/ Al	1.04	4.66	0.46	2.2	(125)
ITO/ PEDOT:PSS/ MDMO-PPV:PCBM/ LiF/ Al	0.82	5.25	0.61	3.3	(126)
ITO/ PEDOT:PSS/ P3HT:PCBM/ TiO <sub>x</sub> / Al	0.61	11.1	0.66	5.0	(127)
ITO/ PEDOT:PSS/ PCPDTBT:PCBM/ Al	0.62	16.2	0.55	5.2	(128)
ITO/ PEDOT:PSS/ PTB7:PCBM/ Al	0.74	14.5	0.69	7.4	(129)
ITO/ PEDOT:PSS/ PTB7:PC <sub>71</sub> BM/ PFN/ Ca/ Al	0.76	15.4	0.71	8.2	(130)
ITO/ PEDOT:PSS/ PTB7-Th:PC <sub>71</sub> BM/ Al	0.81	17.52	0.72	10.28	(79)

#### 1.7.4 Hybrid Planar-Mixed Heterojunction Cells

It is a combination of bilayer and bulk-heterojunction solar cells. In such type of cells, a blend solution of donor and acceptor is inserted in between donor layer and acceptor layer. Electrode1/donor/mixed/acceptor/electrode2 is the device geometry of such solar cells. Xue has investigated the device based on hybrid heterojunction solar cells in which small molecules CuPc and C<sub>60</sub> was coated in between the separate layers of CuPc and C<sub>60</sub>, and achieved the efficiency of about 5.0% (131). Such type of geometry provides efficient photon harvesting and good transport to the photo-generated charge carriers to the respective electrodes. The thickness of each homogenous layer is equal to the diffusion length of the excitons. Consequently, exciton dissociation becomes more efficient as it occurs throughout the mixed layer as well as at the interfaces of the mixed layer and the homogenous layers.

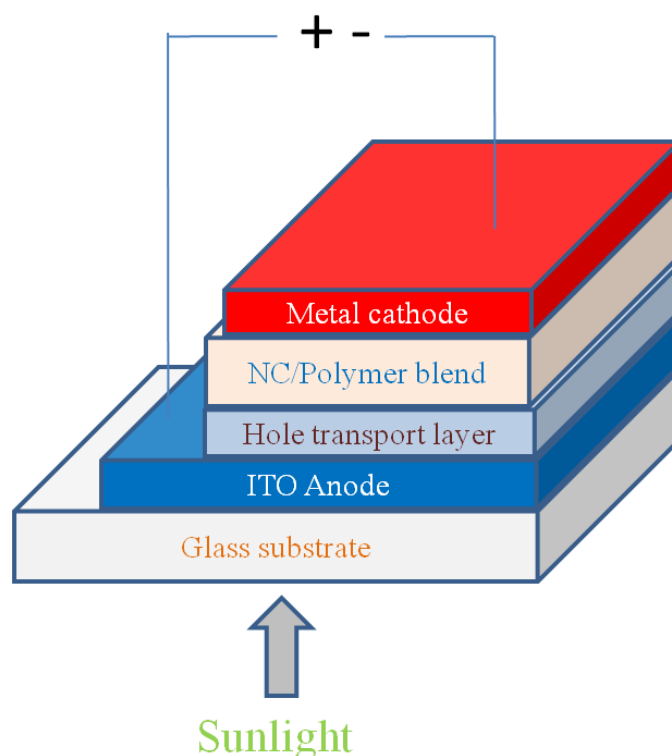


**Figure 1.11** Schematic diagrams of hybrid planar-mixed heterojunction solar cell device.

#### 1.7.5 Tandem Solar Cells

In order to improve the efficiency of organic solar cells, tandem structure was investigated. One reason behind the low efficiency of OPV devices is the inability of organic material to absorb the entire solar spectrum. The first tandem solar cells were prepared by Hiramoto (132). The series connection of two or more solar cells with dissimilar absorption characteristics either in small molecule or in polymer for utilizing a broad series of the solar spectrum is known as tandem configuration of organic solar cells (133-138). During the initial stage of fabrication of tandem structure, there was no major problem in case of small molecule as thin films were prepared through thermal evaporation while in case of solution processable polymers, problem arises during deposition of upper layer which sometime partially or

completely destroy the bottom layer. To overcome such limitation, a suitable interlayer was sandwiched in between these layers which act as cathode for bottom layer and anode for upper layer (139-142).

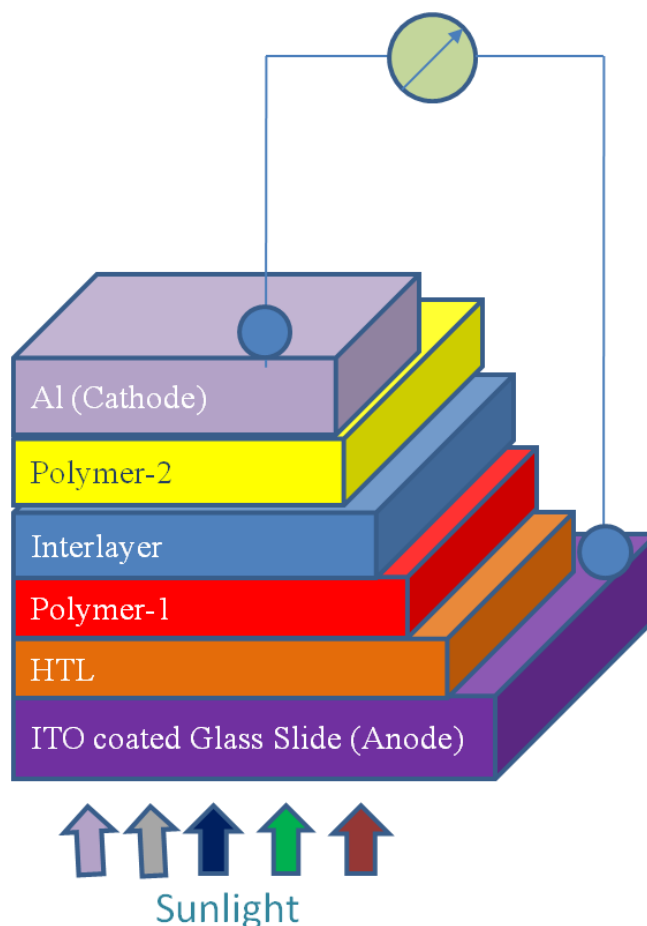


**Figure 1.12** Schematic diagrams of tandem solar cell devices.

#### 1.7.6 Inverted Solar Cells

Inverted solar cells are those polymers based solar cells in which high work function ITO work as cathode while low work function aluminium or silver work as anode. The overall device geometry is inverted in which ETL is coated above to ITO followed by active material(s) and HTL is coated just below to aluminium/ silver. The work function of ITO was customized by metal oxides like titanium oxide, PFN, zinc oxide and cesium carbonate (143-149). The degradation of inverted solar cell is much

lesser as compared to conventional structure of OPV devices due to non-contact of hygroscopic and corrosive hole transporting PEDOT:PSS directly to ITO. Approximately 10% power conversion efficiency has been achieved through ITO/PFN/PTB7:PC<sub>71</sub>BM/MoO<sub>3</sub>/(Al/Ag).

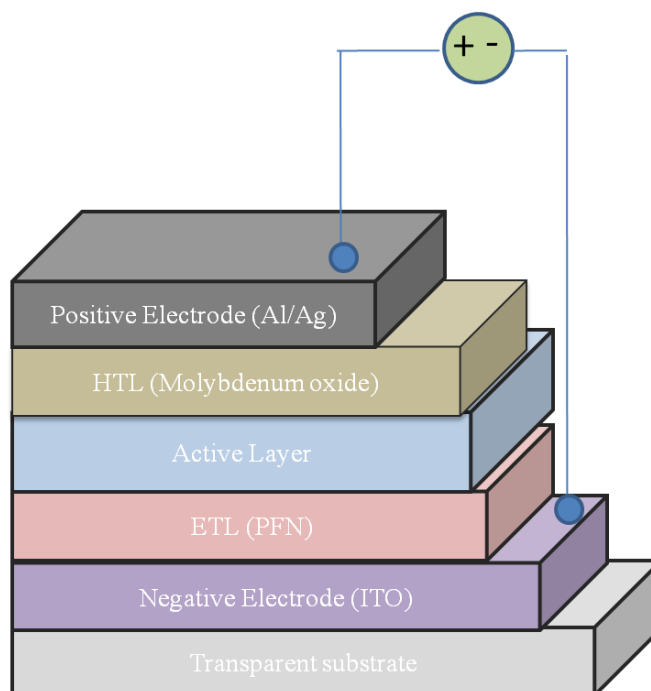


**Figure 1.13** Schematic diagrams of inverted solar cell devices.

#### 1.7.7 Perovskite Solar Cells

Perovskite solar cell is a solar cell in which perovskite material act as active layer which is sandwich in between two electrodes out of which one should be optically transparent. In such solar cells, fluorine doped tin oxide (FTO) is generally use as transparent electrode while other electrode either be silver or aluminium. Perovskite material is composed of most typically a hybrid organic inorganic lead or tin halide based material. Different device geometries of perovskite solar cell have been already developed with improved efficiencies.

Based on device architecture, perovskite solar cells have been divided into two categories: Conventional n-i-p structure and Inverted p-i-n structure. Conventional n-

i-p (n-i-p planar and n-i-p mesoscopic) has device architecture FTO/ETM/Perovskite /HTM /Metal anode while Inverted p-i-n (p-i-n planar and p-i-n mesoscopic) have device architecture ITO/HTM/Perovskite /ETM /Metal cathode as shown in Figure 1.14 (A-D) (150-151). In order to enhance the efficiency perovskite solar cells, hole transporting material (HTM) and electron transporting material (ETM) are inserted with perovskite layer with proper alignment in sequential order.

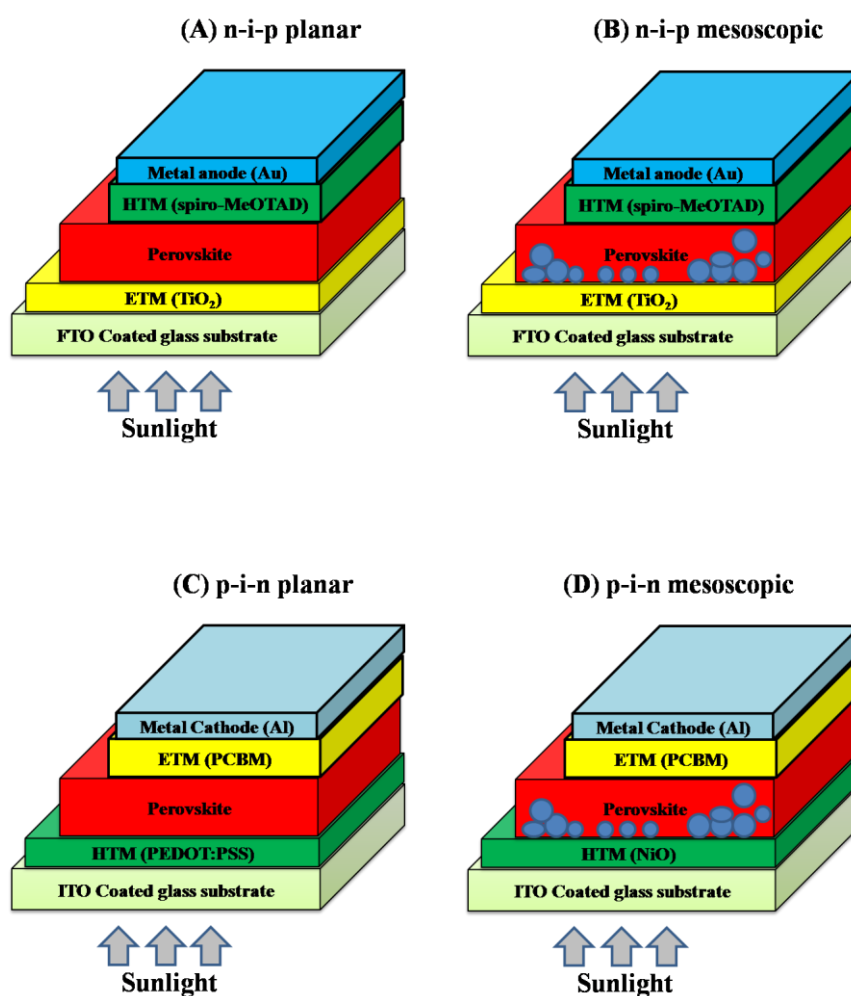


**Figure 1.14** Schematic diagrams of perovskite solar cell devices (A) n-i-p planar, (B) n-i-p mesoscopic, (C) p-i-n planar, (D) p-i-n mesoscopic.

## 1.8 Device Components

Polymer based organic solar cells are consisting of following components:

- Electrodes
  - Anode (ITO/FTO)
  - Cathode (Al/Ag/Au)
- Interface Layers
  - Hole transport layer (HTL)
  - Electron transport layer (ETL)
- Active Layer
  - Donor (P3HT/PCDTBT/PTB7)
  - Acceptor (PC<sub>61</sub>BM/ PC<sub>71</sub>BM)

### 1.8.1 Electrodes (Anode/Cathode)

All the devices based on organic semiconducting materials consisting of two electrodes (152). Out of these two, one electrode should be optically transparent with suitable work function to collect positive charge carriers (holes) for conventional structure of OPV devices. Basically high work function materials are used as anode for a BHJ organic solar cell.

Metal oxides like indium tin oxide (ITO) or fluorine-doped tin oxide (FTO) on glass or plastic substrates were ultimate option for anode due to its high work function, good electrical conductivity, high optical transparency in the visible region, insolubility and high thermal stability. The top metal electrode (cathode) is typically either aluminum, gold or silver with comparable low work function can be coated by thermally deposition technique with suitable vacuum. However, aluminum is the most suitable top electrode in standard structure of solar cells.

### 1.8.2 Interface Layers (HTL/ETL)

The performance of organic solar cells based on BHJ structure are strongly depends upon hole transport layer (HTL) and electrode transport layer (ETL). HTL is sandwich in between ITO anode and active material while ETL is inserted in between active material and metallic cathode in case of conventional cells. Without interface layer, device exhibit poor performance or even no operation so it is compulsory to fabricate interface layers accordingly. The selection of HTLs and ETLs depends upon the energy levels and charge transport properties of the material(s).

#### *Hole Transport Layer (HTL)*

Hole transport layer improves the collection of positive charge holes at anode electrode. A lot of materials like organic, inorganic and self assembled monolayers were used as HTL. Water soluble PEDOT:PSS is the most commonly used HTL in conventional geometry BHJ solar cells, due to its high transparency in the visible range, good electrical conductivity, high work function which match the HOMO level of frequently used donor polymers and also have the ability to reduce the ITO surface roughness (153). Moreover transition metal oxides with a high work function, namely molybdenum oxide ( $\text{MoO}_3$ ) (154), vanadium oxide ( $\text{V}_2\text{O}_5$ ) (155,156) and tungsten oxide ( $\text{WO}_3$ ) (157) so forth have been successfully used as HTL in organic solar cells. In the present thesis copper (I) thiocyanate ( $\text{CuSCN}$ ) (158) and copper iodide ( $\text{CuI}$ ) (159) are also used as alternative hole transporting layer (HTL) for polymeric solar cells.

#### *Electron Transport Layer (ETL)*

Electron transport layer improve the efficiency of cathode electrode for collection and extraction of negative charge electron. Low work function materials having good electronic level matching with the LUMOs of the active material



(polymers) are as ETL used in organic solar cells. Zinc oxide (ZnO) (160) and titanium oxide ( $\text{TiO}_x$ ) (161, 162) are the well-known and widely used ETLs which can be deposited by sol-gel, spray-coating and nanoparticle (NP) deposition. Later on cesium carbonate ( $\text{Cs}_2\text{CO}_3$ ) (163) and niobium pentoxide ( $\text{Nb}_2\text{O}_5$ ) (164) was also used as good ETL for OSCs.

### 1.8.3 Active Material (Donor/Acceptor)

In organic solar cells, active layer composed of organic semiconducting materials are responsible for absorption of light, generation and separation of charge carriers. Typically, the active layer consists of two components in the OSCs: electron donor and acceptor materials.

Polymers and small molecular compounds with conjugated backbones are used as electron donor material in OPV devices. A lot of research has been done on P3HT donor material due to promising photovoltaic properties and good stability although the absorption band of P3HT is not broad enough to get good harvest of the sunlight. In the present thesis a lot of work has done based on low band gap polymer: PCDTBT and PTB7. Fullerene and its derivatives are the most successful electron acceptor materials.  $\text{PC}_{61}\text{BM}$  and its equivalent derivative  $\text{PC}_{71}\text{BM}$  has been dominantly used as acceptors in OSCs.  $\text{PC}_{71}\text{BM}$  shows stronger absorption in visible region compared to  $\text{PC}_{61}\text{BM}$ .

## 1.9 Objectives of the Thesis

The objective of this thesis is to fabricate the organic solar cells based on low band gap polymers deposited through spin coating technique in glove box. All the devices are fabricate on pre-patterned ITO coated glass substrates. The device structure is: ITO (anode) /HTL/ active layer / Al (metal), where active layer corresponds to the low band gap polymers: PCDTBT and PTB7. The fabrication is

carried out in Flexible Organic Energy devices section of CSIR- National Physical Laboratory.

Most of the effort devoted to the fabrication of OPV devices has been based on P3HT:PC<sub>61</sub>BM bulk heterojunction architecture in which P3HT act as electron donor and PC<sub>61</sub>BM act as electron acceptor materials. But the PCE achieved by this photoactive material is unable to reach up to a certain limit due to poor absorption in active layer, which restricts to commercialization. Less investigation has been done on low band gap polymers based solar cells. In the present work, focus has been on low band gap polymers (PCDTBT and PTB7) acting as donor material with PC<sub>71</sub>BM as acceptor material through modification of an interference layer.

The aim of the thesis is to investigate the low band gap polymeric solar cells based on inexpensive and solution-processable HTL and optimization of device efficiency. The thesis is mainly directed towards:

1. Fabrication of organic solar cells based on low band gap polymers (PCDTBT and PTB7) as core problem of the thesis using solution-processable CuSCN as hole transporting layer.
2. Development of low band gap polymeric solar cells using solution-processable CuI as hole transport material.
3. Optimization of composition ratio of P3HT:PC<sub>61</sub>BM in organic solar cells for optimal device efficiency.

## 1.10 Thesis Outline

*Chapter 1* (present chapter) This chapter of the thesis is devoted towards the extensive literature survey on past and present research work done on organic solar cells including working mechanism, various geometry, buffer layers, both hole and

electron transport layers (HTL and ETL) which are used in organic solar cells, are discussed keeping focus on various HTL. It summarizes the general review on various methods for the enhancement in the performance (both stability and efficiency) of organic solar cells by using different HTL, ETL and conducting polymers.

*Chapter 2* This chapter details the various characterization techniques performed to characterize the parameters of organic solar cells e.g. morphology, I-V measurement etc. The detailed process for the fabrication of solution processed optoelectronic devices such as solar cell is discussed. Equipments require for fabrication process like glove box, thermal evaporation systems and spin coating unit with characterization techniques including UV-vis-NIR, XRD, SEM, TEM and AFM etc. are discussed in brief.

*Chapter 3* describes the utilization of copper (I) thiocyanate (CuSCN) as an efficient and solution processable hole transport layer (HTL) in bulk heterojunction solar cells. The work has been discussed in two subsequent sections.

*Chapter 3A* In this section three different combinations of the most studied active layers of P3HT:PC<sub>61</sub>BM, PCDTBT:PC<sub>71</sub>BM and PTB7:PC<sub>71</sub>BM were used for photovoltaic device fabrication with the simplest device structure of ITO/CuSCN/active layer/Al. The use of CuSCN as an HTL has improved light absorption within the active layer and thereby leads to up to 5.94% and 4.60% power conversion efficiencies (PCEs) for these active layers respectively. These results are slightly better when compared to the devices fabricated using thermal deposition of MoO<sub>3</sub> and solution processed deposition of PEDOT:PSS as an HTL under similar conditions.

*Chapter 3B* During past few years, significant research on solution-processable deposition of copper(I)thiocyanate (CuSCN) as an efficient hole

transporting layer (HTL) for excitonic solar cells have been successfully reported. Surprisingly, till now only two solvents diisopropyl sulfide and diethyl sulfide are known which have been used for CuSCN film deposition as a HTL for device fabrication. It is also noticeable that both the solvents are an irritant solvent having very foul smell. In this section we have used eco-friendly and inexpensive solvent dimethyl sulfoxide (DMSO) for solution processed thin film deposition of CuSCN for organic solar cells. The photovoltaic devices were fabricated using two different donor polymers PCDTBT and PTB7 blended with PC<sub>71</sub>BM as an acceptor material with device structure of ITO/CuSCN/active layer/Al. The power conversion efficiency (PCE) based on CuSCN using DMSO as a deposition solvent have been achieved up to 4.20% and 3.64% respectively, with relative higher fill factor (FF) as compared to previously reported values in literature.

In parallel with the above work, investigations were also directed towards development of alternative and universal solvents for copper (I) thiocyanate for fabrication of low band gap polymeric solar cells to boost the utilization of CuSCN. In this connection, we used five different alternative solvents compactable with CuSCN for fabrication of organic solar cells: *N,N*-dimethylformamide, dioxane, acetonitrile, ethylene glycol, propylene carbonate.

*Chapter 4* In this chapter, we have shown the performance of solution-processable copper iodide (CuI) as an alternative hole transporting layer (HTL) for polymeric solar cells. Optical spectra of the CuI thin film reveal highly transparent and practically no absorption in the range vis-NIR region (450-1110 nm). X-ray diffraction (XRD) patterns of CuI exhibits a p-type semiconductor as well as crystalline nature. The power conversion efficiencies (PCEs) based on CuI as an HTL have been achieved up to 3.04% and 4.48% for PCDTBT and PTB7 based donor

materials blended with PC<sub>71</sub>BM as an acceptor material respectively with a configuration based on ITO/CuI(40 nm)/active layer (60 nm)/Al (120 nm). Furthermore, we use a wide range of solvents for solution-processed deposition of copper iodide (CuI) thin films as hole transport layer for efficient polymeric solar cells in general. Three different solvents (dimethyl sulfoxide (DMSO), *N,N*-dimethylformamide (DMF) and diisopropyl sulfide) are used for solution-processable HTL for low band gap solar cells. To examine the feasibility of these deposited solvents for HTL, we used two different combination of active layers based on low band gap polymers (PCDTBT: PC<sub>71</sub>BM and PTB7:PC<sub>71</sub>BM) for fabrication of solar cells with a device configuration based on ITO/CuI(40 nm)/active layer (60 nm)/Al (120 nm).

*In Chapter 5* the effects of different composition ratios of P3HT:PC<sub>61</sub>BM in active layer on photovoltaic parameters were systematically studied in ambient conditions. The P3HT:PC<sub>61</sub>BM composition ratios range from 1.0:0.4 to 1.0:1.2 in active layer shows relatively good PCE and further decrease or increase of P3HT:PC<sub>61</sub>BM ratio the resulted devices show very poor PCE. The devices with various composition ratios clearly demonstrated that 1.0:0.8 weight ratio of P3HT:PC<sub>61</sub>BM has achieved highest power conversion efficiency.

*Chapter 6* This chapter presents the major conclusions derived from the present work and the scope of the future study in this field has been suggested.

**References:**

1. M. A. Green (Ed.), *Silicon Solar Cells: Advanced Principles & Practice*, Centre for Photovoltaic Devices and Systems, University of New South Wales, Kensington, N.S.W., 1995.
2. T. Markvart, and L. Castaner (Eds.), *Solar Cells: Materials, Manufacture and Operation*, Elsevier, Oxford, UK, 2005.
3. A. Goetzberger, J. Knobloch, and B. Voss (Eds.), *Crystalline Silicon Solar Cells*, John Wiley & Sons Ltd., England, 1998.
4. T. Markvart, *Progress in Quantum Electronics*, 24 (2000) 107.
5. R. B. Bergmann, *Applied Physics A Materials Science & Processing*, 69 (1999) 187.
6. R. Schropp, and M. Zeman (Eds.), *Amorphous and Microcrystalline Silicon Solar Cells: Modelling, Materials and Device Technology* Kluwer, Boston, 1998.
7. S. M. Sze (Ed.), *Physics of Semiconductor Devices*, John Wiley & Sons, New York, 1981.
8. A. Goetzberger, J. Luther, and G. Willeke, *Solar Energy Materials Solar Cells*, 74 (2002) 1.
9. A.E. Becquerel, *Comptes Rendus de L'Academie des Sciences*, 9 (1839) 561.
10. C.E. Fritts, *American Journal of Science*, 26 (1883) 465.
11. Jenny Nelson (Ed.), *The Physics of Solar Cells*: Imperial College Press, 2003.
12. M. A. Green, *Progress in Photovoltaic*, 13 (2005) 447.
13. A. Blakers, K. Weber and V. Everett, *Chemistry in Australia* 72 (2005) 9.

14. A. Luque, and S. Hegedus (Ed.), Handbook of Photovoltaic Science and Engineering: John Wiley and Sons, 2003.
15. M. A. Green, K. Emery, D. L. King, S. Igari, and W. Warta, Progress in Photovoltaics: Research and Applications, 9 (2001) 287.
16. L. C. Rogers, W. C. O'Mara, R. B. Herring, and L. P. Hunt (Ed.), Handbook of Semiconductor Silicon Technology: Noyes Publications, New Jersey, USA (1990).
17. W. Wettling, Solar Energy Materials & Solar Cells, 38 (1995) 487.
18. F. Antony, C. Durschner, and K.-H. Remmers (Ed.), Photovoltaics for Professional: Solarpraxis AG, London, 2007.
19. R. E. I. Schropp, and M. Zeman (Eds.), Amorphous and Microcrystalline Silicon Solar Cells: Modelling, Materials and Device Technology, Kluwer Academic Publishers: Boston, MA, 1998.
20. J. Poortmans, and V. Arkhipov (Eds.), Thin Film Solar Cells: Fabrication, Characterization and Applications, John Wiley & Sons Ltd., England, 2006.
21. R. Brendel (Ed.), Thin-Film Crystalline Silicon Solar Cells: Physics and Technology, Wiley-VCH, Weinheim, 2003.
22. R. Noufi, and K. Zweibel (Eds.), IEEE 4<sup>th</sup> World Conference on Photovoltaic Energy Conversion (WCPEC-4), 1 (2006) 317.
23. V. Kumar, S. C. Jain, A. K. Kapoor, W. Geens, T. Aernauts, J. Poortmans, and R. Mertens, Journal of Applied Physics, 92 (2002) 7325.
24. A. K. Kapoor, S. C. Jain, V. Kumar, J. Poortmans, and R. Mertens, Journal of Applied Physics, 92 (2002) 3835.
25. S. Gunes, H. Neugebauer, and N. S. Sariciftci, Chemical Reviews, 107 (2007) 1324.

26. S. C. Jain, A. K. Kapoor, W. Geens, J. Poortmans, R. Mertens, and M. Willander, *Journal of Applied Physics*, 92 (2002) 3579.
27. H. Hoppe, and N. S. Sariciftci, *Journal of Materials Research*, 19 (2004) 1924.
28. H. Kim, W.-W. So, and S.-J. Moon, *Solar Energy Materials & Solar Cells* 91 (2007) 581.
29. M. M. Wienk, M. P. Struijk, and R. A. J. Janssen, *Chemical Physics Letters*, 422 (2006) 488.
30. P. Kumar, S. C. Jain, A. Misra, M. N. Kamalasanan, and V. Kumar, *Journal of Applied Physics*, 100 (2006) 114506.
31. T. L. Benanti, and D. Venkataraman, *Photosynthesis Research*, 87 (2006) 73.
32. V. Kumar, S. C. Jain, A. K. Kapoor, J. Poortmans, and R. Mertens, *Journal of Applied Physics*, 94 (2003) 1283.
33. P. Kumar, A. Misra, M. N. Kamalasanan, S. C. Jain, and V. Kumar, *Journal of Physics D: Applied Physics*, 40 (2007) 561.
34. W. Ma, C. Yang, X. Gong, K. Lee, and A. J. Heeger, *Advanced Materials*, 15 (2005) 1617.
35. J. Nelson, *Current Opinion in Solid State and Materials Science*, 6 (2002) 87.
36. K. M. Coakley, and M. D. McGehee, *Chemistry of Materials*, 16 (2004) 4533.
37. S. C. Jain, W. Geens, A. Mehra, V. Kumar, T. Aernouts, J. Poortmans, R. Mertens, and M. Willander, *Journal of Applied Physics*, 89 (2001) 3804.
38. H. Spanggaard, and F.C. Krebs, *Solar Energy Materials Solar Cells* 83 (2004) 125.
39. W. U. Huynh, X. G. Peng, and A. P. Alivisatos, *Advanced Materials*, 11 (1999) 923.



40. X. J. Wang, E. Perzon, F. Oswald, F. Langa, S. Admassie, M. R. Andersson, and O. Inganas, *Advanced Functional Materials*, 15 (2005) 1665.
41. T. Stoferle, U. Scherf, and R. F. Mahrt, *Nano Letters*, 9 (2009) 453.
42. E. Holder, N. Tesslerb, and A. L. Rogach, *Journal of Materials Chemistry*, 18 (2008) 1064.
43. B. Sun, E. Marx, and N. C. Greenham, *Nano Letters*, 3 (2003) 961.
44. S. Gunes, and N. S. Sariciftci, *Inorganica Chimica Acta*, 361 (2008) 581.
45. B. R. Saunders, and M. L. Turner, *Advances in Colloid and Interface Science* 138 (2008) 1.
46. Y. Zhou, Y. Li, H. Zhong, J. Hou, Y. Ding, C. Yang, and Y. Li, *Nanotechnology* 17 (2006) 4041.
47. M. T. Khan, R. Bhargav, A. Kaur, S. K. Dhawan, and S. Chand, *Thin Solid Films* 519 (2010) 1007.
48. W. U. Huynh, J. J. Dittmer, and A. P. Alivisatos, *Science* 295 (2002) 2425.
49. I. Gur, N. A. Fromer, C.-P. Chen, A. G. Kanaras, and A. P. Alivisatos, *Nano Letters*, 7 (2007) 409.
50. W. U. Huynh, J. J. Dittmer, W. C. Libby, G. L. Whiting, and A. P. Alivisatos, *Advanced Functional Materials*, 13 (2003) 73.
51. L. Han, D. Qin, X. Jiang, Y. Liu, L. Wang, J. Chen, and Y. Cao, *Nanotechnology*, 17 (2006) 4736.
52. M. Pientka, V. Dyakonov, D. Meissner, A. Rogach, D. Talapin, H. Weller, L. Lutsen, and D. Vanderzande, *Nanotechnology*, 15 (2004) 163.
53. B. Sun, and N. C. Greenham, *Physical Chemistry Chemical Physics*, 8 (2006) 3557.

54. J. Seo, W. J. Kim, S. J. Kim, K. S. Lee, A. N. Cartwright, and P. N. Prasad, *Applied Physics Letters*, 94 (2009) 133302.
55. J. Boucle, S. Chyla, M. S. P. Shaffer, J. R. Durrant, D. D. C. Bradley, and J. Nelson, *Advanced Functional Materials*, 18 (2008) 622.
56. T. Z. Wei, Y. Y. Lin, H. H. Lo, C. W. Chen, C. H. Chen, S. C. Liou, H. Y. Huang, and W. F. Su, *Nanotechnology*, 17 (2006) 5387.
57. X. S. Zhou, Z. Li, N. Wang, Y. H. Lin, and C. W. Nan, *Applied Physics Letters*, 88 (2006) 243119.
58. X. Jiang, R. D. Schaller, S. B. Lee, J. M. Pietryga, V. I. Klimov, and A. A. Zakhidov, *Journal of Materials Research*, 22 (2007) 2204.
59. C. Y. Kwong, W. C. H. Choy, A. B. Djurisic, P. C. Chui, K. W. Cheng, and W. K. Chan, *Nanotechnology* 15 (2004) 1156.
60. Y. Kang, N. G. Park, and D. Kim, *Applied Physics Letters*, 86 (2005) 113101.
61. W. J. E. Beek, M. M. Wienk, and R. A. J. Janssen, *Advanced Materials*, 16 (2004) 1009.
62. K. Takanezawa, K. Hirota, Q.-S. Wei, K. Tajima, and K. Hashimoto, *Journal of Physical Chemistry C*, 111 (2007) 7218.
63. W. J. E. Beek, M. M. Wienk, M. Kemerink, X. Yang, and R. A. J. Janssen, *Journal of Physical Chemistry B*, 109 (2005) 9505.
64. D. C. Olson, J. Piris, R. T. Collins, S. E. Shaheen and D. S. Ginley, *Thin Solid Films*, 496 (2006) 26.
65. S. Berson, R. D. Bettignies, S. Bailly, S. Guillerez, and B. Jousset, *Advanced Functional Materials*, 17 (2007) 3363.
66. B. J. Landi, S. L. Castro, H. J. Ruf, C. M. Evans, S. G. Bailey, and R. P. Raffaele, *Solar Energy Materials and Solar Cells*, 87 (2005) 733.

67. [http://www.kaneka.co.jp/kanekae/images/topics/1473811995/1473811995\\_101.pdf](http://www.kaneka.co.jp/kanekae/images/topics/1473811995/1473811995_101.pdf) (accessed 25 October 2016).
68. S. Zhang, X. Pan, H. Jiao, W. Deng, J. Xu, Y. Chen, P. P. Altermatt, Z. Feng, and P. J. Verlinden, *IEEE Journal of Photovoltaics*, 6 (2016) 145.
69. P. J. Verlinden, *PVSEC 26: Singapore*, (2016) 24.
70. J. Meier, J. Sitznagel, U. Kroll, C. Bucher, S. Fay, T. Moriarty, and A. Shah, *Thin Solid Films*, 518 (2004) 451.
71. M. A. Contreras, K. Ramanathan, J. AbuShama, F. Hasoon, D. Young, B. Egaas, and R. Noufi, *Progress in Photovoltaics: Research and Applications*, 13 (2005) 209.
72. H. Sugimoto, 2014 IEEE 40th Photovoltaic Specialist Conference (PVSC), (2014) 2767.
73. First solar press release, First Solar builds the highest efficiency thin film PV cell on record, 5 August 2014.
74. First solar press release. First Solar achieves world record 18.6 % thin film module conversion efficiency, 15 June 2015.
75. B. M. Kayes, H. Nie, R. Twist, S. G. Spruytte, F. Reinhardt, I. C. Kizilyalli, and G. S. Higashi. 37<sup>th</sup> IEEE Photovoltaic Specialists Conference, (2011) 4.
76. L. S. Mattos, S. R. Scully, M. Syfu, E. Olson, L. Yang, C. Ling, B. M. Kayes, and G. He, 38th IEEE Photovoltaic Specialists Conference, (2012) 003187.
77. R. Venkatasubramanian, B. C. O'Quinn, J. S. Hills, P. R. Sharps, M. L. Timmons, J. A. Hutchby, H. Field, A. Ahrenkiel, and B. Keyes, *Conference Record of the Twenty Fifth IEEE Photovoltaic Specialists Conference*, (1997) 31.

78. C. J. Keavney, V. E. Haven, and S. M. Vernon, Conference Record, 21st IEEE Photovoltaic Specialists Conference, (1990) 141.
79. Z. He, B. Xiao, F. Liu, H. Wu, Y. Yang, S. Xiao, C. Wang, T. P. Russell, and Y. Cao, Nature Photonics, 9 (2015) 174.
80. R. Komiya, A. Fukui, N. Murofushi, N. Koide, R. Yamanaka and H. Katayama, Technical Digest: 21st International Photovoltaic Science and Engineering Conference, 2 (2011) 50.
81. J. You, L. Dou, K. Yoshimura, T. Kato, K. Ohya, T. Moriarty, K. Emery, C. C. Chen, J. Gao, G. Li, and Y. Yang, Nature Communications, 4 (2013) 1443.
82. S. Mori, H. Oh-oka, H. Nakao, T. Gotanda, Y. Nakano, H. Jung, A. Iida, R. Hayase, N. Shida, M. Saito, K. Todor, T. Asakura, A. Matsui, and M. Hosoya, MRS Online Proceedings Library, 1737 (2015) 540.
83. M. Hosoya, H. Oooka, H. Nakao, T. Gotanda, S. Mori, N. Shida, R. Hayase, Y. Nakano, and M. Saito, Proceedings of the 93rd Annual Meeting of the Chemical Society of Japan, (2013) 21.
84. W. S. Yang, J. H. Noh, N. J. Jeon, Y. C. Kim, S. Ryu, J. Seo, and S. I. Seok, Science, 348 (2015 ) 1234.
85. <http://en.sjtu.edu.cn/news/a-breakthrough-in-large-area-perovskite-solar-panels-by-sjtu-team/> (accessed 25 October 2016).
86. A. Marti, L. Cuadra, and A. Luque, IEEE Transactions on Electron Devices, 49 (2002) 1632.
87. A. Luque, A. Marti, N. Lopez, E. Antolin, E. canovas, C. Stanley, C. Farmer, L. J. Ca-ballero, L. Cuadra, and J. L. Balenzategui, Applied Physics Letters 87 (2005) 083505.

88. P. J. Verlinden, R. M. Swanson, R. A. Crane, K. Wickham, and J. A. Perkins, Conf. Record, 13th European Photovoltaic Solar Energy Conference, Nice, October (1995) 1582.
89. P. Schilinsky, C. Waldauf, and C. J. Brabec, *Advanced Functional Materials*, 16 (2006) 1669.
90. S. S. Sun, and N. S. Sariciftci (Eds.), *Organic Photovoltaics: Mechanisms, Materials and Devices*, CRC Press, Boca Raton, FL, 2005.
91. J. C. Bernedej, *Journal of the Chilean Chemical Society*, 3 (2008) 1549.
92. J-M. Nunzi, *Comptes Rendus Physique*, 3 (2002) 523.
93. C. Deibel, and V. Dyakonov, *Reports on Progress in Physics*, 73 (2010) 096401.
94. C. J. Brabec, N. S. Sariciftci, and J. C. Hummelen, *Advanced Functional Materials*, 11 (2001) 15.
95. S. Barth, and H. Bassler, *Physical Review Letters*, 79 (1997) 4445.
96. M. A. Green, *Journal of Materials Science - Materials in Electronics*, 18 (2007) 15.
97. J. M. Nunzi, *Comptes Rendus Physique*, 3 (2002) 523.
98. C. Deibel, T. Strobel, and V. Dyakonov, *Advanced Materials*, 22 (2010) 4097.
99. T. M. Clarke, and J. R. Durrant, *Chemical Reviews*, 110 (2010) 6736.
100. L. J. A. Koster, E. C. P. Smits, V. D. Mihailechi, and P. W. M. Blom, *Physical Review B*, 72 (2005) 085205.
101. V. Mihailechi, L. Koster, J. Hummelen, and P. Blom, *Physical Review Letters*, 93 (2004) 216601.
102. C. Deibel, A. Wagenpfahl, and V. Dyakonov, *Physica status solidi (RRL)-Rapid Research Letters*, 2 (2008) 175.

103. T. Kirchartz, B. E. Pieters, K. Taretto, and U. Rau, *Physical Review B*, 80 (2009) 035334.
104. A. Wagenpfahl, D. Rauh, M. Binder, C. Deibel, and V. Dyakonov, *Physical Review B*, 82 (2010) 115306.
105. J-M. Nunzi, *Comptes Rendus Physique*, 3 (2002) 523.
106. A. J. Mozer, and N. S. Sariciftci, *Comptes Rendus Chimie*, 9 (2006) 568.
107. R. N. Marks, J. J. M. Halls, D. D. C. Bradley, R. H. Friend, and A. B. Holmes, *Journal of Physics: Condensed Matter*, 6 (1994) 1379.
108. C. W. Tang, *Applied Physics Letters*, 48 (1986) 183.
109. S. R. Forrest, L. Y. Leu, F. F. So, and W. Y. Yoon, *Journal of Applied Physics*, 66 (1989) 5908.
110. Y. Shao, and Y. Yang, *Advanced Materials*, 17 (2005) 2841.
111. K. Suemori, T. Miyata, M. Yokoyama, and M. Hiramoto, *Applied Physics Letters*, 85 (2004) 6269.
112. J. H. Schön, C. Kloc, E. Bucher, and B. Batlogg, *Nature*, 403 (2000) 408.
113. B. P. Rand, J. Xue, F. Yang, and S. R. Forrest, *Applied Physics Letters*, 87 (2005) 233508.
114. K. L. Mutolo, and E. I. Mayo, *Journal of the American Chemical Society*, 128 (2006) 8108.
115. H. Kumar, P. Kumar, R. Bhardwaj, G. D. Sharma, S. Chand, S. C. Jain, and V. Kumar, *Journal of Physics D: Applied Physics*, 42 (2009) 15103.
116. K. Schulze, C. Uhrich, R. Schuppel, K. Leo, M. Pfeiffer, E. Brier, E. Reinold, and P. Bauerle, *Advanced Materials*, 18 (2006) 2872.
117. C. W. Chu, Y. Shao, V. Shrotriya, and Y. Yang, *Applied Physics Letters*, 86 (2005) 243506.

118. S. Yoo, B. Domercq, and B. Kippelen, *Applied Physics Letters*, 85 (2004) 5427.
119. P. Peumans, and S. R. Forrest, *Applied Physics Letters*, 79 (2001) 126.
120. K. H. Lee, P. E. Schwenn, A. R. G. Smith, H. Cavaye, P. E. Shaw, M. James, K. B. Krueger, I. R. Gentle, P. Meredith, and P. L. Burn, *Advanced Materials*, 23 (2011) 766.
121. G. Yu, and A. J. Heeger, *Journal of Applied Physics*, 78 (1995) 4510.
122. J. J. M. Halls, A. C. Walsh, N. C. Greenham, E. A. Marseglia, R. H. Friend, S. C. Moratti, and A. B. Holmes, *Nature*, 376 (1995) 498.
123. S. E. Shaheen, C. J. Brabec, N. S. Sariciftci, F. Padinger, T. Fromhert, and J. C. Hummelen, *Applied Physics Letters*, 78 (2001) 841.
124. F. Padinger, R. S. Rittberger, and N. S. Sariciftci, *Advanced Functional Materials*, 13 (2003) 85.
125. M. Svensson, F. Zhang, S. C. Veenstra, W. J. H. Verhees, J. C. Hummelen, J. M. Kroon, O. Inganäs, and M. R. Anderson, *Advanced Materials*, 15 (2003) 988.
126. C. J. Brabec, S. E. Shaheen, C. Winder, N. S. Sariciftci, and P. Denk, *Applied Physics Letters*, 80 (2002) 1288.
127. J. Y. Kim, S. H. Kim, H. H. Lee, K. Lee, W. Ma, X. Gong, and A. J. Heeger, *Advanced Materials*, 18 (2006) 572.
128. J. Peet, J. Y. Kim, N. E. Coates, W. L. Ma, D. Moses, A. J. Heeger, and G. C. Bazan, *Nature Materials*, 6 (2007) 497.
129. Y. Liang, Z. Xu, J. Xia, S. T. Tsai, Y. Wu, G. Li, C. Ray, and L. Yu, *Advanced Materials*, 22 (2010) 135.
130. Z. He, C. Zhong, S. Su, M. Xu, H. Wu, and Y. Cao, *Nature Photonics*, 6 (2012) 591.

131. J. Xue, S. Uchida, B. P. Rand, and S. R. Forrest, *Advanced Materials*, 17 (2005) 66.
132. M. Hiramoto, H. Fujiwara, and M. Yokohama, *Journal of Applied Physics*, 72 (1992) 3781.
133. J. Xue, S. Uchida, B. P. Rand, and S. R. Forrest, *Applied Physics Letters*, 85 (2004) 5757.
134. G. Dennler, H. J. Prall, R. Koeppe, M. Egginger, R. Autengruber, and N. S. Sariciftci, *Applied Physics Letters*, 89 (2006) 73502.
135. A. Yakimov, and S. R. Forrest, *Applied Physics Letters*, 80 (2002) 1667.
136. A. Colsmann, J. Junge, C. Kayser, and U. Lemmer, *Applied Physics Letters*, 89 (2006) 203506.
137. V. Shrotriya, E. H. E. Wu, G. Li, Y. Yao, and Y. Yang, *Applied Physics Letters*, 88 (2006) 64104.
138. K. Kawano, N. Ito, T. Nishimori, and J. Sakai, *Applied Physics Letters*, 88 (2006) 73514.
139. A. Hadipour, B. De Boer, J. Wildman, F. B. Kooistra, J. C. Hummelen, M. G. R. Turbiez, M. M. Wienk, R. A. J. Janssen, and P. W. M. Blom, *Advanced Functional Materials*, 16 (2006) 1897.
140. S. Sista, M. H. Park, Z. Hong, Y. Wu, J. Hou, W. L. Kwan, G. Li, and Y. Yang, *Advanced Materials*, 22 (2010) 380.
141. J. Gilot, M. M. Weink, and R. A. J. Janssen, *Applied Physics Letters*, 90 (2007) 143512.
142. J. Gilot, M. M. Weink, and R. A. J. Janssen, *Advanced Materials*, 22 (2010) 67.
143. G. Li, C. W. Chu, V. Shrotriya, J. Huang, and Y. Yang, *Applied Physics Letters*, 88 (2006) 253503.



144. C. Waldauf, M. Morana, P. Denk, P. Schilinsky, K. Coakley, S. A. Choulis, and C. J. Brabec, *Applied Physics Letters*, 89 (2006) 233517.
145. J. Huang, G. Li, and Y. Yang, *Advanced Materials*, 20 (2008) 415.
146. T. Ameri, G. Dennler, C. Waldauf, H. Azimi, A. Seemann, K. Forberich, J. Hauch, M. Scharber, K. Hingerl, and C. J. Brabec, *Advanced Functional Materials*, 20 (2010) 1592.
147. T. Yang, W. Cai, D. Qin, E. Wang, L. Lan, X. Gong, J. Peng and Y. Cao, *Journal of Physics Chemistry C*, 114 (2010) 6849.
148. Y. M. Sun, J. H. Seo, C. J. Takacs, J. Seifert, and A. J. Heeger, *Advanced Materials*, 23 (2011) 1679.
149. C. E. Small, S. Chen, J. Subbiah, C. M. Amb, S. W. Tsang, T. H. Lai, J. R. Reynolds, and F. So, *Nature Photonics*, 6 (2012) 115.
150. Z. Song, S. C. Wathage, A. B. Phillips, and M. J. Heben, *Journal of Photonics for Energy*, 6 (2016) 022001.
151. D. T. Grant, K. R. Catchpole, K. J. Weber, and T. P. White, *Optics Express*, 24 (2016) 1454.
152. A. Becquerel, *Comptes Rendus des Séances Hebdomadaires*, 9 (1839) 561.
153. S. A. Carter, M. Angelopoulos, S. Karg, P. J. Brock, and J. C. Scott, *Applied Physics Letters*, 70 (1997) 2067.
154. C. Tao, S. Ruan, X. Zhang, G. Xie, L. Shen, X. Kong, W. Dong, C. Liu, and W. Chen, *Applied Physics Letters*, 93 (2008) 193307.
155. R. Lampande, G. W. Kim, J. Boizot, Y. J. Kim, R. Pode, and J. H. Kwon, *Journal of Materials Chemistry A*, 1 (2013) 6895.
156. K. Zilberberg, S. Trost, J. Meyer, A. Kahn, A. Behrendt, D. Ltzenkirchen-Hecht, R. Frahm, and T. Riedl, *Advanced Functional Materials*, 21 (2011) 4776.

157. C. Tao, S. Ruan, G. Xie, X. Kong, L. Shen, F. Meng, C. Liu, X. Zhang, W. Dong, and W. Chen, *Applied Physics Letters*, 94 (2009) 043311.
158. N. Chaudhary, R. Chaudhary, J. P. Kesari, A. Patra, and S. Chand, *Journal of Materials Chemistry C*, 3 (2015) 11886.
159. N. Chaudhary, J. P. Kesari, R. Chaudhary, and A. Patra, *Optical Materials*, 58 (2016) 116.
160. A. K. K. Kyaw, X. W. Sun, C. Y. Jiang, G. Q. Lo, D. W. Zhao, and D. L. Kwong, *Applied Physics Letters*, 93 (2008) 221107.
161. S. Sakohara, M. Ishida, and M. A. Anderson, *Journal of Physical Chemistry B*, 102 (1998) 10169.
162. S. Monticone, R. Tufeu, and A. V. Kanaev, *Journal of Physical Chemistry B*, 102 (1998) 2854.
163. T. Hasegawa, S. Miura, T. Moriyama, T. Kimura, I. Takaya, Y. Osato, and H. Mizutani, *Journal of the Society for Information Display*, 35 (2004) 154.
164. O. Wiranwetchayan, Z. Liang, Q. Zhang, G. Cao, and P. Singjai, *Materials Sciences and Applications*, 2 (2011) 1697.





# ***Chapter:2***

**Experimental Methods and Characterization Techniques**

---

**2.1 Introduction**

Fabrication of organic solar cell devices involves many fundamental steps and each step has its own importance. Particularly, processing of device is prompt to changes when different active materials with different interfacial layers are used. Often, even processing of device with the same active material using different HTL can result in different requirements for device processing. In order to obtain the optimal device efficiency from the available materials, much iteration of experiments is essential to establish the best processing conditions for fabrication of OPV devices.

In this chapter, experimental details including various steps involved in device preparation and fabrication equipments like thermal evaporator, spin coating unit, laser scribing system, UV ozone cleaner and glove box integrated with vacuum coating unit have been presented. Further, techniques used in the characterization of OPV devices such as solar simulator to illuminate the devices, Keithley source meter for J-V characteristics, atomic force microscopy (AFM), X-ray diffraction (XRD), UV-Vis absorption spectroscopy, transmission electron microscopy (TEM), scanning electron microscope (SEM) are discussed.

**2.2 Materials Used**

Different organic materials including anode, cathode, active materials and materials for HTL are illustrated in Table 2.1

**Table 2.1** List of materials required for fabrication of OPV devices.

S. No.	Material	Vendor	Layer
1	ITO	Vin Karola Instruments	Anode Electrode
2	PEDOT:PSS	Ossila Ltd	Hole Transport Layer
3	MoO <sub>3</sub>	Alfa Aesar	
4	CuSCN	Sigma-Aldrich	
5	CuI	Alfa Aesar	
6	P3HT	1-Material	Active Materials
7	PTB7	1-Material	
8	PCDTBT	1-Material	
9	PC <sub>61</sub> BM	1-Material	
10	PC <sub>71</sub> BM	1-Material	
11	Aluminium	Alfa Aesar	Cathode Electrode

Following organic solvents were used to dissolve active layer materials (donor and acceptor) and interface layer materials.

- Chlorobenzene
- Dichlorobenzene
- 1,8-diiodooctane (DIO)
- Diisopropyl sulphide
- Dimethyl sulfoxide (DMSO)
- *N,N*-Dimethylformamide
- Dioxane
- Acetonitrile
- Ethylene glycol
- Propylene carbonate

### 2.3 Brief Experimental Detail

The standard conventional bulk heterojunction (BHJ) organic solar cells were fabricated using following layers: a transparent anode layer coated with hole transport layer (HTL), followed by the active layer and a metal cathode with a low work function. ITO (indium tin oxide) coated glass substrate is used as anode due to its good electrical conductivity and optical transparency. Before deposition of any layer, these substrates should be cleaned with soap solution in ultrasonic-bath followed by heating in acetone, trichloroethylene and isopropyl alcohol (10 min each solvent-step). First, hole transport layer (HTL) is deposited by spin-coating or thermal evaporation technique (depending upon the nature of the material). Next, the active layer prepared by blend solution of donor and acceptor at a particular weight ratio (depending upon the polymer used) is deposited through spin coating method. Finally, aluminium electrode (low work function metal) is evaporated in high-vacuum through

thermal evaporation technique. Entire device fabrication takes place inside a glove-box in nitrogen inert atmosphere. Basic device structure is illustrated in Figure 2.1.

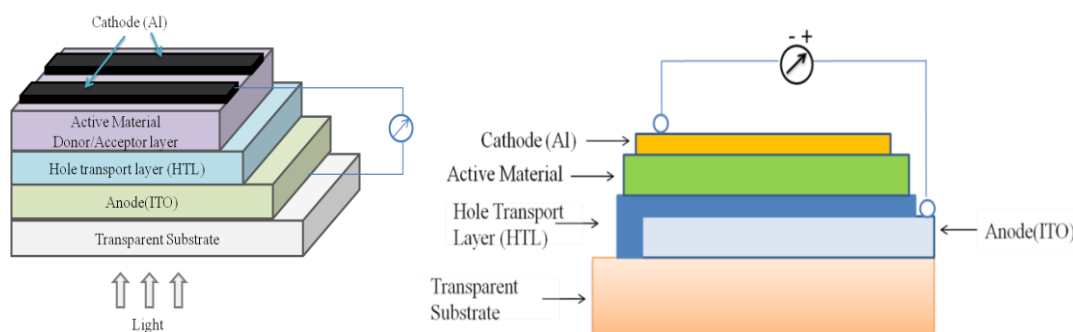


**Figure 2.1** Schematic diagram of standard structure of conventional organic solar cells.

## 2.4 Device Fabrication Process

### 2.4.1 Patterning of ITO coated glass substrates

To measure the performance of organic solar cell device(s) accurately, it is essential to identify precisely the active area which results from the vertical overlap of ITO and aluminium. Therefore, it is extremely essential to control the patterning of both the electrodes.

In the first step, ITO coated glass sheet was cut in 25 mm×25 mm size slides through glass cutter. The glass substrate used for device fabrication is entirely covered by ITO. During the initial stage in the laboratory, etching was done by exposing these ITO substrates to the solution of dilute hydrochloric acid (HCl) solvent and zinc dust powder through proper masking of desired pattern, either through cello tape or photolithography that involved the steps of photo resist coating called wet-etching technique. But later, patterning was done using a laser scribing system. Using this system, ITO substrates were patterned and etched in a single step dry ablative etching process, performed in ambient conditions which provide a good replacement over chemical etching. Laser scribing system (LSS) is shown in Figure 2.3. The whole



etching operation of LSS was corresponding to the drawing made in Corel Draw. We make two strips of ITO having 2 mm width. The patterned ITO strips on glass substrate is shown Figure 2.2.

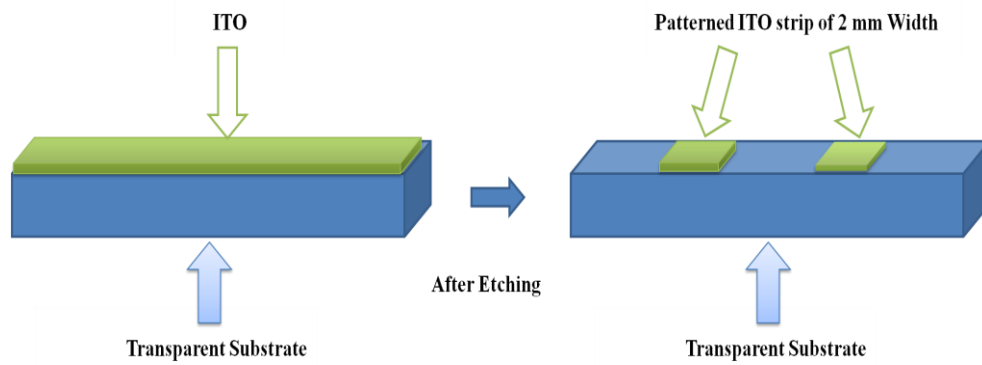


**Figure 2.2** ITO coated glass substrates before and after patterning the strip of 2 mm width.

Benefits and Characteristics of Laser Patterning:

- ❖ Processing time is very less, 45 second required for etching 1 inch substrate.
- ❖ Big substrate size can be patterned without any problem.
- ❖ Patterning can be done up to 10 microns size of pixel.
- ❖ No requirement of any mask for patterning i.e. the process can be done in a single step with ease.
- ❖ Any type of patterning is possible by making drawing on CorelDraw.
- ❖ Patterning and etching is very much environment friendly as there is no pollution during the process.
- ❖ It is a dry etching process unlike other etching processes.
- ❖ Substrates are not heated during the process.
- ❖ Etching can be done without damaging glass or plastic.

- ❖ It also helps to get rid of toxic chemicals that are otherwise used in chemical etching process.

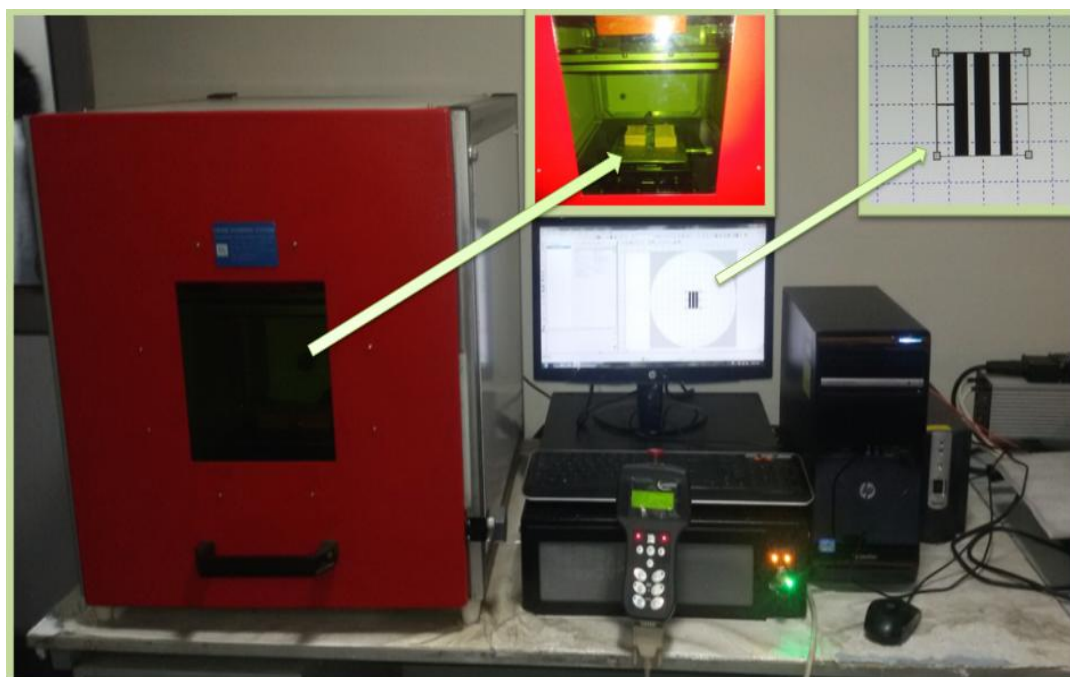


**Figure 2.3** Laser scribing system for patterning and etching of ITO substrates as per required design.

For the realization of patterning of aluminium (cathode), shadow-masks made from either aluminium sheet or cast iron sheet were used as shown in Figure 2.4. These masks were cut through cutter (in case of thin flexible aluminium sheet) or in workshop (thin cast iron sheet), with a width of 2.5 mm, that can easily fix to the sample holder of evaporator plate. The two strips are 3 mm distant, as in the anode. Active area of the device is  $2\text{ mm} \times 2.5\text{ mm} = 5\text{ mm}^2$ , obtained with  $90^\circ$  superposition of strip-shaped electrodes. In this technique, four different pixels for a device which are electrically isolated from one another in the same substrate can be obtained.

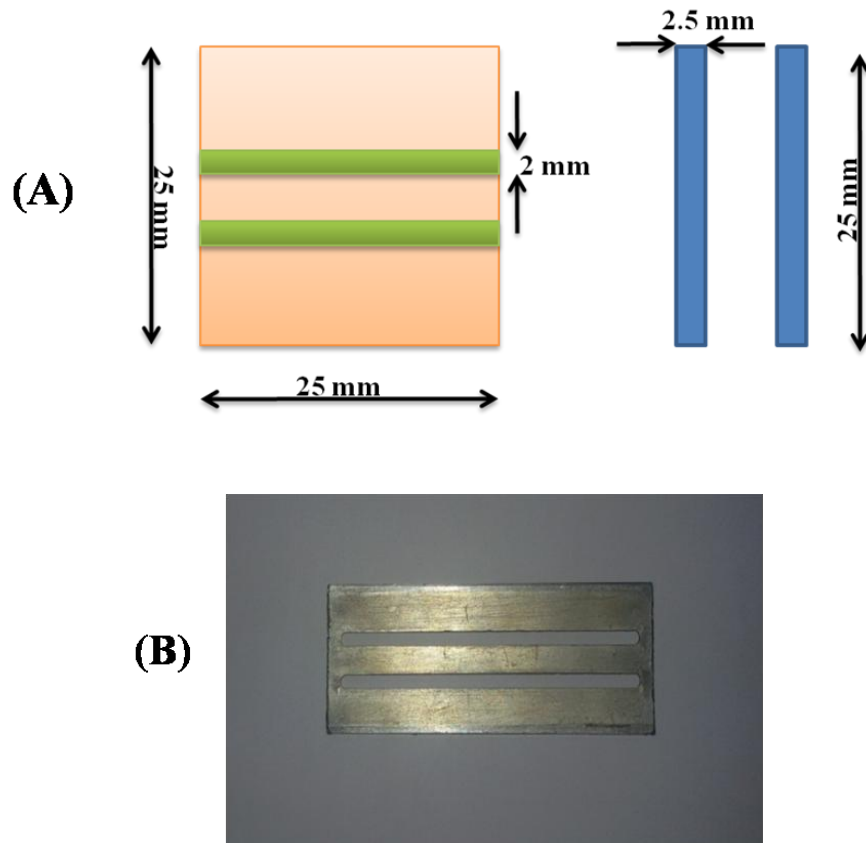
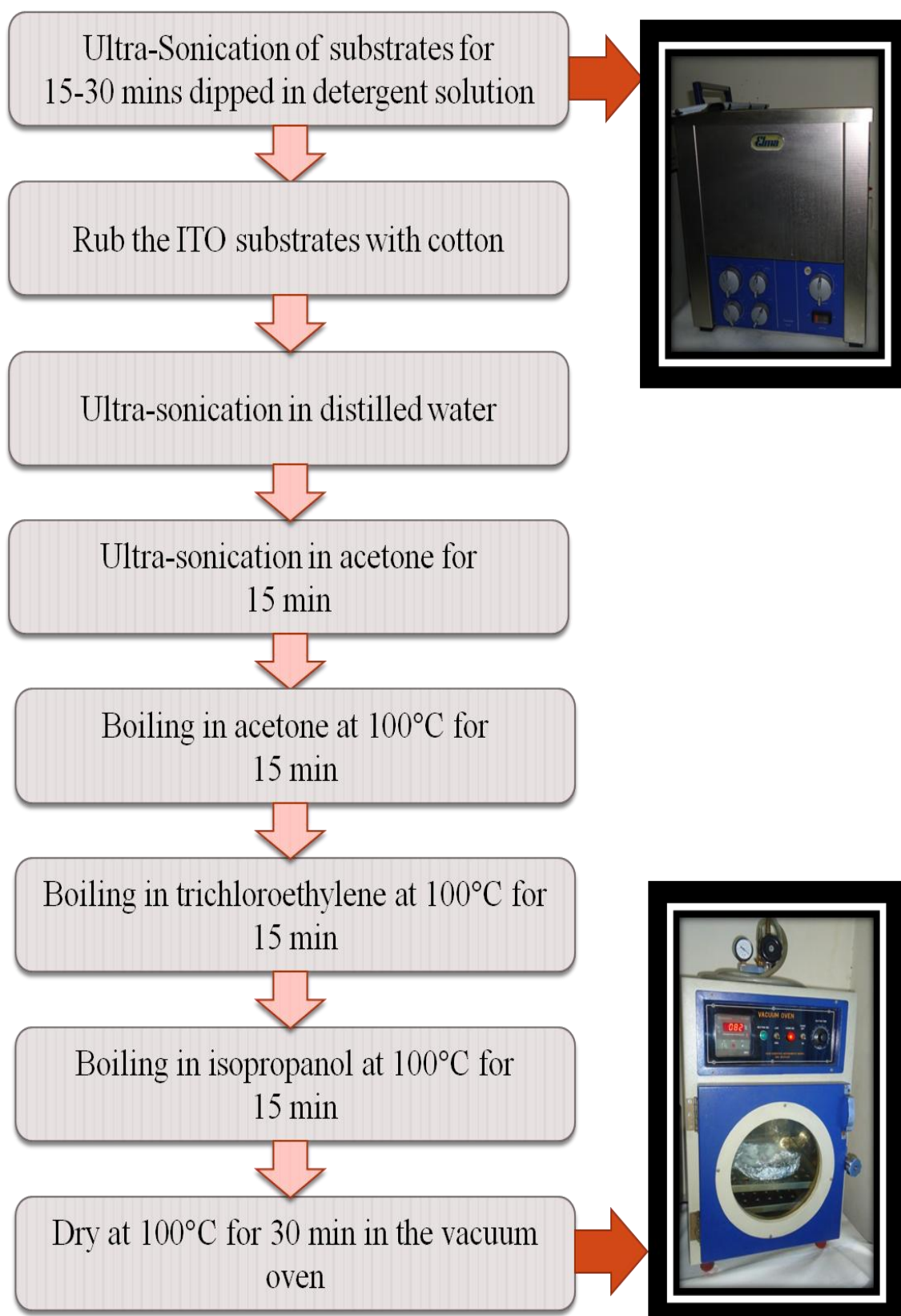


**Figure 2.4** (a) Realization of patterned devices, (b) Shadow-mask used for aluminium evaporation.

#### 2.4.2 Cleaning of patterned ITO glass substrates

Prior to deposition of thin film(s), ITO coated glass substrates with patterned strips should be cleaned appropriately according to the techniques listed in the flow chart as shown in Scheme 2.1.



**Scheme2.1** Flowchart representing the cleaning procedure for cleaning the ITO substrates.

### 2.4.3 UV ozone cleaning of cleaned ITO glass substrates

The ITO coated glass substrates were cleaned using UV ozone cleaning to remove stain on ITO, which cannot be removed by water and organic solvents. These stains are of nanometre size and form organic contaminants which cannot see through eyes. Hence, these substrates should be further cleaned by treating in UV ozone cleaner, which also facilitates to reduce the surface pollution created by solvents. The samples exposed to UV ozone cleaner are shown in Figure 2.5. UV ozone cleaner also leads to the supplementary cleaning of these ITO substrates by removing the nano impurities from surface. Moreover, it also increases the adhesiveness of ITO substrates leading to better bonding between anode (ITO) and HTL. Apart from this, it also enhances the work function of ITO which helps holes and electrons to shift toward respective electrodes as high work function anode and low work function cathode; as in case of conventional structure is the essential obligation for proper running of devices.



**Figure 2.5** Photograph of UV ozone cleaner placed in glove box.

#### 2.4.4 Deposition of hole transport layer (HTL) on ITO coated substrates

In the present work, four different materials as hole transport layer: poly(3,4 ethylenedioxythiophene):poly(styrene sulfonate) (PEDOT:PSS), molybdenum oxide ( $\text{MoO}_x$ ), copper thiocyanate ( $\text{CuSCN}$ ), and copper iodide ( $\text{CuI}$ ) have been used.

PEDOT:PSS is most commonly used as hole transport layer (HTL) in organic solar cells, due to its favourable work function that corresponds to HOMO level of donor polymers, good electrical conductivity, high transparency, and the ability to reduce the surface roughness of ITO that helps to make active layer deposition more uniform. A thin film of PEDOT:PSS (shown below) was spin coated onto pre cleaned and UV ozone treated ITO coated glass substrates at 3000 rpm for 90 second under ambient conditions followed by annealing at  $120^\circ\text{C}$  for 30 min in vacuum oven. The thickness of the layer is about 80 nm that usually depends on the concentration of the solution and rotating speed (rpm) of spin coating unit. The functional solution is typically volatile, and concurrently evaporates. As a result, higher the angular speed of spinning, thinner would be the obtained film.

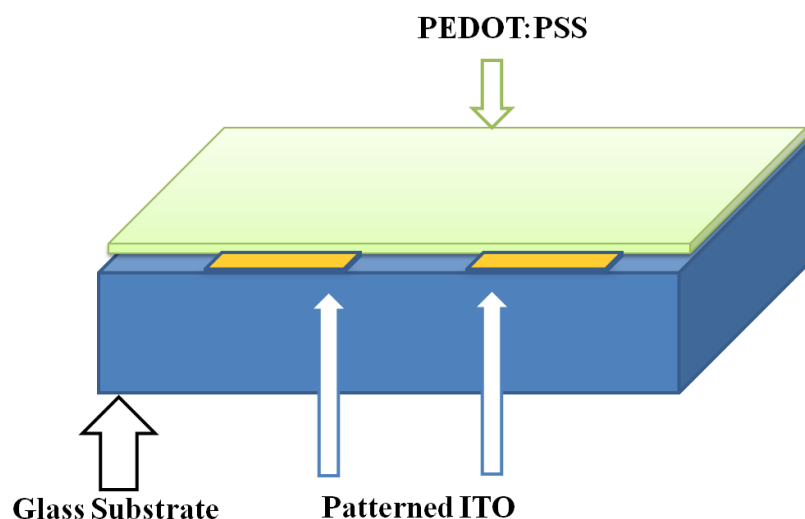


**Figure 2.6** Thin layer of PEDOT:PSS coated on the top of ITO coated glass substrate.

Spin coating unit as shown in diagram of Figure 2.7 is equipment used to deposit uniform thin film(s) of the solution to substrate. A small amount of solution is applied in the centre of the substrate, and then these substrates are rotated to spread the coating solution by centrifugal force. Various parameters such as choice of solvent, concentration of solution, rotating speed and spin time should be optimized in order to attain the controlled deposition of thin film of uniform thickness.

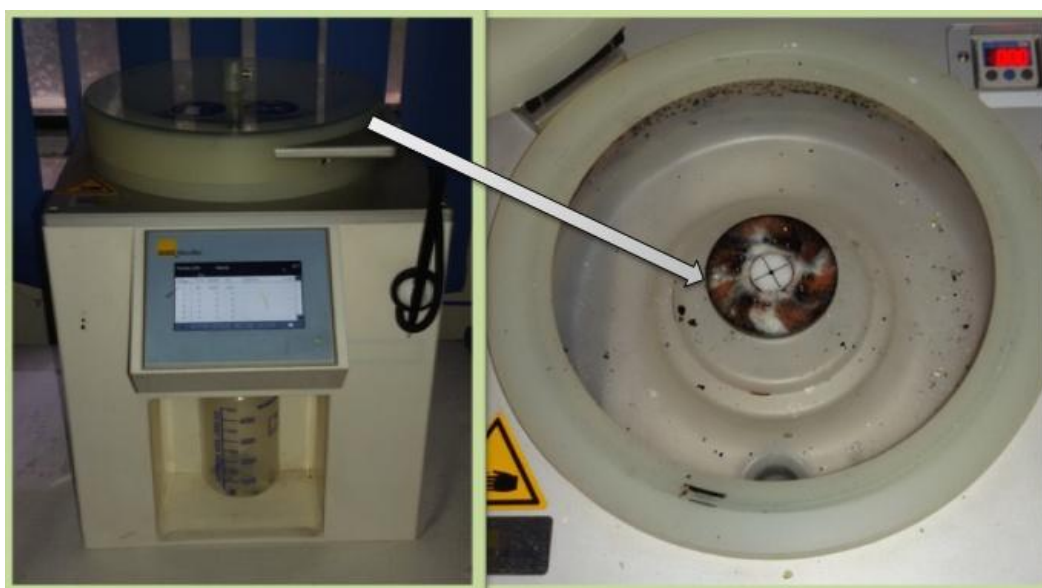


**Figure 2.7** Spin coating unit for deposition of HTL in environment.

Due to presence of hygroscopic, acidic and protonation nature of PSS in PEDOT:PSS, device stability is influenced and results in degradation which limits their possible commercial applications. It is also noted that other PSS based HTL materials like polyaniline influences the device stability as well. To overcome such limitation, molybdenum oxide ( $\text{MoO}_3$ ) as hole transport layer was deposited on the pre-cleaned ITO coated glass substrates through thermal evaporation technique in vacuum coating unit (VCU). VCU is equipment which is used for deposition of thin film on substrate(s) by evaporating the material in high vacuum. The vacuum allows vapour particles of material to move freely towards the substrate, where they



condense back to a solid state. Evaporation and condensation are two basic procedure of the system. The uniformity of thin film by evaporation of source material(s) depends upon the level of vacuum inside the chamber of VCU. In high vacuum, evaporated particles can move directly to the substrates without colliding with the background gas molecules. On the other hand, if evaporation is performed in poor vacuum, the consequential deposition is generally non-uniform and tends not to be continuous throughout the entire surface of substrates as the evaporated material move to substrate mostly from a single direction, protruding features block the evaporated material from some areas.



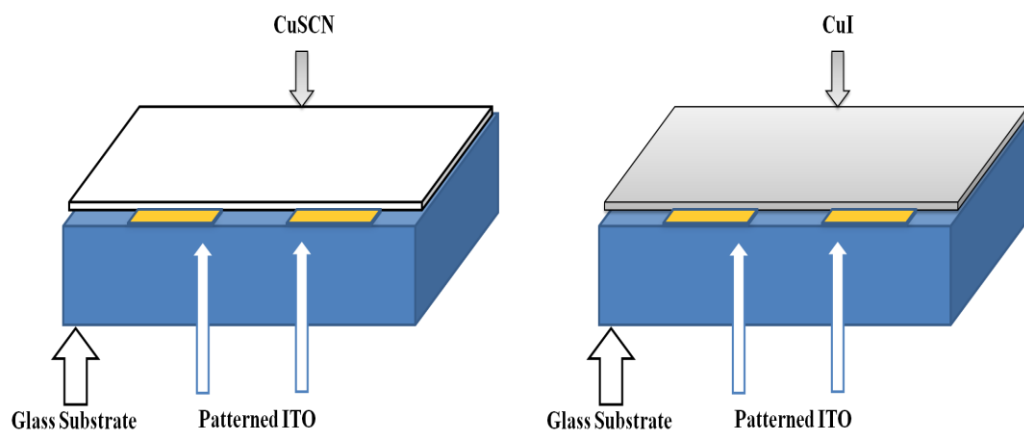
**Figure 2.8** Boat containing  $\text{MoO}_3$  fixed between two electrodes in a thermal evaporating system.

Copper thiocyanate (CuSCN) is effectively used as hole transport layer due to high optical transparency and *p*-type conductivity. First of all, CuSCN powder was dissolved in diisopropylsulfide in 10 mg/mL and mix through ultra sonic bath for 4 hrs. After sonication the mixture was kept for 6 hrs and the resulting clear solution



was used for solution-processable HTL in organic solar cells. A thin film CuSCN solution was deposited by spin coating unit onto the pre-patterned ITO coated glass substrate for device fabrication at 3000 rpm for 60 seconds in ambient conditions. The resulted thin films were annealed (at 90°C for 20 minutes and 120°C for 20 minutes) and then dried at room temperature for 1 hour at ambient conditions. The main drawback related to CuSCN as HTL is nasty and unusual smell of diisopropyl sulfide solvent. In order to overcome this problem, a systematic study was done by using a series of environment friendly and economic solvents: dimethyl sulfoxide (DMSO), *N,N*-dimethylformamide (DMF), acetonitrile (MeCN), propylene carbonate (PC), dioxane and ethylene glycol (EG).

The main limitation related to CuSCN as HTL is the poor solubility which resists the OPV devices for commercial application. Copper(I) iodide (CuI) is also used as an excellent solution processable hole transport layer as it is easily soluble in various solvents and bears good electrical conductivity and optical transparency. First, 10 mg of copper iodide (CuI) was dissolved in 1.0 mL of acetonitrile and the resulting suspension mixture was sonicated for 1 hour at room temperature. After sonication the mixture was kept for 10 minutes and the resulting clear solution was used for solution-processable HTL in organic solar cells. A thin film of CuI layer was deposited by spin coating over ITO coated glass slides at 3500 rpm for 60 seconds. The resulting substrates were annealed at 100°C for 15 minutes followed by drying at room temperature for 1 hour.

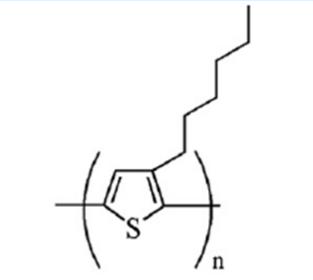
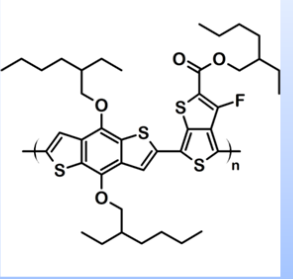
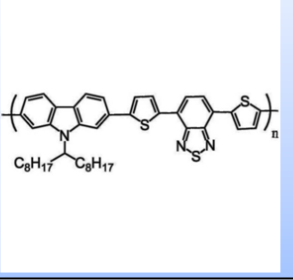
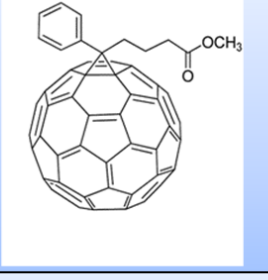
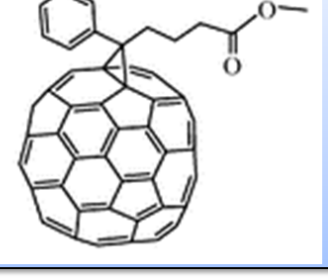


**Figure 2.9** Thin layer of (a) CuSCN, (b) CuI coated on the top of ITO coated glass substrate.

#### 2.4.5 Deposition of active layer thin film over the hole transport layer

The performance of an organic solar cell strongly depends upon active layer and its parameters like thickness and morphology. It is very significant to map the preparation of the blend solution to attain the required performance for device. In this thesis, most of the devices were fabricated using blend solutions of low band gap polymer: PTB7: PC<sub>71</sub>BM and PCDTBT: PC<sub>71</sub>BM. One of the experiments was also done on bulk-heterojunction solution of P3HT:PC<sub>61</sub>BM. All the devices were fabricated with simplest device structure of ITO/HTL/active layer/Al. The chemical structure of all the polymers used in this thesis is shown in Table 2.2.

**Table 2.2** Conjugated polymers and their chemical structure used for fabrication of polymer solar cells.

<b>Conjugated Polymers</b>	<b>Chemical Structure</b>
<b>P3HT</b> (Electron Donor)	
<b>PTB7</b> (Electron Donor)	
<b>PCDTBT</b> (Electron Donor)	
<b>PC<sub>61</sub>BM</b> (Electron Acceptor)	
<b>PC<sub>71</sub>BM</b> (Electron Acceptor)	

The composition ratio of donor and acceptor play a very important role to determine the maximum performance of OPV devices as it strongly influences optical and electrical properties. In case of low band gap solar cells based PTB7:PC<sub>71</sub>BM as active layer: the compositions ratio of PTB7:PC<sub>71</sub>BM is 1:1.5 which was dissolved in a mixture of chlorobenzene and 1,8-diiodoctane(97:3 vol %) in a concentration of 25 mg/mL. Other low band gap solar cells based PCDTBT:PC<sub>71</sub>BM as active layer: the composition ratio of PCDTBT:PC<sub>71</sub>BM is 1:4 that was dissolved in a mixture of chlorobenzene and dichlorobenzene (1:3 ratio) in a concentration of 35 mg/mL. This composition ratio recorded the best performance of OPV devices. The composition ratio of P3HT:PC<sub>61</sub>BM based conventional BHJ solar cell has also been optimized for best possible performance in ambient conditions without protective atmosphere. The composition ratios of P3HT:PC<sub>61</sub>BM materials range from 1.0:0.4 to 1.0:1.2 dissolved in 20 mg/mL of chlorobenzene shows comparatively good performance. Further decrease or increase of P3HT:PC<sub>61</sub>BM ratio resulted in devices showing very bad performance. It was also demonstrated that 1.0:0.8 weight ratio of P3HT:PC<sub>61</sub>BM has achieved relatively best performance.

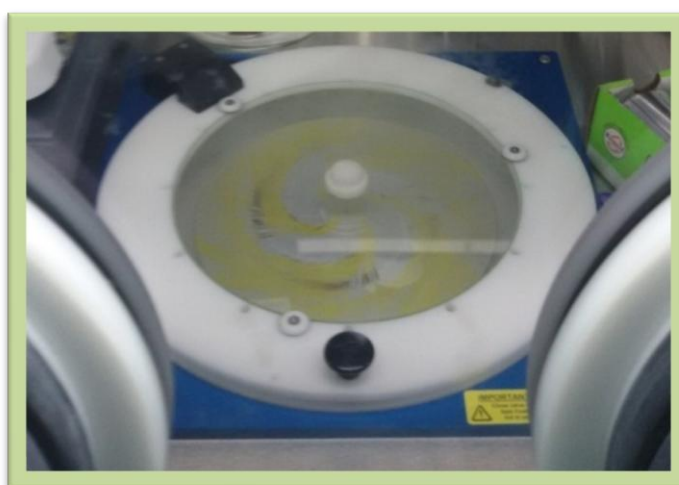


**Figure 2.10** Spin coating unit for deposition of active material(s) in glove box.

The active layer was deposited on top of the HTL by spin coating technique (Figure 2.6) inside a nitrogen glove box with O<sub>2</sub> and H<sub>2</sub>O levels below 0.1 ppm. The spin-coating technique was composed of three steps: first step involve the extension of the solution over the surface of substrate which was accelerated to its final rotating speed. Consequently, during the second step, the substrate was rotated at a constant rate where viscous forces control the thinning behaviour of the active layer. During this step the film is slowly formed which can be observed by the change in colour of the reflected light. In the last step, the active layer is dried during rotation of substrate at a constant lower rate and the solvent evaporation rate dominates the thinning behaviour.

All the active materials used for fabrication of OPV devices are very sensitive to environment. To prevent the degradation of these materials caused by the oxidation in air, the device should be fabricated under inert atmosphere. The glove box is intended to permit manipulation of chemicals sensitive to oxygen and moisture under an inert atmosphere. The glove box is a sealed container working within a very high purity nitrogen or argon gas. The glove-box is fitted with UV ozone cleaner, spin coating unit, hot plate, and other equipments used for ozone cleaning, deposition, annealing and encapsulation of active layer. The glove box is directly and internally connected with a thermal evaporating system for the deposition of small organic molecules and cathode electrodes. The glove box integrated with vacuum coating unit is shown in Figure 2.11

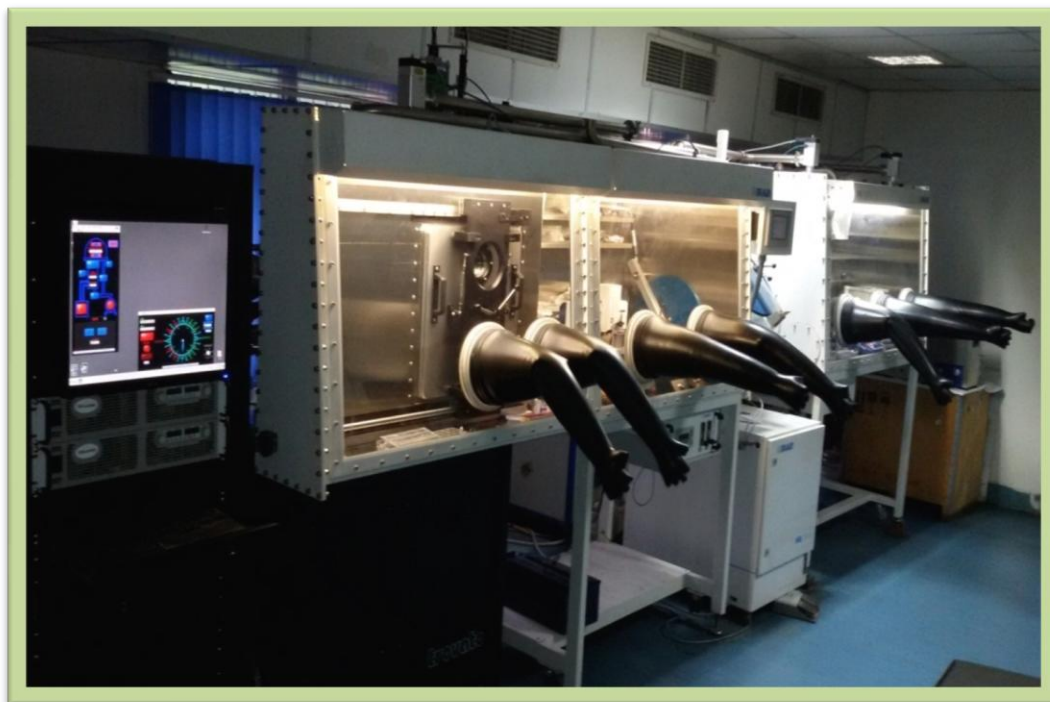


**Figure 2.11** Glove Box (MBRAUN) used for deposition of active material(s).

#### 2.4.6 Deposition of cathode electrode

The top electrode was deposited by thermal evaporation technique at a base pressure of  $10^{-6}$  mbar with a shadow mask as already shown in Figure 2.2. In this thesis, aluminium was used as the top electrode in conventional structure of OPV devices. Au, Mg, Ag, Ca, and their alloys can also be used as cathode due to its low work function. The metal deposition system included evaporation filament as sources situated at the base of the evaporating chamber supported by shutter to load the aluminium beads. In case of Al deposition, filaments are made up of tungsten wire while molybdenum sheets are employed for deposition of silver and gold. The deposition rate can be controlled by the applied electrical power. The metallic chamber used for the deposition of Al electrode is shown in photograph of Figure 2.12. Schematic diagrams of OPV devices fabricated in the thesis are shown in Figure 2.13.

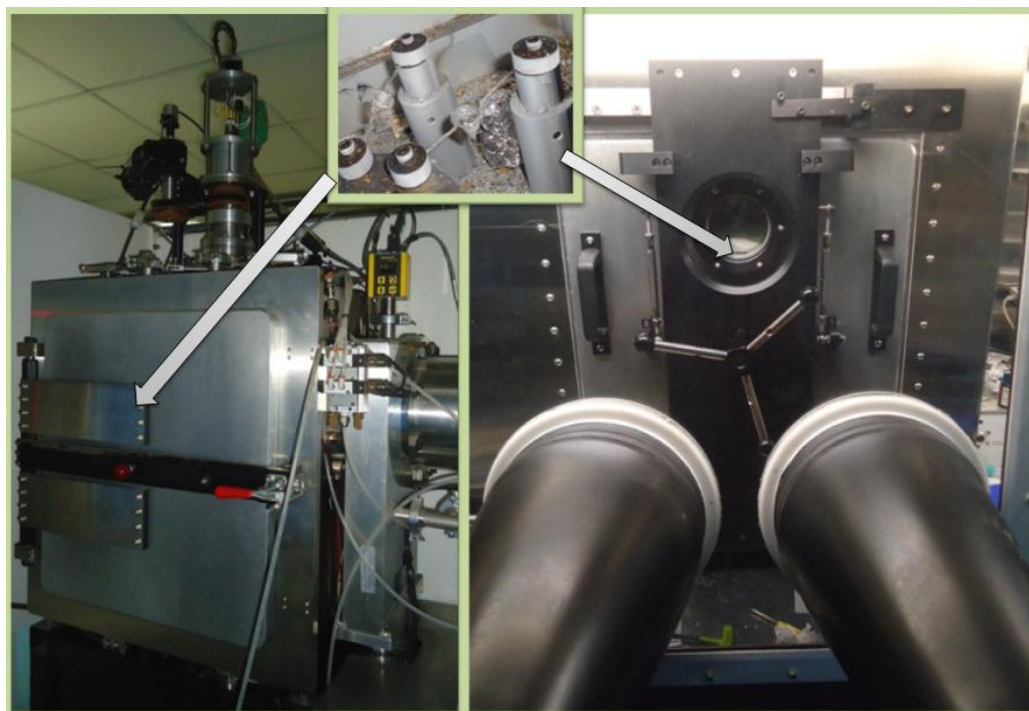


**Figure 2.12** Thermal evaporation systems (back side on LHS and front side on RHS) along with filament used for deposition of metal cathode (Al).

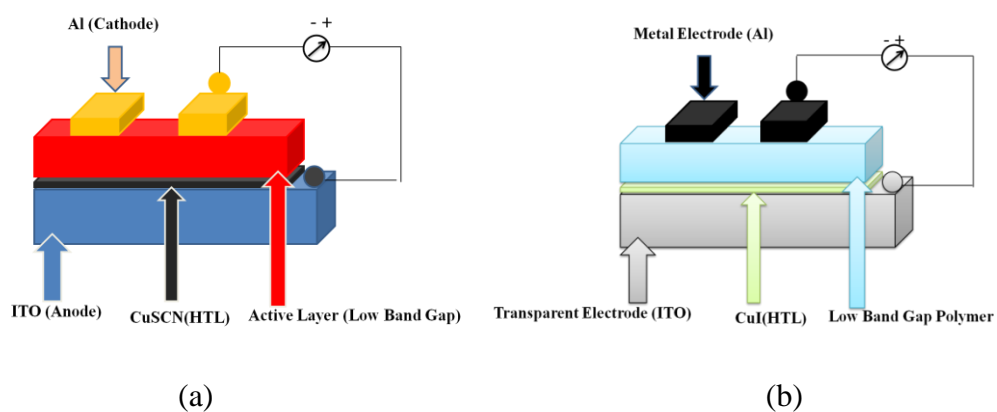


**Figure 2.13** Schematic diagrams of low band gap OPV devices using (a) CuSCN as HTL (b) CuI as HTL.

## 2.5 Measurement of Solar Cell Characteristics in Dark and under Illumination

The J-V characteristics of the all OPV devices were measured with computer-controlled Keithley 2400 source meter under dark and one sun illumination. To measure the current density under illumination, the devices were illuminated from the ITO side using shutter controlled SCIENCETECH solar simulator (as shown in Figure 2.14) with an air mass 1.5 (AM 1.5) and the light intensity  $100 \text{ mW/cm}^2$ . The light intensity was determined by a standard silicon photodiode. Current density can be calculated by dividing the values of current in IV curve by area of pixel. All measurements were performed at room temperature. After obtaining the values of short circuit current density ( $J_{sc}$ ) and open circuit voltage ( $V_{oc}$ ), we can easily calculate the other parameters such as fill factor (FF) and power conversion efficiency ( $\eta$ ) of devices as mentioned in the previous chapter.

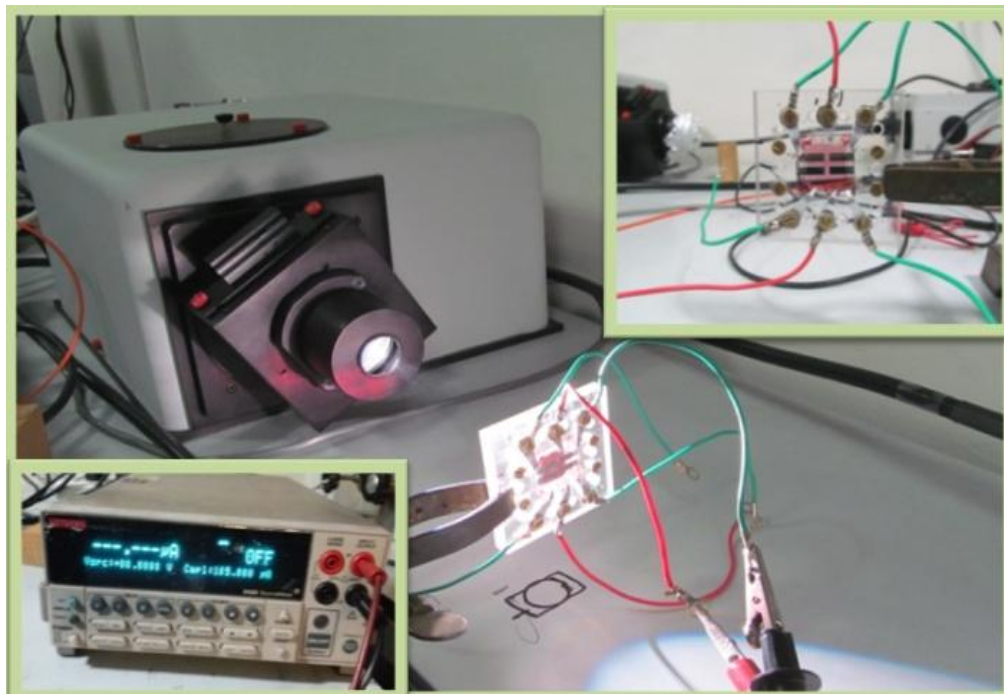


**Figure 2.14** Solar simulator showing the experimental set-up for J-V characteristics of solar cell devices under illumination with Keithley 2400 source meter.



## 2.6 Devices Fabrication

Lot of devices based on low band gap polymers have been fabricated during the entire period of PhD work. The device geometry employed for processing OPV devices are illustrated in Table 2.3.

**Table 2.3** Device configurations used for fabrication of OPV devices in this Thesis.

S. No.	Anode	HTL	Active Layer		Cathode
			Donor	Acceptor	
1	ITO	PEDOT:PSS	P3HT	PC <sub>61</sub> BM	Al
2	ITO	MoO <sub>3</sub>	P3HT	PC <sub>61</sub> BM	Al
3	ITO	PEDOT:PSS	PTB7	PC <sub>71</sub> BM	Al
4	ITO	MoO <sub>3</sub>	PTB7	PC <sub>71</sub> BM	Al
5	ITO	PEDOT:PSS	PCDTBT	PC <sub>71</sub> BM	Al
6	ITO	MoO <sub>3</sub>	PCDTBT	PC <sub>71</sub> BM	Al
7	ITO	CuSCN	P3HT	PC <sub>61</sub> BM	Al
8	ITO	CuSCN	PTB7	PC <sub>71</sub> BM	Al
9	ITO	CuSCN	PCDTBT	PC <sub>71</sub> BM	Al
10	ITO	CuI	PTB7	PC <sub>71</sub> BM	Al
11	ITO	CuI	PCDTBT	PC <sub>71</sub> BM	Al

- In S. No. 1, a study based on different weight ratios of P3HT: PC<sub>61</sub>BM has been investigated to obtain the best efficiency from the available material(s)
- In S. No. 2-6, the devices were fabricated to compare the performance of low band gap polymer solar cells with well established hole transport layer like PEDOT:PSS and MoO<sub>3</sub> with new introduce HTLs.
- In S. No. 7-9, copper thiocyanate (CuSCN) as an effective solution processable HTL has been investigated for low band gap polymer solar cells. Parallel with this, so many experiments have been also performed to explore the application of CuSCN with environment friendly and economic solvent(s) as a solution processable HTL.
- In S. No. 10-11, same type of study has been done on copper iodide (CuI) as solution processable HTL for fabrication of OPV devices based in low band gap polymer solar cells with different solvents.

## 2.7 Characterization Equipments

### 2.7.1 Atomic force microscope (AFM)

To optimize the surface thin film at nanoscale level, AFM has been proved as one of the powerful tools due to its higher resolution and magnification. The precursor for AFM was invented by Gerd Binnig and Heinrich Rohrer in 1980 at IBM Research -Zurich, and got the Nobel Prize for Physics in 1986. G. Binnig, C. F. Quate, and C. Gerber invented the first atomic force microscope in 1986 (1). The first commercially available AFM was introduced in 1989. A 10×10 mm specimen is used for AFM measurements in the tapping mode. During AFM measurement the cantilever (the AFM tip) scans the surface and records the topology in 2D as well as 3D topology information with a colour code for the height scale. To study the magnetic and electric response of surface AFM is found to be useful. The cantilever is typically made up of

either silicon or silicon nitride material having a tip radius of curvature in nanometres scale. Scratched film is used to measure the thickness and afterwards the step height which is the difference between the averaged heights was measured at one edge of the scratch.

During the process when the tip is brought into the contact of a sample surface, forces between the tip and the sample results into a deflection of the cantilever as per Hooke's law (2). AFM modes of operation can be classified into contact mode, non contact mode and tapping mode depending on the purpose of specimen.

In contact mode, the cantilever remains in contact with the surface during scanning. When it encounters variations in the surface it responds by deflecting to follow the contours. In Non-contact mode, there is no direct contact between the tip and surface and the tip remains a few nanometre above the surface of the material vibrating at a little higher frequency little higher than the resonance frequency of tip (3). This result into very small vibrations. In the tapping mode, the cantilever arm resonates at a frequency as it scans the surface. When the tip comes in contact with the surface, a sensor reverses the motion of the cantilever to continue the oscillation. If scanning is processed at a constant height of tip then there is chance of damaging the tip due to non uniformity of film on substrate as the tip can collides with the surface and break. Therefore, generally a feedback mechanism is employed to regulate the tip-to-sample distance to maintain a constant force between the tip and the sample.

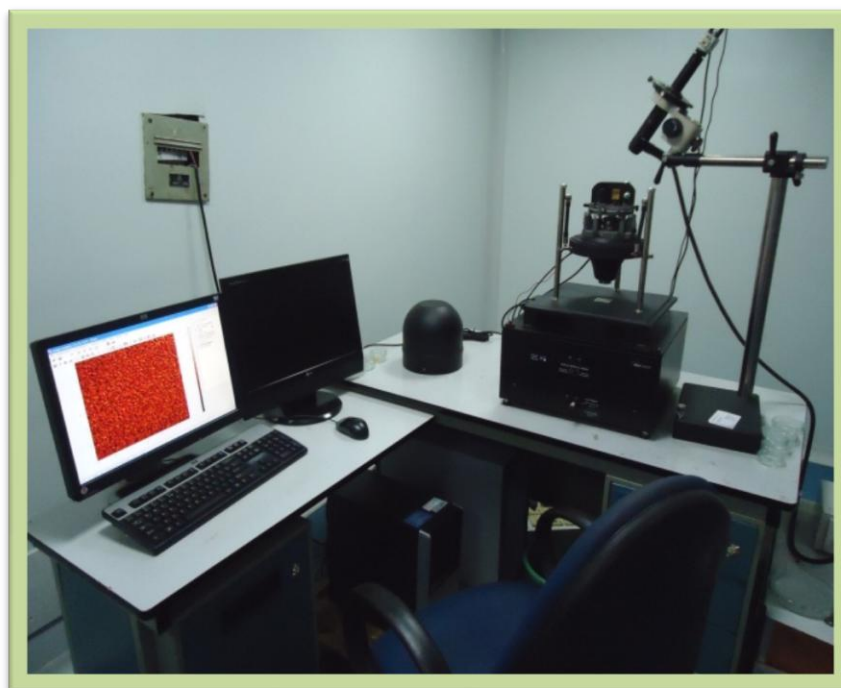


**Figure 2.15** AFM setup

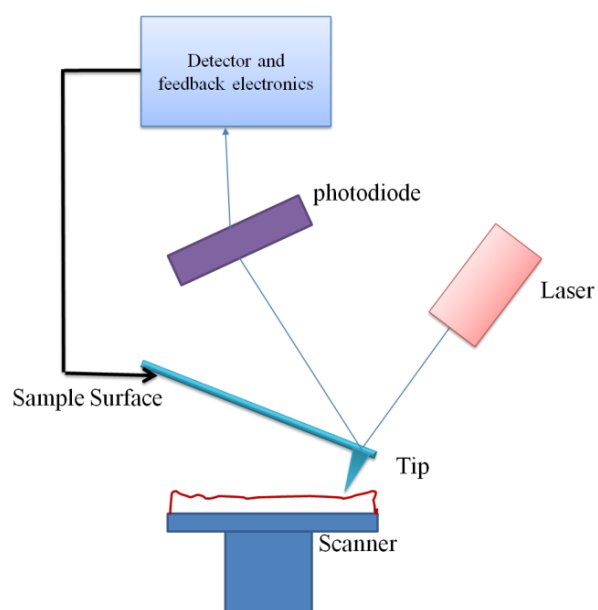


**Figure 2.16** Block diagram of atomic force microscope.

### 2.7.2 X-ray Diffraction (XRD)

X-ray diffraction is non-destructive measurement which is used to determine the structure, crystallinity (amorphous or crystalline nature) and identification of materials (4, 5). Figure 2.17 depicts the pictorial representation of X-ray diffractometer. Due to the characteristic peaks of crystalline material X-ray powder diffraction can be used as a "fingerprints" to characterize these materials. In this method, monochromatic beam of X-rays is focused onto crystalline materials which interact with the structural planes of the lattice and construct a diffraction pattern as per the lattice point of each plane. Constructive interference of reflected X-rays from lattice plane can be expressed by Bragg's law (6).

$$n\lambda = 2d \sin\theta \quad \dots\dots\dots(1)$$

Where,  $n$  is an integer (1, 2, 3),  $\lambda$  is the wavelength of a beam of X-rays incident on a crystal with lattice planes,  $d$  is inter planer spacing, and  $\theta$  the angle between the incident ray and the scattering planes. According to law, for a given set of parallel planes the diffraction will give maxima only in that direction for which the angle will satisfy the Bragg's law.

The X-rays, generated via a cathode ray tube are filtered to turn out monochromatic radiation, collimated and directed towards the sample. X-ray interact mostly with electrons in atoms, collide and some photons from the incident beam are deflected away from original. The X-rays interfere constructively and destructively producing a diffraction pattern on the detector.



**Figure 2.17** XRD setup

### 2.7.3 UV-Vis absorption spectroscopy

The UV-Vis spectroscopy is an effective technique for the determination of size and optical properties of nanosized materials. This spectrometer gives the spectrum between absorbance (A) versus wavelength ( $\lambda$ ). This spectrum corresponds to degree of absorption at each wavelength. In this spectroscopy the electrons get excited from valence band to conduction band by the absorption of appropriate amount of energy. To determine the nature of charge transition across the optical band gap, variation of optical coefficient with wavelength is calculated. Tauc's expression is used to relate between the absorption and band gap energy as shown in equation (2) (7-9).

$$(\alpha h\nu) = A (h\nu - E_g)^n \quad \dots\dots\dots(2)$$

Where ' $\alpha$ ' is the absorption coefficient of the nano materials, A is a constant related to the effective masses associated with the bands,  $E_g$  is the band gap energy,  $h\nu$  is the energy of photon and n is the transition.

The block diagram of the computer controlled UV-VIS-NIR model spectrophotometer is shown in Figure 2.18. The samples measurements were carried out using Varian 500 Scan UV-VIS-NIR spectrophotometer for various measurements like absorbance, transmittance, specular and diffuse reflectance measurements. All absorbance spectrophotometers must contain the light source, wavelength selection device, sample holder and photon detector. This type of spectrophotometer features a continuous change in wavelength and an automatic comparison of light intensities of samples and reference material; the ratio of the latter is the transmittance/reflectance of the sample, which is plotted as a function of wavelength. The automatic operation eliminates many time consuming adjustments and provides a rapid spectrogram.



**Figure 2.18** UV-vis absorption spectroscopy

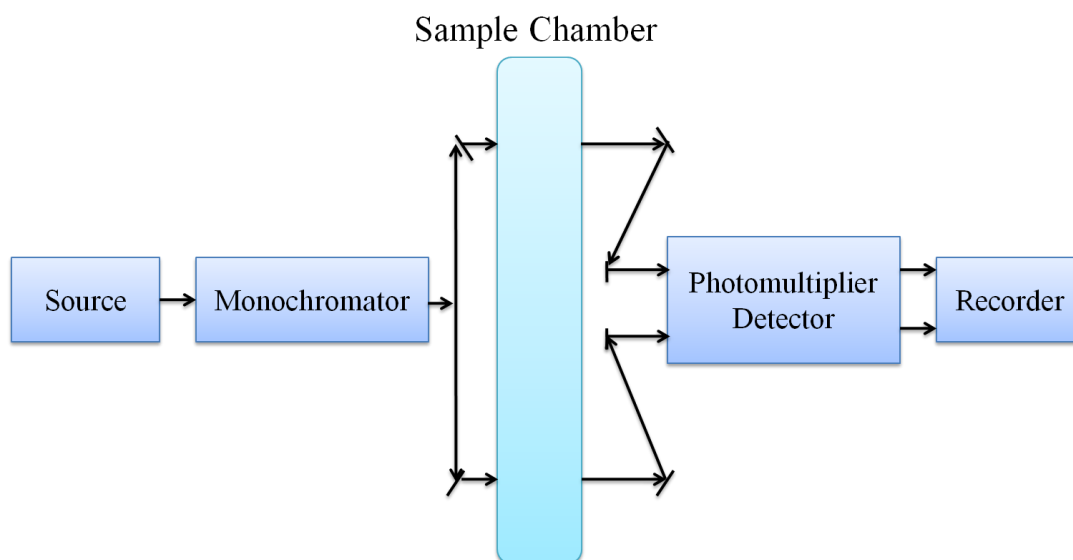


**Figure 2.19** Block diagram of UV-vis absorption spectroscopy.

#### 2.7.4 Transmission electron microscope (TEM)

Transmission electron microscope (TEM) is used for characterization of nano particles owing to its high resolution and chemical microanalysis (10). This instrument provides information regarding direct identification of the chemistry of even single nanocrystal along with the atomic resolution images and chemical information at a spatial resolution of 1nm or better (11-13).

TEM is based on the principle of amplitude or scattering contrast of the electron beam owing to the fact that the electron beam is scattered by crystalline material. It is composed of two modes of images which are bright field and dark field images. Simultaneous examination of micro structural features having high resolution along with the acquisition of chemical and crystallographic information from small region of the specimen are some of the characteristic features of this spectroscopy.

TEM consist of four major parts: electron source, aberration corrected lens, sample holder and imaging system as illustrated in Figure 2.20. Electromagnetic lenses and the metal apertures are used to focus the electron beam coming from the source. The



system allows the electrons to pass through in a small energy range, so the electrons in the electron beam will have a well defined energy. This beam interacts with the sample contained in sample holder and transmitted beam replicates the patterns on the sample. This transmitted beam is projected onto a phosphor screen. In the present work, TEM images were recorded by Tecnai G2 F30 STWIN transmission electron microscope at an accelerating voltage of 300 kV, magnification upto 1000 kX, specimen heating holder upto 1000 °C, TEM point resolution 0.205 nm, TEM line resolution 0.144 nm and EDAX Resolution 136 eV. To obtain the images, particles were dissolved in ethanol followed by ultrasonication for 30 minutes. A drop of solution was coated onto the copper grid and TEM images were obtained.

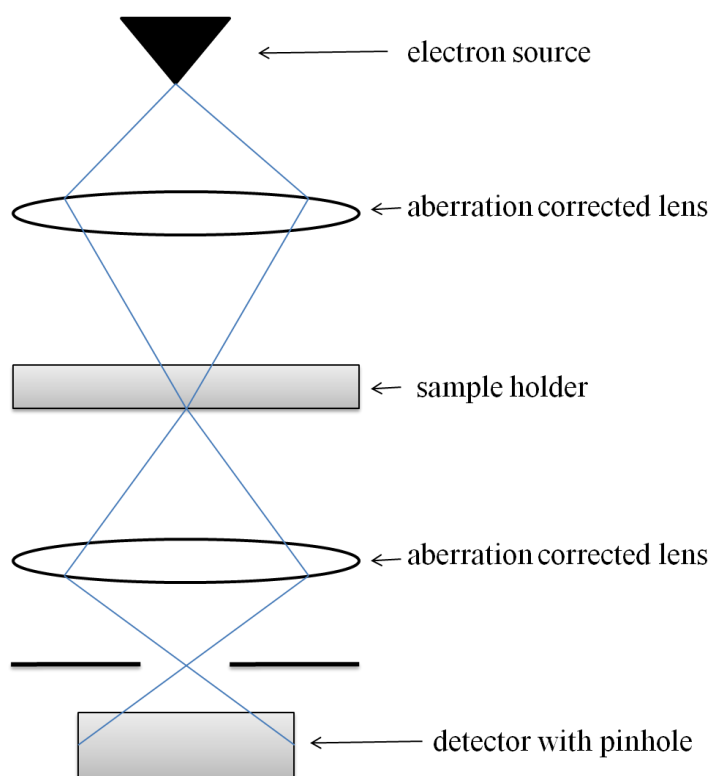


**Figure 2.20** Schematic diagram of the conventional TEM.

### 2.7.5 Scanning electron microscopy (SEM)

Scanning electron microscopy is a powerful technique which produces images via scanning with a focused beam of electrons on a specimen. The electrons of the beam interact with the electrons in the specimen resulting into the various signals. Detector detects these signals containing information of surface topography and composition of the specimen. The electron beam follows a rectangular pattern during scanning, and the beam's position is combined with the detected signal to create an image (14). SEM can achieve resolution less than 1 nm. Samples can be observed in both high and low vacuum and have advantage of resolution less than 1 nm. SEM is able to produce characteristic three-dimensional images and is useful for judging the surface structure of the sample (13, 15).

The SEM is an instrument that produces a largely magnified image by using electrons instead of light to form an image. A schematic diagram of the SEM is illustrated in Figure 2.21. Electron gun which is at the top of microscope is used to produce the electron beam. This beam follows a vertical path through the microscope held within vacuum. The beam travels through electromagnetic fields and lenses, which focus the beam down toward the sample. Once the beam hits the sample, electrons and X-rays are evicted from the sample. Detectors collect these X-rays, back scattered electrons and secondary electrons and convert them into a signal that is sent to screen which produces the final image. In this research work, the samples have been prepared by spin coating of solution on 10×10 mm glass slide. SEM images were recorded by EVO MA 10VPSEM modal with resolution 3 nm SEI MODE @30kV, 5 nm BSE MODE, magnification 7X to 10,00,000X and ac voltage 200V-30kV.

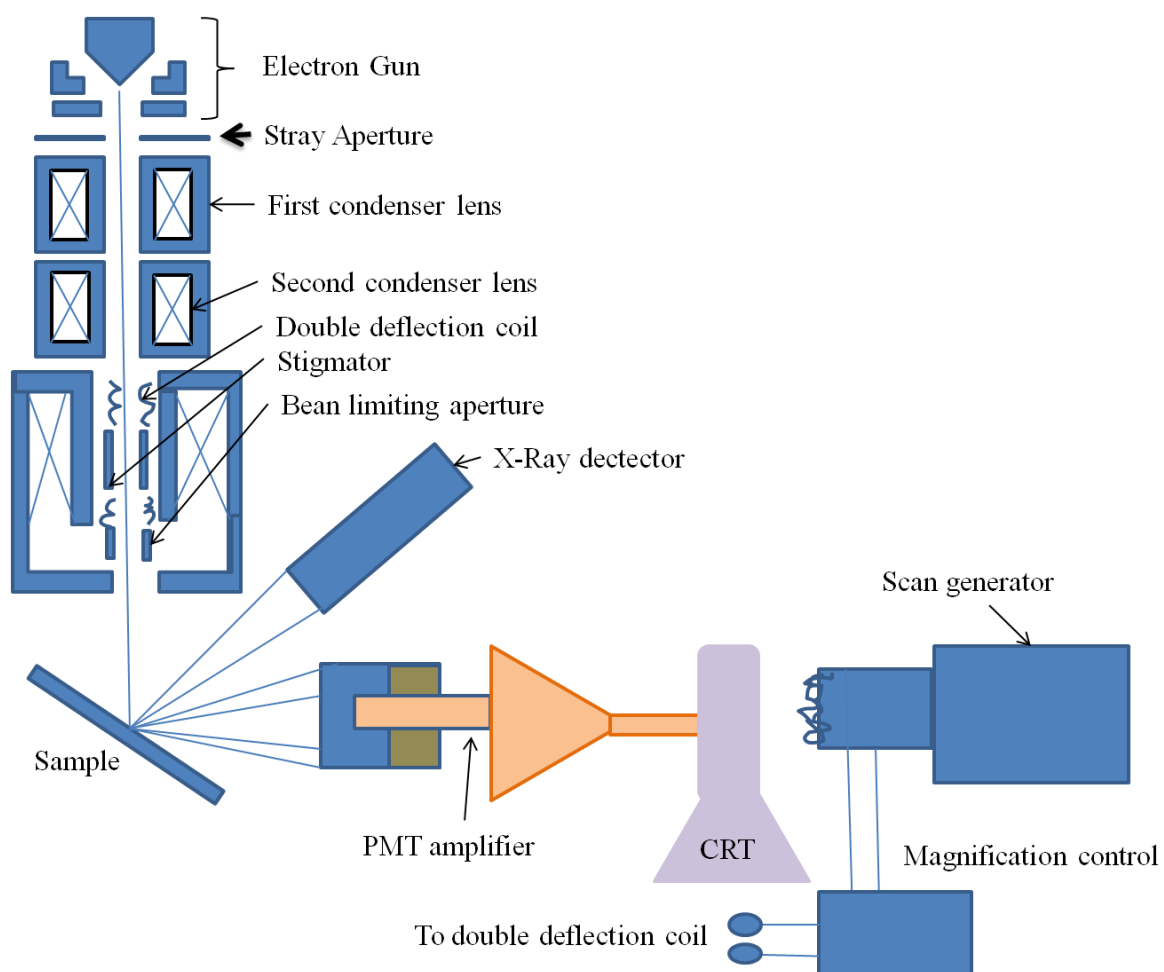


**Figure 2.21** Schematic diagram of SEM.

**References:**

1. G. Binnig, C. F. Quate, and C. Gerber, *Physical Review Letters*, 56 (1986) 930.
2. B. Cappella, and G. Dietler, *Surface Science Reports*, 34 (1999) 1.
3. P. J. Bryant, R. G. Miller, R. Yang, *Applied Physics Letters*, 52 (1988) 2233.
4. C. Kittel (8<sup>th</sup> Ed.), *Introduction to Solid State Physics*, John Wiley & Sons, 2005.
5. B.D. Cullity (Ed.), *Elements of X-Ray Diffraction*, Addison-Wesley Publishing Company, 1956.
6. H. P. Myers (Eds.), *Introductory Solid State Physics*, Taylor & Francis, 2002.
7. K. P. Acharya, Ph.D. Thesis, Bowling Green State University, 2009.
8. B. S. Rao, B. R. Kumar, V. R. Reddy, T. S. Rao, and G. V. Chalapath, *Chalcogenide Letters*, 8 (2011) 39.
9. A. B. El-Bially, R. Seoudi, W. Eisa, A. A. Shabaka, S. I. Soliman, R. K. A. El-Hamid, and R. A. Ramadan, *Journal of Applied Sciences Research*, 8 (2012) 676.
10. J. Z. Zhang, Z-L. Wang, J. Liu, S. Chen, and G-Y. Liu (Eds.), *Self-Assembled Nanostructures*, 2003.
11. Z. L. Wang (Ed.), *Characterization of Nanophase Materials*, 2000.
12. Z. L. Wang, *Advanced Materials*, 15 (2003) 1497.
13. G. B. Sergeev (Ed.), *Nanochemistry*, Elsevier, 2006.
14. D. McMullan, *Scanning*, 17 (1995) 175.
15. C. W. Oatley, *Journal of Applied Physics*, 53 (2016) R1.



# ***Chapter:3***

**Efficient Low Band Gap Polymer Solar Cells using Copper (I) Thiocyanate (CuSCN) as Solution Processable Hole Transport Layer**

---

**3.1 Introduction**

Power conversion efficiency (PCE) with adequate stability in polymeric solar cells is the most crucial challenge for their possible commercial applications at large scale. Conventional bulk heterojunction (BHJ) solar cells has been fabricated from a blend of active layer of a conjugated material (donor material) and a fullerene derivative (acceptor material) sandwiched between hole transport layer (HTL) on an indium tin oxide (ITO) positive electrode and electron transport layer (ETL) on a low-work-function metal negative electrode. Various methodologies have been developed for realizing this goal, among them active layer optimization and engineering are most studied (1, 2). While with great to effort on active layer very little is known about HTL, which can be the electrical contacts between active layers, and electrodes, and leads to enhance charge transport and collection. Thus HTL in photovoltaic device plays a pivotal role for device stability, power conversion efficiency (PCE); influence the work function of the electrode and properties of active layer. It's also mentioned here that with respect to thousands of active materials (i.e. donor and acceptor materials) reported in literature (3-5), the types of organic HTL materials are limited to poly(3,4-ethylenedioxythiophene)-poly(styrenesulfonate) (PEDOT:PSS), polyaniline:poly (styrene sulfonate), graphene-based materials, carbon nanotubes (CNTs) etc (6).

Water soluble PEDOT:PSS is the most widely used HTL in organic solar cells, while several investigations have been demonstrated that due to presence of

hygroscopic, acidic and protonation nature of PSS in PEDOT:PSS, it's influences the device stability and degradation which limits their possible commercial applications (7, 8). It is also noted that other PSS based HTL materials like polyaniline based has influences the device stability (9, 10). Small molecules (11), graphene-based materials (12, 13) and CNTs are also used as HTL for organic solar cells, while the PCE of these devices are poor compared to PEDOT:PSS used as an HTL. Alternatively transition metal oxides, like nickel oxide (NiO), molybdenum oxide ( $\text{MoO}_x$ ), vanadium oxide ( $\text{V}_2\text{O}_5$ ) and tungsten oxide ( $\text{WO}_3$ ) etc have been widely used as an efficient HTL as replacements of PEDOT:PSS in organic solar cells (14-20). It is also noted that for some transition metal oxides, thermally deposited HTL is required for better photovoltaic performance. For example thermal deposition of  $\text{MoO}_x$  has been reported an excellent HTL in organic solar cells and shows very promising performances compared to PEDOT:PSS as an HTL (14).

Copper (I) thiocyanate ( $\text{CuSCN}$ ) (21-25) is successfully used as HTL that exhibits both high optical transparency and *p*-type conductivity (26). Most importantly,  $\text{CuSCN}$  is working excellent from solution using right solvents and concentration at room temperature (27), thus making it a suitable solution-processable HTL for cost effective, large area and flexible plastic substrate applications.  $\text{CuSCN}$  was reported as an efficient HTL for dye synthesized solar cells (27) and hybrid perovskite solar cells (28). Recently, electrodeposited  $\text{CuSCN}$  as an efficient HTL for BHJ solar cells (29) and perovskite solar cells (30) have been appeared. Poor solubility of  $\text{CuSCN}$  limits its application as a solution-processable HTL for solar cells applications. So far diisopropyl sulfide and diethyl sulfide two useful solvents have been reported for  $\text{CuSCN}$  at proper concentration to reach the minimum thickness required for HTL in solar cell applications.

Best of our knowledge, very recently, only two studies have been demonstrated for CuSCN as a solution-processable and transparent HTL in BHJ solar cells using different combinations of donor and acceptor materials (31, 32). Yaacobi-Gross et al. first demonstrated solution-processable CuSCN as HTL material for high efficiency organic solar cells using bilayer Sm/Al (10/90 nm) cathode for device fabrication (31). CuSCN as an solution-processable HTL was not studied for most used active materials of poly(3-hexylthiophene) and phenyl-C<sub>61</sub>-butyric acid methyl ester (P3HT:PC<sub>61</sub>BM) (33), poly[N-9'-heptadecanyl-2,7-carbazole-alt-5,5-(4',7'-di-2-thienyl-2',1',3'-benzothiadiazole)] (PCDTBT) (34) and poly[[4,8-bis[(2-ethylhexyl)oxy]benzo[1,2-b:4,5-b']dithiophene-2,6-diyl][3-fluoro-2-[(2-ethylhexyl)carbonyl]thieno[3,4-b]thiophenediyl]] (PTB7) (35,36) blend with phenyl-C<sub>71</sub>-butyric acid methyl ester (PC<sub>71</sub>BM).

Here we report CuSCN as an efficient and solution-processable HTL in conventional BHJ solar cells. Three different combinations of active layers of P3HT:PC<sub>61</sub>BM, PCDTBT:PC<sub>71</sub>BM and PTB7:PC<sub>71</sub>BM were used for photovoltaic device fabrication with simplest device structure of ITO/CuSCN/active layer/Al. Details investigation of the effect of annealing temperature of HTL on photovoltaic performances were studied. In this present work, the resulted HTLs were characterized by UV-vis-NIR spectroscopy, scanning electron microscope (SEM), atomic force microscope (AFM) and transmission electron microscope (TEM) for better understanding to achieve the highest possible efficiency.

## 3.2 Results and discussion

### 3.2.1 Photovoltaic properties

Inspired by many potential importance of CuSCN as a solution-processable HTL over PEDOT:PSS and other transition metal oxides, we decided to explore the



solution-processable CuSCN as an HTL in organic solar cells in general. To examine the CuSCN films as HTL in photovoltaic devices, BHJ solar cells were fabricated using simplest device geometry of ITO/CuSCN/active layer/Al as presented in Figure 3.1. It is well-known that P3HT:PC<sub>61</sub>BM, PCDTBT:PC<sub>71</sub>BM and PTB7:PC<sub>71</sub>BM are the most studied and successful used donor: acceptor combinations in organic solar cell based on PEDOT:PSS and other transition metal oxide as HTL. We have examined the efficiency of this donor: acceptor combinations using solution-processable CuSCN as HTL in order to make more universal applications. The chemical structures and band diagram of the materials used are presented in Figures 3.2 and 3.3 respectively.

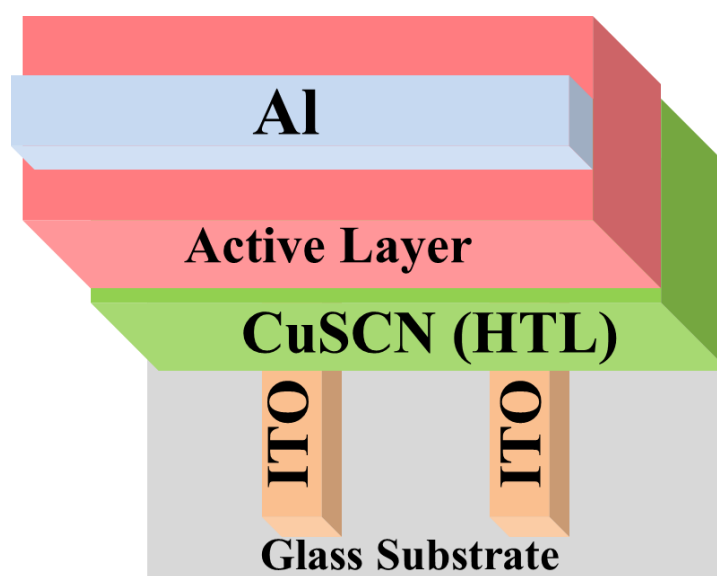


**Figure 3.1** Schematic of the conventional BHJ solar cell in which the HTL is sandwiched between an ITO cathode and active layer.

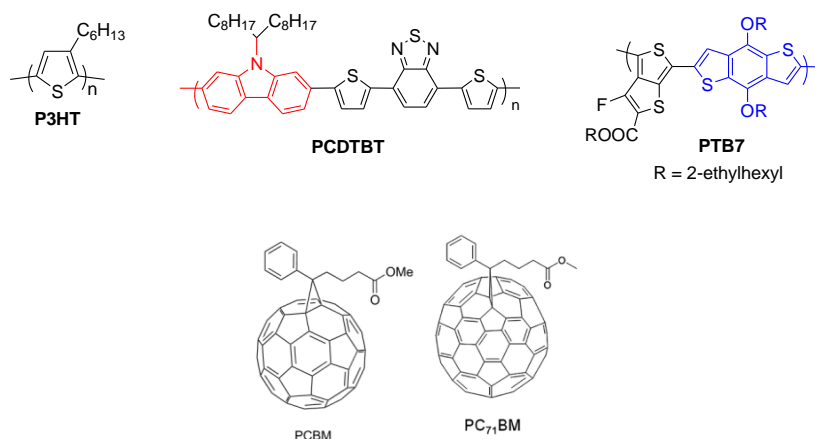


**Figure 3.2** Chemical structures of P3HT, PCDTBT, PTB7, PC<sub>61</sub>BM and PC<sub>71</sub>BM.

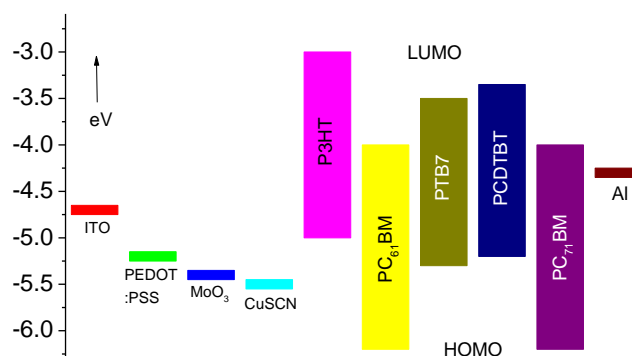


**Figure 3.3** Electronic energy levels of the materials used in organic solar cells.

Blend of P3HT and PC<sub>61</sub>BM active materials are the most studied donor and acceptor materials respectively in organic solar cells. To examine the performance of the active layer using CuSCN as an HTL for fabrication of OPV devices with the geometry of ITO/CuSCN/P3HT:PC<sub>61</sub>BM/Al, CuSCN in diisopropyl sulfide was spin-coated onto pre-patterned ITO electrode on a glass substrate for device fabrication. The thickness of the HTL was varied by using different concentration of the solution and rpm during spin casting followed by annealing. Then the P3HT:PC<sub>61</sub>BM (1.0:0.8 wt %) active layer from a solvent of chlorobenzene was deposited and finally device was completed by deposition of 120 nm aluminium layer at a pressure of  $5 \times 10^{-6}$  mbar.

We have observed that these devices show poor performance. This may be due to the compatibility issue between the HTL and active layer namely interfacial energy alignment occur from the significant difference between the work function of CuSCN (-5.35 eV) and HOMO level of P3HT (-4.90 eV), but further studies will be needed to confirm this proposal.

To demonstrate solution-processable CuSCN as a potential member of HTL for low band gap donor polymers, BHJ solar cells were fabricated with well studied PCDTBT as a donor polymer with PC<sub>71</sub>BM as an acceptor material using a simple device structure of ITO/CuSCN/PCDTBT:PC<sub>71</sub>BM/Al. All the devices were fabricated and characterized under identical condition in ambient condition and photovoltaic results under AM 1.5 G illumination with 100 mW/cm<sup>2</sup> are summarized in Table 3.1. The CuSCN as an HTL layer was deposited from a solution of diisopropyl sulfide solution and the thickness of the layer is about 30 nm. The resulted HTL was thermally annealed by heating at 90°C for 20 minutes. Then the active material PCDTBT:PC<sub>71</sub>BM (1.0:4.0 wt%) was deposited on the annealed HTL followed by further annealing and deposition of 120 nm aluminium layer at a pressure of 5x10<sup>-6</sup> mbar. We have found that the resulted device shows PCE of 4.22% with open circuit voltage ( $V_{oc}$ ), short-circuit current ( $J_{sc}$ ) and fill factor (FF) are 0.77 V, 14.89 mA/cm<sup>2</sup> and 37.39% respectively as shown in Figure 3.5. We have noted that thermal annealing of HTL has influence on device performances namely FF. Under identical condition, when the HTL was thermally annealed by heating at 120°C for 20 minutes, significant improvement of PCE up to 5.94% has been achieved with  $V_{oc}$ ,  $J_{sc}$  and FF are 0.76 V, 15.15 mA/cm<sup>2</sup> and 51.52% respectively (Figure 3.5 and Table 3.1, entry 2). This improvement of PCE is due to significant increase of FF with slightly improve of  $J_{sc}$ , while no noticeable change of  $V_{oc}$  has been observed. Thus annealed

of HTL at 120°C for 20 minutes may have improved the mobility, morphology and nano scaled phase separation for better contact which causes enhancement of the PCE (37). Both the corresponding dark curves are shown in Figure 3.4.

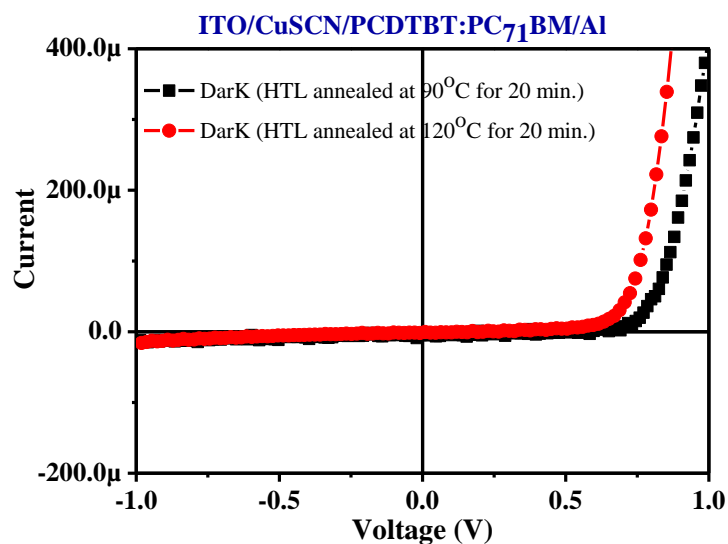


**Figure 3.4** Dark curves for OPV devices for ITO/CuSCN/PCDTBT:PC<sub>71</sub>BM/Al geometry.

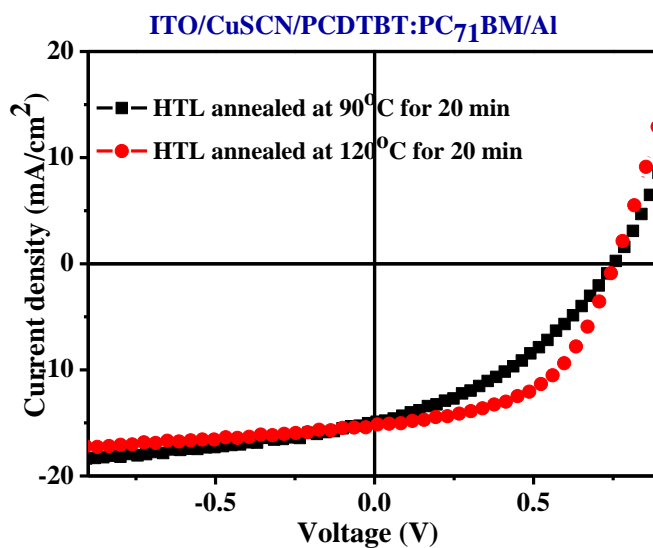


**Figure 3.5** J-V curves for OPV device performance for ITO/CuSCN/PCDTBT:PC<sub>71</sub>BM/Al geometry. (black line) HTL was annealed at 90°C for 20 minutes; (red line) HTL was annealed at 120°C for 20 minutes.

For comparison purpose, photovoltaic devices have been fabricated using  $\text{MoO}_3$  by thermal deposition as a HTL with the geometry of  $\text{ITO}/\text{MoO}_3$  (10 nm)/PCDTBT:PC<sub>71</sub>BM/Al and PCE 5.25% with  $J_{sc}$ ,  $V_{oc}$  and FF are 10.8  $\text{mA}/\text{cm}^2$ , 0.89V and 54.9% respectively under similar condition. We have found that in case the device made from  $\text{MoO}_3$  as HTL shows under performance compared to CuSCN as an HTL by solution-processable (Figure 3.6). This is due to the lower values of  $J_{sc}$  and  $V_{oc}$ , while no noticeable change of FF has been found.

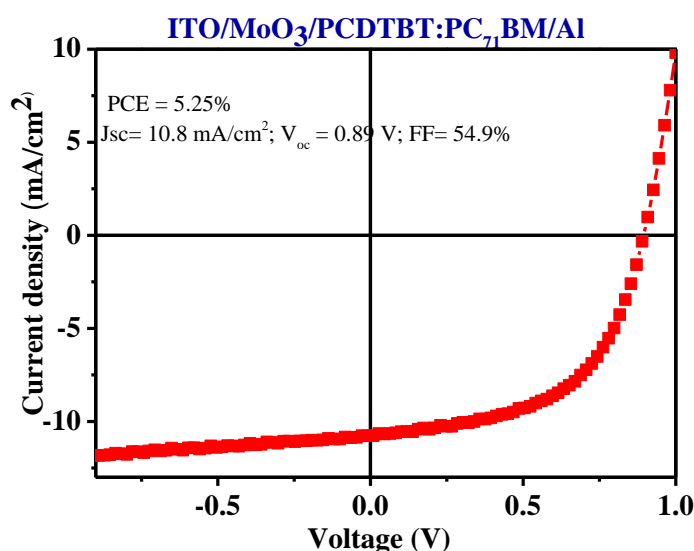


**Figure 3.6** *J-V curves for OPV device performance for  $\text{ITO}/\text{MoO}_3/\text{PCDTBT:PC}_{71}\text{BM}/\text{Al}$  geometry.*

For other comparison purpose, photovoltaic devices have been fabricated using PEDOT:PSS by solution-processed as a HTL with the geometry of  $\text{ITO}/\text{PEDOT:PSS}/\text{PCDTBT:PC}_{71}\text{BM}/\text{Al}$  and achieve PCE 3.22% with  $J_{sc}$ ,  $V_{oc}$  and FF are 10.29  $\text{mA}/\text{cm}^2$ , 0.82V and 38.28% respectively under similar condition which show significantly lower performance as shown in figure 3.7. This results clearly demonstrated that solution-processable CuSCN is even better HTL compared to both

thermal deposited  $\text{MoO}_3$  and solution-processed PEDOT:PSS respectively for photovoltaic applications.

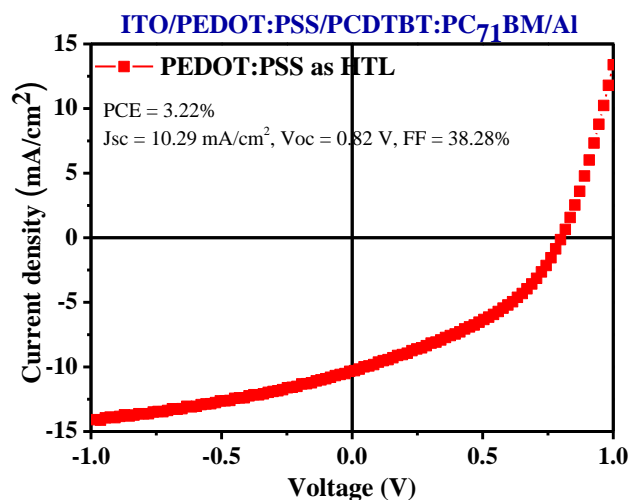


**Figure 3.7** J-V curves for OPV device for ITO/PEDOT:PSS/PCDTBT:PC<sub>71</sub>BM/Al geometry.

In order to further examine the CuSCN as an efficient HTL for low band polymer, we have considered the most successful used PTB7 as a donor material blended with PC<sub>71</sub>BM as an acceptor. CuSCN as an HTL was deposited from diisopropyl sulfide solution on ITO coated glass. The obtained HTL was annealed by heating 90°C for 20 minutes. Then the active layer and metal cathode were deposited successively to complete the photovoltaic device with structure of ITO/CuSCN/active layer/Al. The resulted device exhibits PCE of 3.71% with V<sub>oc</sub>, J<sub>sc</sub> and FF are 0.74 V, 16.25 mA/cm<sup>2</sup> and 30.77% respectively (Figure 3.9 and Table 3.1, entry 3). When HTL was annealed at 120°C for 20 minutes significant improvement of PCE up to 4.60% has been achieved (Figure 3.9, Table 3.1, entry 4) as previously found for PCDTBT:PC<sub>71</sub>BM active layer. FF is lower due to the little S-shape of the J-V curve originated from surface recombination and blocking contacts caused by interfacial layers.

PTB7 is lower band gap polymer compared to PCDTBT and earlier studies demonstrated that devices made with PCDTBT polymer are more stable than PTB7. Since the devices measurement and transfer under ambient condition and during this process the device made with PTB7 is slightly oxide. As a results device made with PTB7 show lower FF. Alternately, may be originated from the interfacial energy alignment that is the HOMO level of PTB7 (-5.15 eV) is 0.2 eV higher lying compared to energy level of CuSCN (work function  $\sim$ -5.35 eV), where as HOMO level of PCDTBT is 0.15 eV lower lying ( $\sim$ -5.5 eV) which are influence the ohmic contact and charge collection. The corresponding dark curves and light are presented in Figure 3.8 and 3.9.

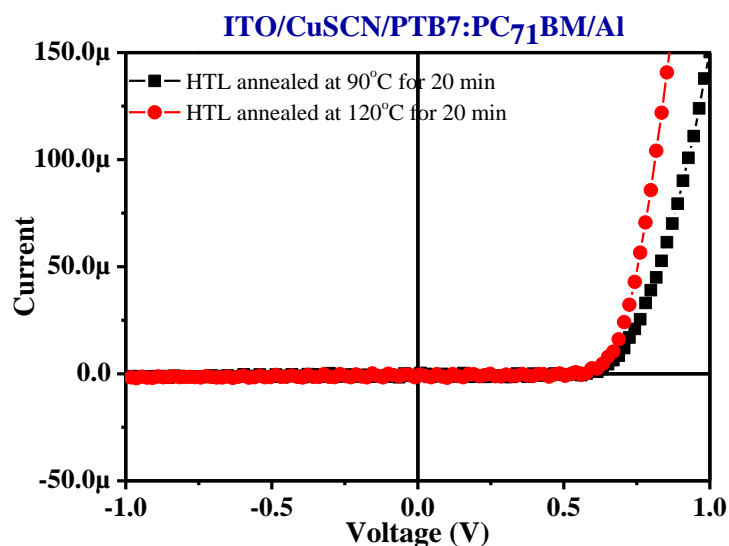


**Figure 3.8** Dark curves for OPV devices for ITO/CuSCN/PTB7:PC<sub>71</sub>BM/Al geometry.

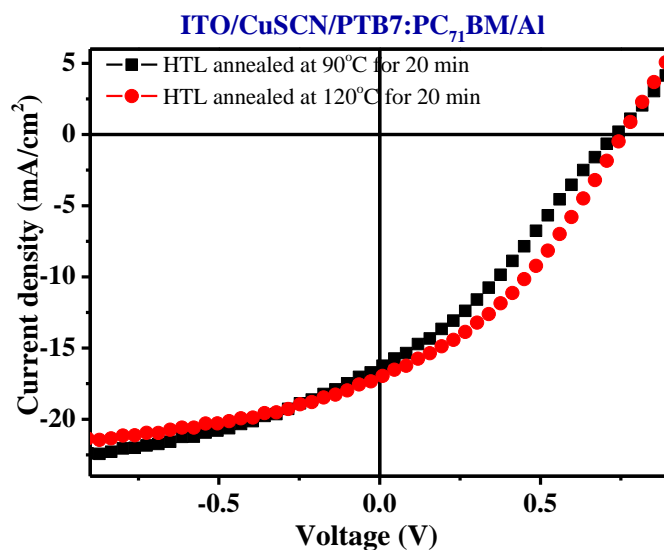


**Figure 3.9** J-V curves for OPV device performance for ITO/CuSCN/PTB7:PC<sub>71</sub>BM/Al geometry. (black line) HTL was annealed at 90°C for 20 minutes; (red line) HTL was annealed at 120°C for 20 minutes.

**Table 3.1** Solar cells parameters of the devices from the solution-processable HTL of CuSCN and donor materials with PC<sub>71</sub>BM of active area 6.0 mm<sup>2</sup>.

Entry	Annealed condition for HTL	Donor materials	J <sub>sc</sub> mA/cm <sup>2</sup>	V <sub>oc</sub> (V)	FF (%)	PCE (%) <sup>a</sup>
1	90°C for 20 min.	PCDTBT	14.89	0.76	37.39	4.22 (4.07)
2	120°C for 20 min.	PCDTBT	15.15	0.76	51.52	5.94 (5.65)
3	90°C for 20 min.	PTB7	16.25	0.74	30.77	3.71 (3.62)
4	120°C for 20 min.	PTB7	16.93	0.76	35.58	4.60 (4.42)

<sup>a</sup>In parenthesis average PCE of 4 devices



### 3.2.2. Absorption and transmission of HTL

Optical absorption of CuSCN thin film on quartz substrate were measured to investigate the absorption across the range of solar spectrum (Figure 3.10). Due to wide optical band gap (2.3) of CuSCN film shows partially nothing absorption in the range 500-1110 nm, while shows absorption in VU region ( $<500$  nm). It is noted that PEDOT:PSS films exhibit significant absorption in the vis-NIR region due to presence of polarons and bipolarons, which are generated by oxidative doping. Thus it is clear that CuSCN layer shows significant lower parasitic absorption which makes it as an efficient HTL in solar cells for further improvement of PCE. The absorption and transmission spectra are hump at around 350 nm (Figures 3.10 and 3.11 respectively) may be due to excitation of electrons from sub bands in the valence band to the conduction band. We note that earlier studies of optical properties on CuSCN were report similar behavior.

In order to understand the improvement of PCE of the devices behind the annealing of HTL, experiments were undertaken to measure the effect of temperature on the optical properties of the HTL. Absorption and transmission measurements of the as prepared CuSCN thin film and annealed CuSCN thin films (at  $90^{\circ}\text{C}$  for 20 minutes and  $120^{\circ}\text{C}$  for 20 minutes) are presented in Figures 3.10 and 3.11 respectively. Remarkably, we do not observed any significant difference in absorption and transmission spectra of the CuSCN film after annealed. This indicates that the enhancement may be originated from morphological improvement of the HTL due to anneal at higher temperature (38, 39). This may be originated from the higher boiling point of diisopropyl sulfide ( $120^{\circ}\text{C}$ ) used for deposition of CuSCN as an HTL.

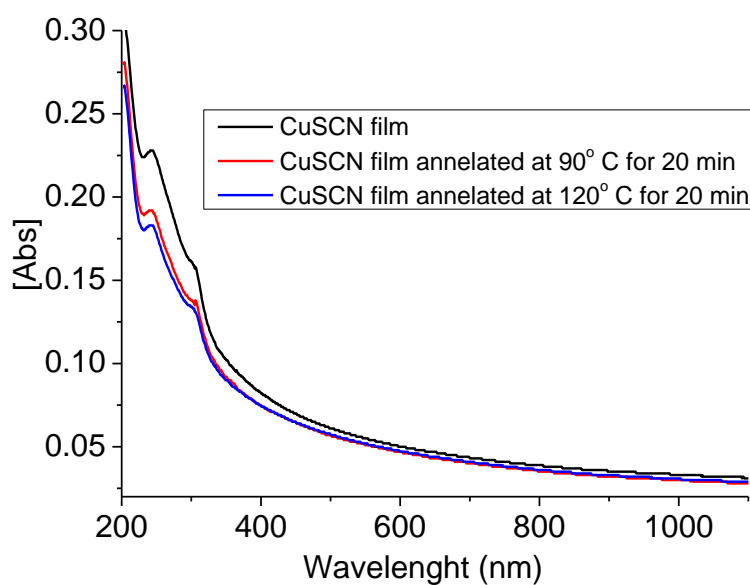


**Figure 3.10** UV-vis-NIR absorption spectra of CuSCN thin films on quartz substrate. (black) as prepared, (red) annealed at 90°C for 20 min and (blue) annealed at 120°C for 20 min.

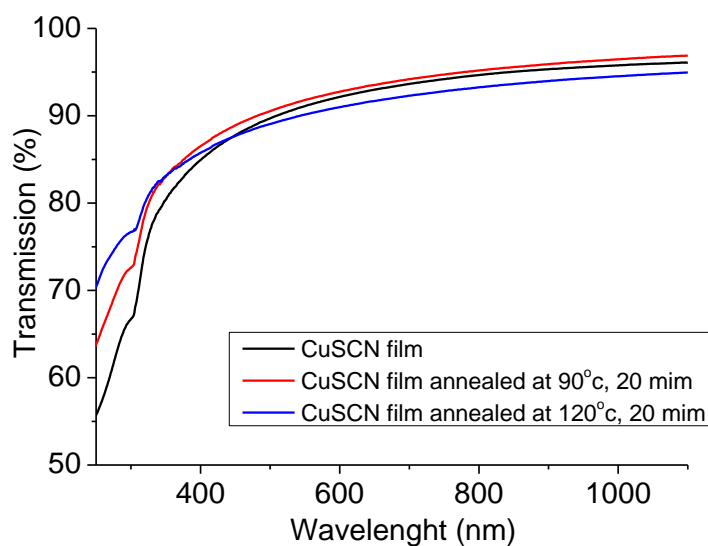


**Figure 3.11** Transmission spectra of CuSCN thin films on quartz substrate. (black) as prepared, (red) annealed at 90°C for 20 min and (blue) annealed at 120°C for 20 min.

### 3.2.3 Morphological studies

In order to understand the better photovoltaic performance behind the annealing temperature, the SEM images of CuSCN films were shown in Figure 3.12. The films were prepared by spin coated on a glass substrate followed by annealing at 90°C for 20 minutes and 120°C for 20 minutes respectively. We have found that both the films have smooth surface rather than rough surface like flattened which may be facilitated good contact between HTL and active layer. SEM images of the HTL from thermal deposition of MoO<sub>3</sub> and solution processed PEDOT:PSS were also illustrated in Figure 3.13. To understand the films morphology at even better scale, AFM studies in air was performed on CuSCN film. The annealed CuSCN film was relatively smooth; with a root mean square (RMS) roughness and average roughness are 1.82 nm and 1.12 nm respectively (Figure 3.14). It is also mentioned here that PEDOT:PSS film shows smoother morphology, while CuSCN films appear as a nano crystalline surface. The spin-coated CuSCN film has been studied by TEM. The TEM image of the CuSCN film indicates the presence of nonowires type structure reveals the mounds to be nanocrystalline as shown in Figure 3.15.

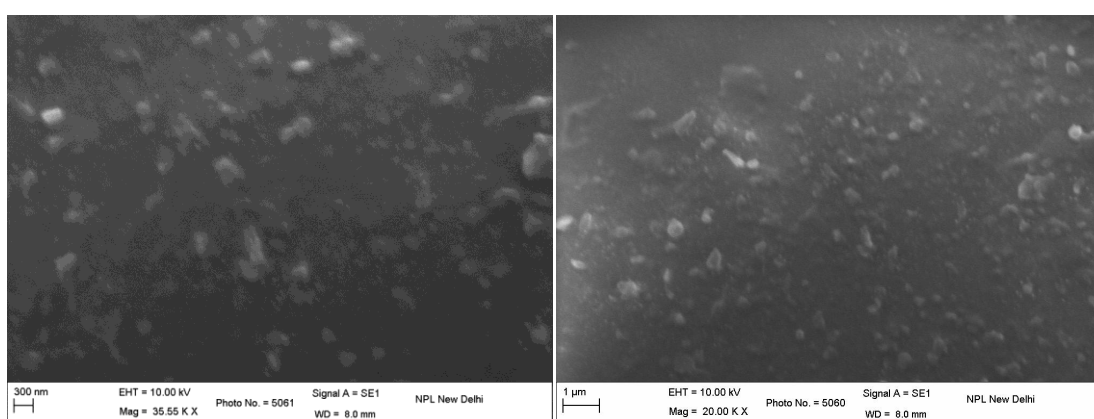


**Figure 3.12** SEM image of CuSCN film annealed at (left) 90°C for 20 minutes and (right) 120°C for 20 minutes on ITO.

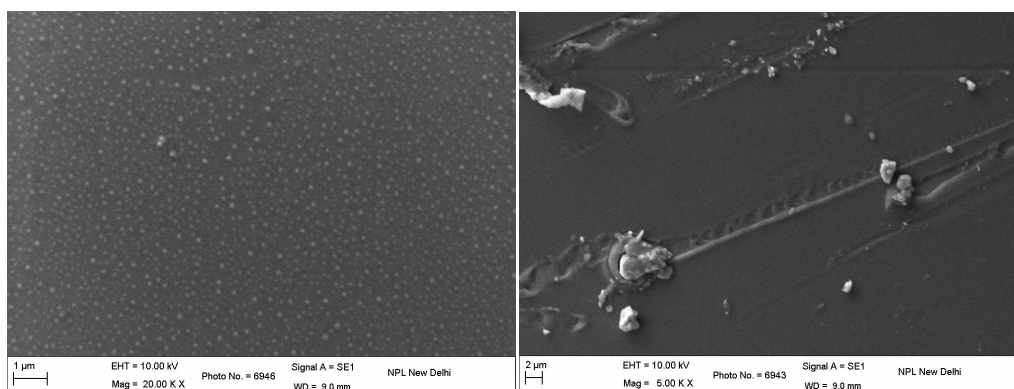


**Figure 3.13** SEM image of (left)  $\text{MoO}_3$  film and (right) PEDOT:PSS on ITO.

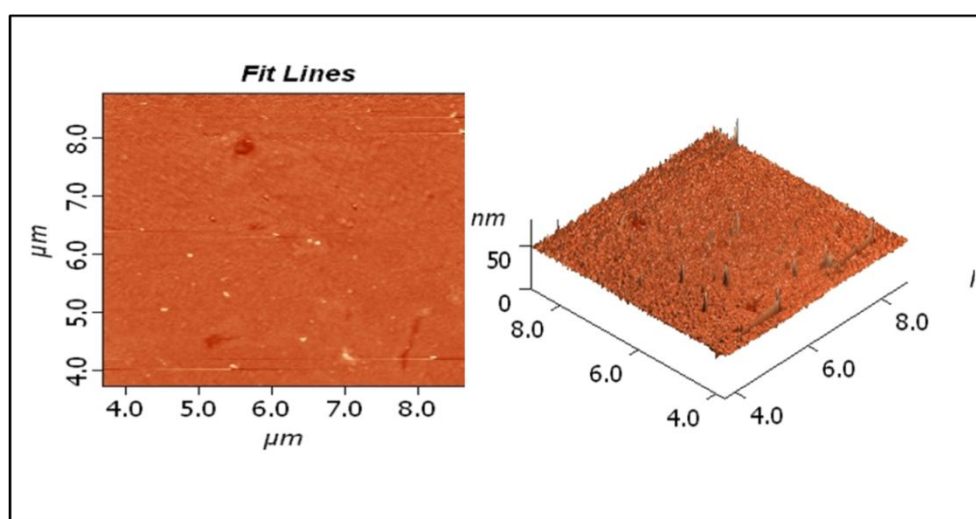


**Figure 3.14** AFM surface images of a spin coated of CuSCN film on glass after annealed at  $120^\circ\text{C}$  for 20 minutes, (left) 2D image and (right) 3D image.

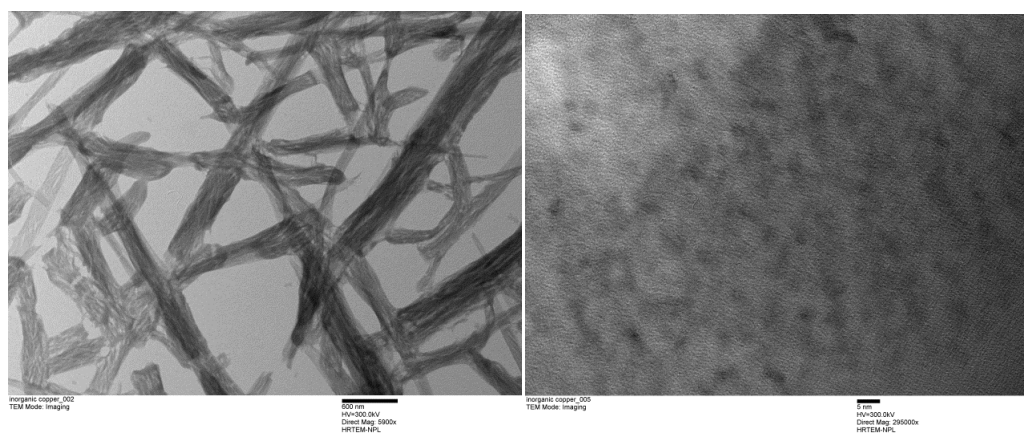


**Figure 3.15** TEM images of the CuSCN film (left, scale bar 600 nm and right scale bar 5 nm).

### 3.3 Experimental

#### 3.3.1 Materials

All chemicals and materials were purchased from sigma-aldrich and Alfa Aesar and used without further purification unless otherwise stated. P3HT ( $M_n \sim 54,000$  and  $PDI < 2.5$ ) and were purchased from sigma-aldrich. PCDTBT, PTB7, PC<sub>61</sub>BM and PC<sub>71</sub>BM were purchased from 1-material, Canada.

#### 3.3.2 Preparation of CuSCN Hole Transport Layer (HTL)

10 mg of copper (I) thiocyanate (CuSCN) was dissolved in 1 mL of diisopropyl sulfide and the resulting suspension mixture was sonicated for 4 hrs at room temperature. After sonicated the mixture was kept for 1 hr at room temperature and the insoluble portion was settle down. The clear solution was used for solution-processable HTL in organic solar cells.

#### 3.3.3 Preparation of MoO<sub>3</sub> Hole Transport Layer (HTL)

10 nm Thickness HTL of MoO<sub>3</sub> was deposited by thermal evaporation at a pressure of  $5 \times 10^{-6}$  mbar.

#### 3.3.4 Preparation of Active Materials

- ✓ P3HT:PC<sub>61</sub>BM:P3HT and PC<sub>61</sub>BM were dissolved in chlorobenzene in the weight ratios from 1:0.8 and the concentration of the solution mixture of P3HT and PC<sub>61</sub>BM was 30 mg/mL in total.
- ✓ PCDTBT:PC<sub>71</sub>BM: The composition ratio of PCDTBT:PC<sub>71</sub>BM is 1:4 that dissolved in a mixture of chlorobenzene and dichlorobenzene (1:3 ratio) in a concentration of 35 mg/mL.
- ✓ PTB7:PC<sub>71</sub>BM: The compositions ratio of PTB7:PC<sub>71</sub>BM is 1:1.5 that dissolved in a mixture of chlorobenzene and 1,8-diiodooctane(97:3 vol%) in a concentration of 25 mg/mL.

### 3.3.5 Device Fabrication

The organic photovoltaic devices with geometry of glass/ITO/CuSCN/active layer/Al were fabricated on ITO coated glass substrates. Prior to use, the substrates were cleaned with soap solution followed by deionized water. Then the substrates were reflux in acetone followed by trichloroethane and isopropanol respectively. After drying the substrates and UV-ozone treatment of ITO substrate, thin film of CuSCN (30 nm) layer was spin coated at 3000 rpm for 60 seconds. The resulted thin films were annealed (at 90°C for 20 minutes and 120°C for 20 minutes) and then dry at room temperature for 1 hour at ambient condition. Three different active materials (P3HT:PC<sub>61</sub>BM, PCDTBT:PC<sub>71</sub>BM and PTB7:PC<sub>71</sub>BM) were used to investigate the efficiency of the HTL. Active materials were spin coated on top of CuSCN as an HTL using 1000 rpm for 90 seconds and resulted substrates were further annealed at 70°C for 10 minutes (for P3HT:PC<sub>61</sub>BM was baked for 120°C for 10 minutes). Finally the devices were completed by deposition of 120 nm aluminium layer at a pressure of  $5 \times 10^{-6}$  mbar.

### 3.3.6 Device Characterization

All the devices measurements were performed in ambient condition without a protective atmosphere. The current-voltage (J-V) characteristics and PCE were measured with a computer controlled Keithley 2400 source meter. To measure the current density under illumination, the devices were illuminated from the transparent ITO electrode side using solar simulator with an air mass 1.5G (AM 1.5G) (100 mW/cm<sup>2</sup>). UV/Vis spectra were obtained on UV-1800, Shimadzu spectrophotometer and AFM images were obtained on model number NT-MDT Solver Pro. SEM and TEM images of CuSCN films were measured at Zeiss EVO MA-10, variable pressure and EDS on Oxford INCA Energy 250 and Tecani, TF30 M/s FEI respectively.

### 3.4 Conclusion

In summary, conventional BHJ solar cells based on the solution-processable CuSCN as HTL has been fabricated using simplest device geometry of ITO/CuSCN/active layer/Al. Three different combinations of most studied and successful used donor: acceptor materials (P3HT:PC<sub>61</sub>BM, PCDTBT:PC<sub>71</sub>BM and PTB7:PC<sub>71</sub>BM) were used and demonstrated that the solution-processable CuSCN as an HTL leads to efficient hole extraction. The use of the CuSCN is improved light absorption within the active layer and thereby leads up to 5.94 % and 4.60 % PCEs for active layers of PCDTBT:PC<sub>71</sub>BM and PTB7:PC<sub>71</sub>BM respectively. These results are slightly better when compared to the cells fabricated using thermal deposition of MoO<sub>3</sub> and solution processed deposition of PEDOT:PSS as HTLs under similar condition. Annealing temperature for HTLs in organic solar cells has significant effect on PCE specifically the FF and J<sub>sc</sub>. We have provided further examples of solution-processable CuSCN as an efficient HTL in organic solar cells, in general. This study clearly demonstrates that there is further opportunity to optimize the solution-processable CuSCN as an HTL to improve the PCE and lifetime of the device with wide range of materials is under process in our laboratory.

**Chapter: 3; Part: B****An Eco-friendly and Inexpensive Solvent for Solution Processable CuSCN as a Hole Transporting Layer in Organic Solar Cells**

---

**3.5 Introduction**

Power conversion efficiency (PCE) with adequate stability in excitonic solar cells is the most difficult challenge for their possible commercial applications (40, 41). Particularly, solution processable organic solar cells are most often referred due to their easy fabrication process, cost effectiveness and large area devices (42). Commonly, conventional bulk heterojunction (BHJ) solar cells have been fabricated based on five different components as active layer (donor/acceptor materials), hole transport layer (HTL), electron transport layer (ETL), indium tin oxide (ITO) as a positive electrode and metal as a negative electrode. Among them, active layer is widely studied to achieve the highest possible performance (3-5). With respect to effort on active layer, very scanty is known about solution processed HTL, while HTL in photovoltaic device plays an important role for device stability and PCE (43, 44). It is observed that water soluble poly(3,4-ethylenedioxythiophene):poly(styrene sulfonate) (PEDOT:PSS) is frequently used HTL in organic solar cells, although it influences the device stability and degradation (21,22,23,27,28). Transition metal compounds (14,15,17,18,20,45) are also well reported for efficient HTL in organic solar cells including copper(I)iodide (CuI) (46) and copper(I)thiocyanate (CuSCN) (21,22,23,27,28). Nowadays CuSCN has been successfully used as an efficient HTL in excitonic solar cells such as organic solar cells (PCE; 8.22%) (47), dye sensitized solar cells (DSSCs) and perovskite (30) solar cells (PCE; 15.6%).



In past few years, significant research on solution-processable deposition of CuSCN as an hole transporting layer for fabrication of efficient electronic devices namely field effect transistors (25, 26), organic light emitting diodes (24) and solar cells have been successfully reported. Recently, our group reported CuSCN as an efficient and solution-processable HTL in low band gap polymeric solar cells using diisopropyl sulfide solvent for thin film deposition (48). Anthopoulos and co-workers reported CuSCN as a solution-processable transparent anodic interface material as a replacement of PEDOT:PSS for highly efficient solution processable BHJ device using different combination of donor and acceptor materials (31). In 2015, another report on advantages of solution-processable CuSCN used as a hole collection/transport layer for polymer/fullerene based organic solar cells have been reported (32). Very recently, Mishra et al. reported solution-processable CuSCN as an interfacial hole transporting layer in organic solar cells using acceptor-donor-acceptor type oligomers and achieved PCE to 8.22%. However, it is shocking that all the cases, diisopropyl sulfide and diethyl sulfide were used as a solvent for thin film deposition of CuSCN as a HTL. It is also noticeable that diisopropyl sulfide is an irritant solvent having very foul smell. The use of these solvents for CuSCN thin film deposition is limited its application as a solution-processable HTL for cost effective, large area and flexible substrate applications. This is due to harmful, irritant, foul smell and expensive nature of these two solvents. Indeed, Ivlentina and co-workers reported electrodeposited CuSCN nano wires as hole transporting layer in conventional polymeric solar cells (29).

Here we use CuSCN as solution-processable HTL for low band gap organic solar cells. Dimethyl sulfoxide (DMSO) was used for solution processed thin film deposition of CuSCN to examine the effectiveness of the solvents in solar cells. The

photovoltaic devices were fabricated using two different low band gap polymers Poly[*N*-9'-heptadecanyl-2,7-carbazole-alt-5,5-(4',7'-di-2-thienyl-2',1',3'-benzothiadiazole)](PCDTBT) (34) and Poly[[4,8-bis[(2-ethylhexyl)oxy]benzo[1,2-b:4,5-b']dithiophene-2,6-diyl][3-fluoro-2-[(2-ethylhexyl)carbonyl]thieno[3,4-b]thiophenediyl]] (PTB7) (35, 36) as donor materials blended with phenyl- $C_{71}$ -butyric acid methyl ester (PC $_{71}$ BM) as an acceptor material with device structure of ITO/CuSCN/active layer/Al (120 nm). The PCE based on CuSCN using DMSO as a HTL deposited solvent have been up to 4.20% and 3.64% respectively. In this present work, the resulted HTLs were achieved characterized by UV-vis-NIR spectroscopy, scanning electron microscope (SEM) and atomic force microscope (AFM) for better understanding to achieve the highest possible efficiency.

### 3.6 Results and discussion

CuSCN is well known *p*-type transparent conductor material. Due to wide band gap and excellent optical transparency, CuSCN is used as a semiconductor for optoelectronic devices (49). Previously reported, CuSCN has relatively good solubility in diisopropyl sulfide and diethyl sulfide for solution-processable optoelectronic devices fabrication. Here in, we dissolved CuSCN in DMSO (10 mg in 1 mL) using sonicator for 2 hrs and this solution was kept for 30 min. In contrast to previous report, in which CuSCN dissolve partially in diisopropyl sulfide solvent, while in this study CuSCN dissolved completely in DMSO for thin film deposition.

Considering significant and even better performance of solution-processable CuSCN as a HTL over PEDOT:PSS and other traditional transition metal oxides, we decided to explore eco friendly and inexpensive DMSO solvent for CuSCN thin film deposition as an HTL in organic solar cells as a replacement of diethyl sulfide solvent and diisopropyl sulfide. To examine the effectiveness of the DMSO solvent for

CuSCN films deposition as HTL in photovoltaic devices, BHJ solar cells were fabricated using device geometry of ITO/CuSCN/active layer/Al as presented in Figure 3.16. It is worthy to mention here that PCDTBT and PTB7 are the most studied low band gap donor polymers in combination with PC<sub>71</sub>BM acceptor for PEDOT:PSS and other traditional HTL in efficient solar cells fabrication. The chemical structures and band diagram of the materials are shown in Figure 3.17 and 3.18 respectively.

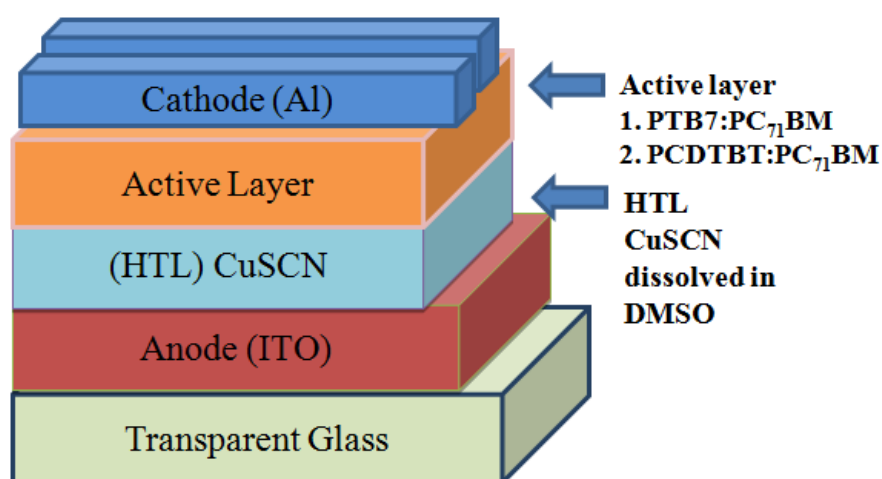


**Figure 3.16** Device geometry of organic solar cells in which CuSCN (HTL) thin film was deposited from DMSO solvent.

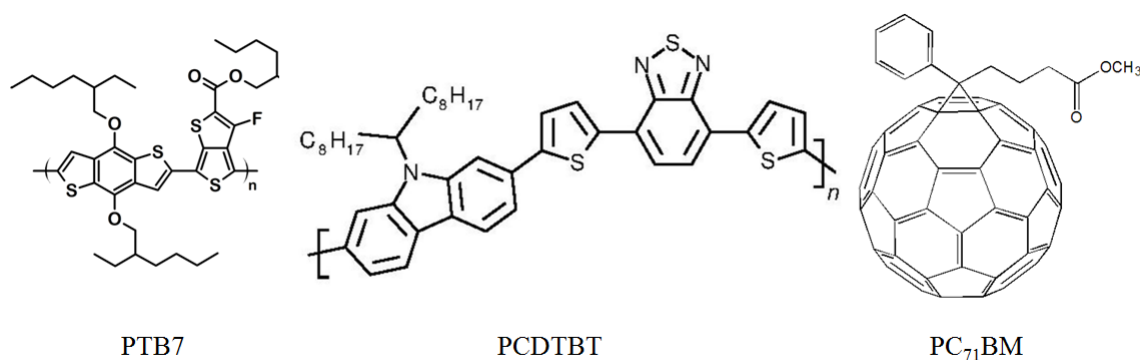


**Figure 3.17** Chemical structures of PTB7, PCDTBT and PC<sub>71</sub>BM.

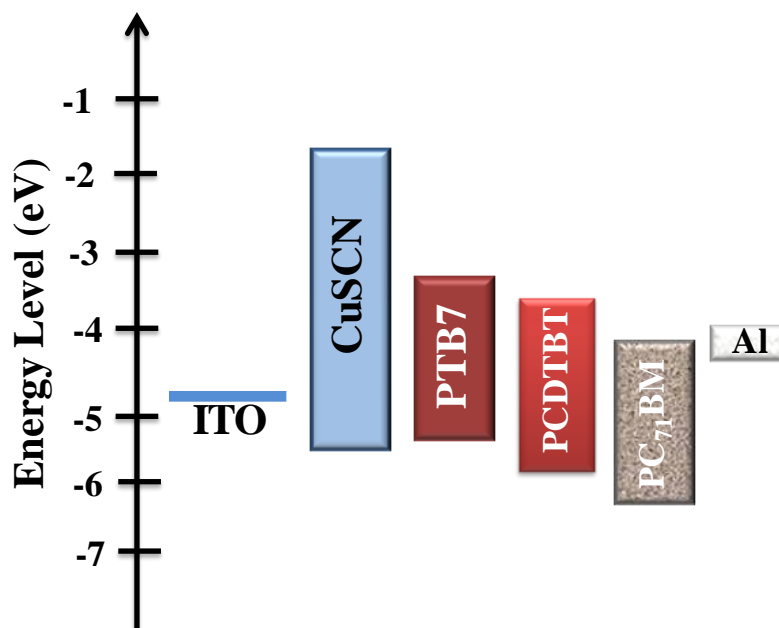


**Figure 3.18** Energy level diagram of materials.

Figure 3.19 shows the optical spectra of CuSCN thin films to investigate the absorption and transmission across the range of the solar spectrum. CuSCN film shows very little absorption in the range vis-NIR. The transmission spectrum reveals that the CuSCN thin film is highly transparent in the vis-NIR region. Thus, CuSCN thin film exhibits good optical transparency compared to other efficient. To examine the crystalline nature of the CuSCN thin film, we performed X-ray diffraction (XRD) studies on thin films (on glass deposited from DMSO and diisopropyl sulfide) and powder (Figure 3.20). Even though both the thin films are significantly disordered, compared to powder samples (strong and sharp peaks observed at  $2\theta = 16, 20, 22, 24, 25, 27, 29, 30, 33, 35, 37, 38, 43, 47, 49, 50, 51, 52, 53, 55, 58$ ). A broad peak was observed for both thin films of CuSCN. While the thin film was deposited from DMSO ( $2\theta = 16, 23, 27, 32, 34, 36, 47, 50$ ) is more ordered compared to the thin film deposited from diisopropyl sulfide ( $2\theta = 16, 27, 32$ ).

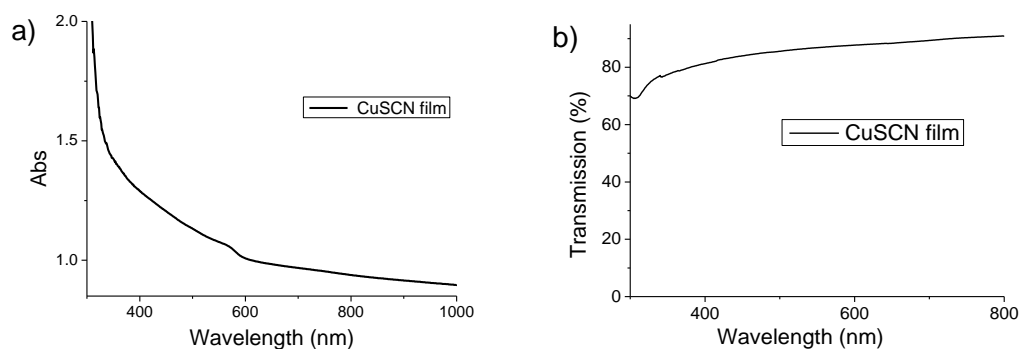


**Figure 3.19** Optical spectra of CuSCN thin films were deposited using DMSO solution on glass substrates, a) absorption and b) transmission.

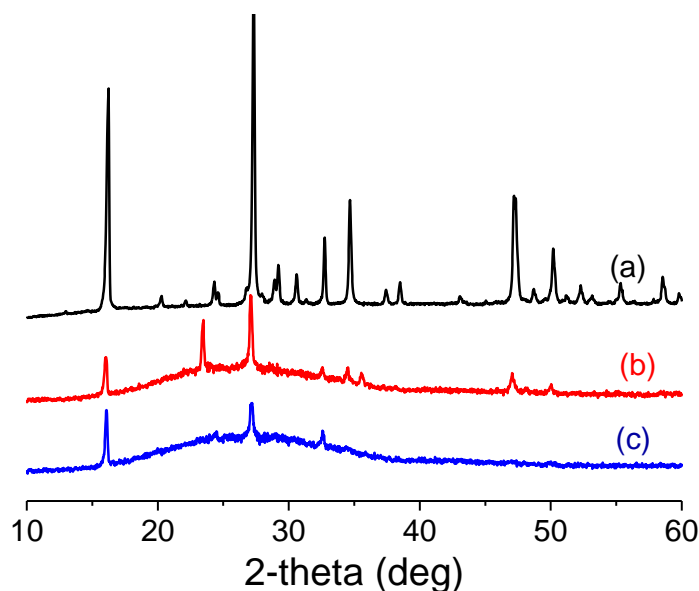


**Figure 3.20** XRD spectra of CuSCN (a) solid power, film on glass deposited from (b) DMSO and (c) diisopropyl sulfide.

To study the performance of dimethyl sulfoxide (DMSO) as a deposited solvent for CuSCN thin film as HTL in solar cells, we have fabricated the device using PCDTBT as a donor polymer with PC<sub>71</sub>BM as an acceptor material with geometry of ITO/CuSCN/PCDTBT:PC<sub>71</sub>BM/Al. The CuSCN film was deposited from a solution of DMSO (10 mg/mL) followed by the active material PCDTBT:PC<sub>71</sub>BM (1.0:4.0 wt%) deposition on the annealed HTL and finally 120 nm

aluminum layer was deposited by thermal evaporation. We have observed that the resulting devices show average PCE of 4.20% with open circuit voltage ( $V_{oc}$ ), short-circuit current ( $J_{sc}$ ) and fill factor (FF) are 0.72 V, 10.55 mA/cm<sup>2</sup> and 54.98% respectively (Figure 3.20 a). In this work the device show excellent average photovoltaic parameters which are presented in Table 3.2. We observed small deviations of the results, which show that our devices are reliable and reproducible. Since the PCE of the device shows slightly lower performance than that of previously reported CuSCN thin film deposited from diisopropyl sulfide as HTL under identical conditions. The lower performance of the device is mainly due to the slightly lower  $J_{sc}$  of the device as compared to previously reported which may be related to the ohmic contact between the CuSCN and active layer.

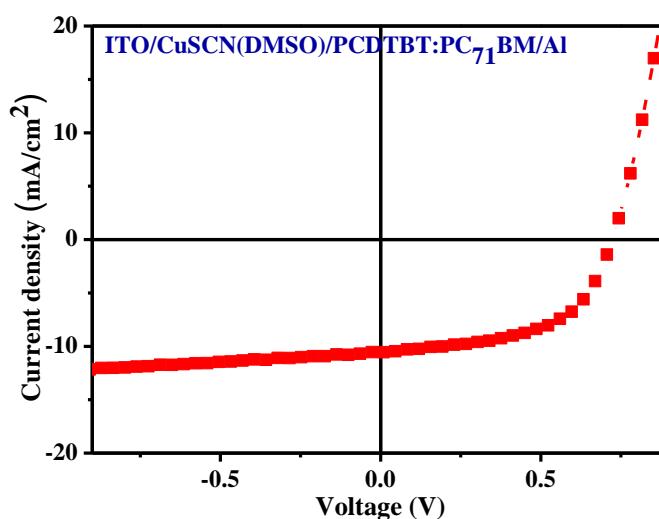


**Figure 3.21** Current density versus voltage ( $J$ - $V$ ) curves of photovoltaic device based PCDTBT:PC<sub>71</sub>BM as active layer.

In order to further examine the DMSO as an efficient solvent for CuSCN thin film deposition as HTL, we have chosen PTB7 as a donor material blended with PC<sub>71</sub>BM as an acceptor. The HTL layer of CuSCN film using DMSO solution (10 mg/mL) on ITO coated glass and annealed for device fabrication. Finally device

structure ITO/CuSCN/PTB7:PC<sub>71</sub>BM/Al was completed by deposition of active layer and metal cathode as previously mentioned. The resulting device shows PCE of 3.64 % with  $V_{oc}$ ,  $J_{sc}$  and FF are 0.61 V, 15.67 mA/cm<sup>2</sup> and 36.41% respectively (Figure 3.22 and Table 3.2). In contrast to PCDTBT, device based on the PTB7 show lower FF. While both the results with low band gap polymeric solar cells based on PCDTBT and PTB7 clearly demonstrate that DMSO as an alternative, efficient and inexpensive solvent for solution processable CuSCN as HTL for organic solar cells.

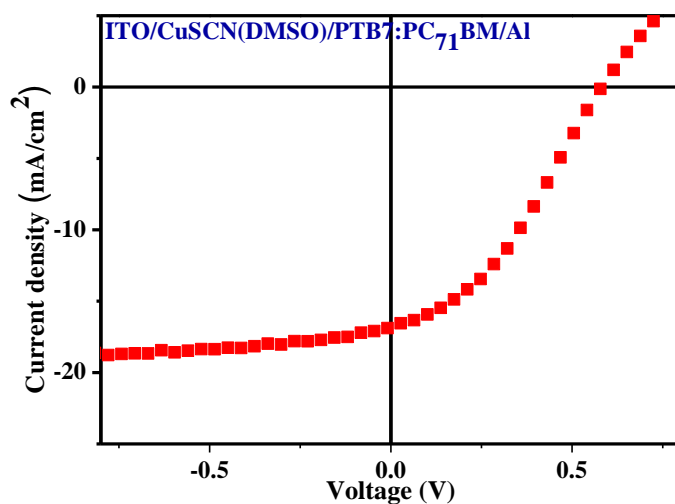


**Figure 3.22** Current density versus voltage ( $J$ - $V$ ) curves of photovoltaic device based PTB7:PC<sub>71</sub>BM active layers.

**Table 3.2** Solar cell parameters of the devices from the solution-processable CuSCN as an HTL and donor materials with PC<sub>71</sub>BM of active area 6.0 mm<sup>2</sup> (average of 4 devices).

Entry	Active materials	J <sub>sc</sub> (mA/cm <sup>2</sup> )	V <sub>oc</sub> (V)	FF (%)	PCE (%)
1	PCDTBT:PC <sub>71</sub> BM	10.55 (±0.32)	0.72 (±0.02)	54.98 (±2.03)	4.20 (±0.25)
2	PTB7:PC <sub>71</sub> BM	16.7 (±0.63)	0.60 (±0.03)	36.41 (±1.63)	3.64 (±0.20)

In parallel with the above work, investigations were also directed towards development of alternative and universal solvents for copper (I) thiocyanate for fabrication of low band gap polymeric solar cells to boost the utilization of CuSCN.

In this connection, we used five different alternative solvents compactable with CuSCN for fabrication of organic solar cells: *N,N*-dimethylformamide, dioxane, acetonitrile, ethylene glycol, propylene carbonate. Solutions of the CuSCN in representative solvents for present study are shown in Figure 3.23.

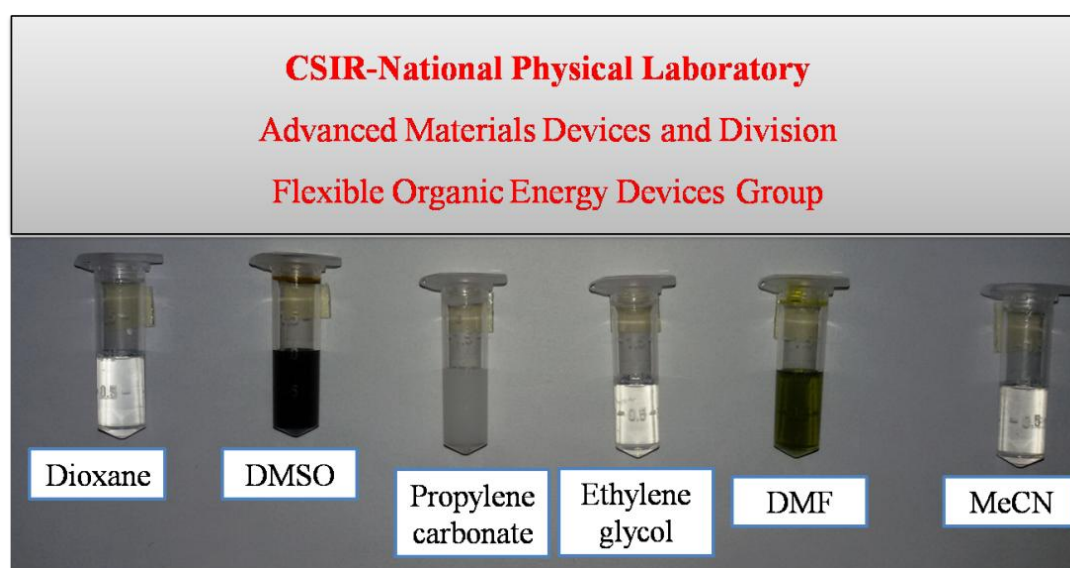


**Figure 3.23** Photograph of CuSCN solution in representative solvents.



To demonstrate the performance of low band gap solar cells based on PCDTBT:PC<sub>71</sub>BM as active material in which PCDTBT a donor polymer with PC<sub>71</sub>BM as an acceptor material to follow the device geometry ITO/CuSCN/PCDTBT:PC<sub>71</sub>BM/Al.

In this experiment, CuSCN dissolved in five solvents (each 10 mg/mL): *N,N*-dimethylformamide, dioxane, acetonitrile, ethylene glycol, propylene carbonate. Each solutions of CuSCN were deposited as thin layer on ITO coated glass substrates by spin coating technique followed by annealing. Afterward active material PCDTBT:PC<sub>71</sub>BM (1:4 wt%) was spin coated on the top of each CuSCN layer followed by deposition of aluminum layer as cathode. The J-V curve under light of each device is illustrated in Figure 3.24. The active area of the device is 5.0 mm<sup>2</sup> (2 mm x 2.5 mm) and photovoltaic parameters of each device are presented in Table 3.3. It was observed that the resulting devices exhibit the PCE of 4.25%, 2.05%, 3.03%, 1.74% and 2.54% using CuSCN dissolved in *N,N*-dimethylformamide, dioxane, acetonitrile, ethylene glycol and propylene carbonate respectively. The parameters like open circuit voltage ( $V_{oc}$ ), short-circuit current ( $J_{sc}$ ) and fill factor (FF) are illustrated in Table 3.3.

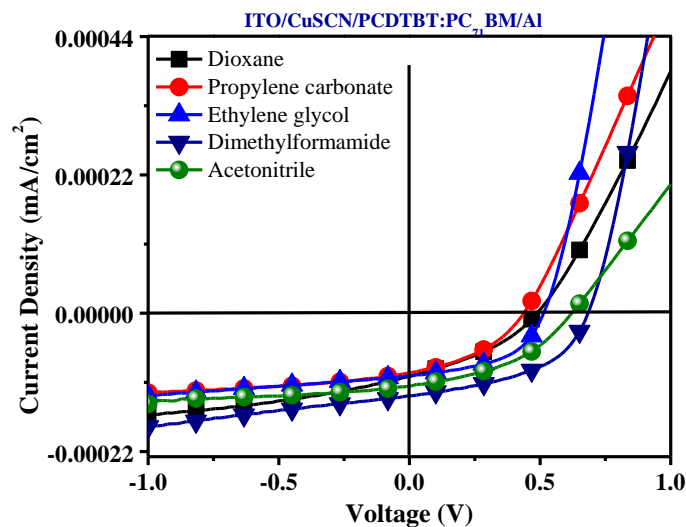


**Figure 3.24** *J-V curves for OPV device performance for ITO/CuSCN/PCDTBT:PC<sub>71</sub>BM/Al in which CuSCN (HTL) dissolved in five different solvents.*

**Table 3.3** *Photovoltaic parameters of the OPV device using CuSCN as HTL dissolved in different solvents having ITO/CuSCN/PCDTBT:PC<sub>71</sub>BM/Al architecture with 0.05 mm<sup>2</sup> of active area.*

S. No.	Solvent used for HTL (CuSCN)	Active Layer (Donor:Acceptor)	V <sub>oc</sub> (V)	J <sub>sc</sub> (mA/cm <sup>2</sup> )	FF (%)	PCE (%)
1	<i>N,N</i> -Dimethylformamide	PCDTBT: PC <sub>71</sub> BM	0.69	13.13	47.04	4.25
2	Dioxane	PCDTBT: PC <sub>71</sub> BM	0.45	11.76	38.83	2.05
3	Acetonitrile	PCDTBT: PC <sub>71</sub> BM	0.63	11.53	41.55	3.03
4	Ethylene glycol	PCDTBT: PC <sub>71</sub> BM	0.50	9.95	34.70	1.74
5	Propylene carbonate	PCDTBT: PC <sub>71</sub> BM	0.52	9.95	48.82	2.54

In order to further examine the CuSCN as an efficient HTL for low band polymer, we have considered the most successful used PTB7 as a donor material blended with PC<sub>71</sub>BM as an acceptor to follow the device architecture ITO/CuSCN/PTB7:PC<sub>71</sub>BM/Al. CuSCN as an HTL dissolved in given five solvents

with same concentration was deposited on top of cleaned ITO coated glass substrates followed by annealing on hot plate. After that, blend solution of PTB7: PC<sub>71</sub>BM (1:1.5) was spin coated on the top of each layer inside glove box followed by deposition of aluminum layer under high vacuum. The J-V curve under light of each device is illustrated in Figure 3.25. The active area of the device is 5.0 mm<sup>2</sup> and photovoltaic parameters of each device are presented in Table 3.3. It was observed that the resulting devices exhibit the PCE of 4.56%, 2.05%, 3.31%, 2.58% and 2.51% using CuSCN dissolved in *N,N*-dimethylformamide, dioxane, acetonitrile, ethylene glycol and propylene carbonate respectively. The parameters like open circuit voltage ( $V_{oc}$ ), short-circuit current ( $J_{sc}$ ) and fill factor (FF) are illustrated in Table 3.4.

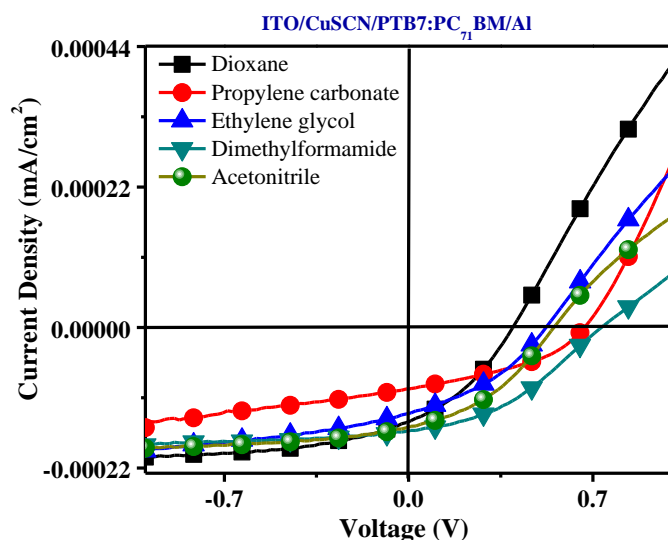


**Figure 3.25** J-V curves for OPV device performance for ITO/CuSCN/PTB7:PC<sub>71</sub>BM/Al in which CuSCN (HTL) dissolved in five different solvents.

**Table 3.4** Photovoltaic parameters of the OPV device using CuSCN as HTL dissolved in different solvents having ITO/CuSCN/ PTB7:PC<sub>71</sub>BM /Al architecture with 0.05 mm<sup>2</sup> of active area.

S. No.	Solvent used for HTL (CuSCN)	Active Layer (Donor:Acceptor)	V <sub>oc</sub> (V)	J <sub>sc</sub> (mA/cm <sup>2</sup> )	FF (%)	PCE (%)
1	N,N-Dimethylformamide	PTB7:PC <sub>71</sub> BM	0.74	16.11	38.13	4.56
2	Dioxane	PTB7:PC <sub>71</sub> BM	0.41	14.58	34.06	2.05
3	Acetonitrile	PTB7:PC <sub>71</sub> BM	0.56	15.46	38.21	3.31
4	Ethylene glycol	PTB7:PC <sub>71</sub> BM	0.52	13.37	36.85	2.58
5	Propylene carbonate	PTB7:PC <sub>71</sub> BM	0.67	9.56	39.23	2.51

For better insight of the comparative studies a bar diagram has been presented in Figure 3.26 (a) and (b) which clearly indicates that the device which has been fabricated using DMF and DMSO as a solvent in HTL gave better efficiency as compared to other solvents in both PTB7:PC<sub>71</sub>BM and PCDTBT:PC<sub>71</sub>BM blend.

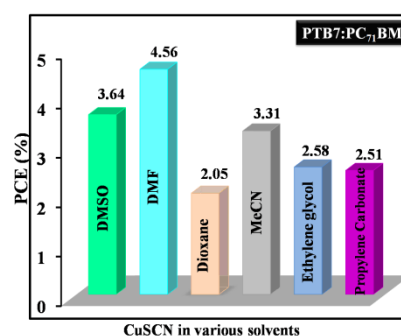
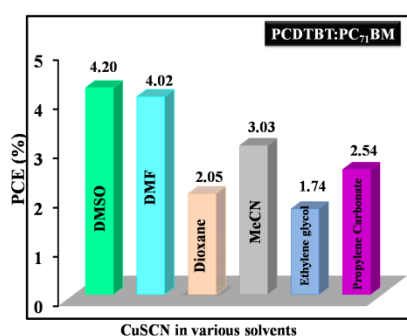


**Figure 3.26** A bar diagram representation of device efficiency of polymer blend (a) PCDTBT:PC<sub>71</sub>BM and (b) PTB7:PC<sub>71</sub>BM in solvents used for the present studies.

To understand the surface morphology of the CuSCN thin film deposited from DMSO solvent, the films were characterized by scanning electron microscopy (SEM) (Figure 3.27) and atomic force microscope (AFM) (Figure 3.28). The film was prepared by spin coating on glass substrates. The SEM image of CuSCN exhibits discontinuous path like structure in contrast to previously reported smooth surface. The AFM image of CuSCN film is rough which supports the SEM image as shown in Figure 3.27 and 3.28.

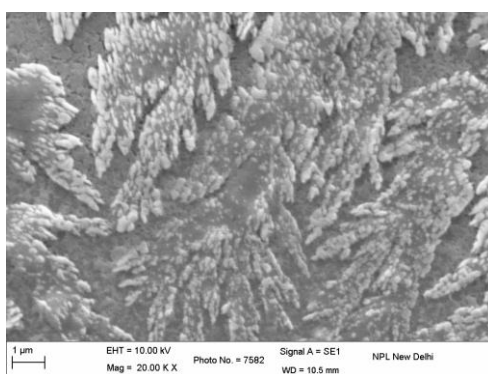


**Figure 3.27** SEM images of CuSCN thin films deposited from DMSO solution on glass substrate.

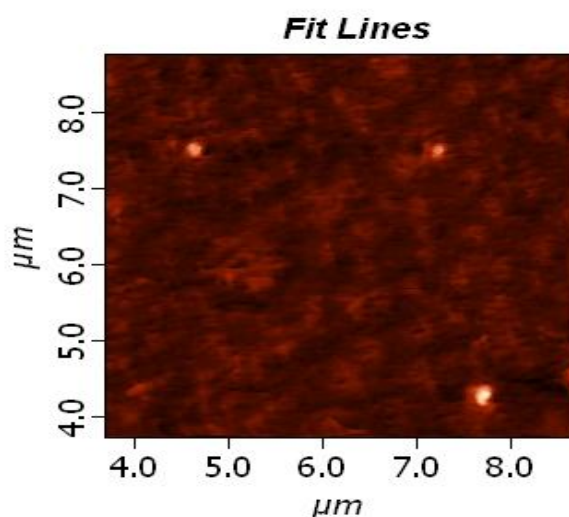


**Figure 3.28** AFM images of CuSCN thin films deposited from DMSO solution on glass substrate.

### 3.7 Experimental Section

#### 3.7.1 Materials

Active materials including low band gap polymer (PTB7 and PCDTBT) along with PC<sub>71</sub>BM were purchased from 1-material, Canada whereas different solvents were purchased from sigma-aldrich, and alfa-aesar and used as received without further purification.

#### 3.7.2 Preparation of CuSCN solutions

10 mg of copper (I) thiocyanate (CuSCN) was dissolved in 1.0 mL dimethyl sulfoxide (DMSO), and the resulting suspension mixture was sonicated for 2 hours at room temperature. After sonication the mixture was kept for 30 min and the resulting clear solution was used for solution-processable HTL in organic solar cells.

Similarly, we have prepared CuSCN solution in *N,N*-Dimethylformamide, Dioxane, Acetonitrile, Ethylene glycol and Propylene carbonate by using 10 mg of CuSCN in 1.0 mL respective solvents in same way as already mentioned in case of DMSO and diisopropyl sulfide solvents. Each solution was sonicated for 2 hours at room temperature. On completion of sonication, mixture kept standing for 30 min and a clear solution was used for fabrication of HTL.

#### 3.7.3 Preparation of Active Materials

The standard weight ratio of PTB7:PC<sub>71</sub>BM is 1:1.5 to dissolved in a combination of chlorobenzene and 1,8-diiodooctane (97:3 vol%) in a concentration of 25 mg/ml. while in case of PCDTBT:PC<sub>71</sub>BM, the weight ratio of PCDTBT:PC<sub>71</sub>BM is 1:4 to dissolved in a blend of chlorobenzene and dichlorobenzene (1:3 ratio) in a concentration of 35 mg/mL. Both solutions were stirred overnight inside the glove box.

#### 3.7.4 Device Fabrication

All OPV devices were manufactured on ITO coated glass slide (80 nm thickness, 15  $\Omega$ /sq sheet resistance) which act as anode while low work function metal aluminum was used as cathode for the fabrication of organic solar cells with the device geometry ITO/CuSCN/active layer/Al. ITO was etched with 2.5 mm width by using laser scribing system. The etched ITO slides were cleaned with distilled water through ultrasonication to remove oil particles. These slides were further cleaned in hot acetone followed by trichloroethylene and isopropanol for 10 min each, further, these were dried in a vacuum oven at 100 °C and then exposed to UV ozone cleaner for 10 min to modify its surface into hydrophilic state for better adhesion. Thin film of prepared solution of CuSCN (act as HTL) dissolved in DMSO was deposited by spin-coating process over it at 3500 rpm for 60 seconds, drying in oven at 100°C for 15 min followed by drying at room temperature for 1 h. Afterward, the mixed solutions consisting of PCDTBT:PC<sub>71</sub>BM and PTB7:PC<sub>71</sub>BM were spin coated at 1000 rpm for 90 seconds in a nitrogen-filled glove-box to form the active layer. Then the slides were directly dried for 10 min on a hot plate at 70°C. Finally, aluminum metal (cathode) of 120 nm thickness was deposited by thermal evaporation under high vacuum of  $5 \times 10^{-6}$  mbar with a rate of 0.3 nm/s.

Correspondingly, we have also deposited thin film of CuSCN layer (dissolved in five different solvents: DMSO, DMF and diisopropyl sulfide using 10 mg of CuSCN in 1.0 mL respective solvents by spin coating technique at 3500 rpm for 60 seconds. The resulting substrates were annealed at 100 °C for 15 minutes followed by dried at room temperature for 1 h. Each device follows the same device architecture: ITO/CuSCN/active layer/Al. Further fabrication process was same as above.

### 3.7.5 Device Characterization

All the device measurements were performed under ambient atmosphere without encapsulation at room temperature. The current-voltage (J-V) characteristics and PCEs were measured with a computer programmed Keithley 2400 source/meter. To measure the current density under illumination, the devices were illuminated from the transparent ITO electrode side using solar simulator with an air mass 1.5G (AM 1.5G) ( $100 \text{ mW/cm}^2$ ). UV/Vis spectra were obtained on UV-1800, Shimadzu spectrophotometer in chlorobenzene, fluorescence spectra were recorded on a fluorolog fluorimeter in a 1 cm quartz cuvette, atomic force microscope (AFM) images were obtained on model number NT-MDT Solver Pro and SEM images were obtained on model number NT-MDT Solver Pro and Zeiss EVO MA-10, variable pressure.

### 3.8 Conclusion

We have demonstrated an eco-friendly solution-processable deposition of CuSCN using DMSO solvent as HTL in efficient organic solar cells. The CuSCN thin films were obtained by spin casting from DMSO solvent and found to be highly transparent. The photovoltaic devices were fabricated with the device structure of ITO/CuSCN/active layer/Al and PCE up to 4.20 % has been achieved with relatively higher FF as compared to literature. We have observed that the solvent DMSO provides compatible interface layers suitable for organic solar cells fabrication which are comparable to diisopropyl sulfide and diethyl sulfide which exhibit displeasing properties like unpleasant smell, detrimental and irritant nature.

In parallel with the above work, investigations were also directed towards development of alternative and universal solvents for CuSCN for fabrication of low band gap polymeric solar cells. In this connection, we used five different alternative



solvents compactable with CuSCN for fabrication of organic solar cells: *N,N*-Dimethylformamide, dioxane, acetonitrile, ethylene glycol and propylene carbonate to develop the OPV devices based on low band gap polymers. Hence these studies open up a new approach to improve device performances via proper choice of solvents in HTL in the field of solar cells.

**References:**

1. Z. B. Henson, K. Müllen, and G. C. Bazan, *Nature Chemistry*, 4 (2012) 699.
2. Y-J. Cheng, S-H. Yang, and C-S. Hsu, *Chemical Reviews*, 109 (2009) 5868.
3. P. M. Beaujuge, and J. M. J. Fréchet, *Journal of the American Chemical Society*, 133 (2011) 20009.
4. H. Dong, H. Zhu, Q. Meng, X. Gongb, and W. Hu, *Chemical Society Reviews*, 41 (2012) 1754.
5. L. Ye, S. Zhang, L. Huo, M. Zhang, and J. Hou, *Accounts of Chemical Research*, 47 (2014) 1595.
6. Z. E. Jouad, M. Morsli, G. Louarn, L. Cattin, M. Addou, and J. Bernède, *Solar Energy Materials and Solar Cells*, 141 (2015) 429.
7. B. Roth, G. A. dos Reis Benatto, M. Corazza, R. R. Søndergaard, S. A. Gevorgyan, M. Jørgensen, and F. C. Krebs, *Advanced Energy Materials*, 5 (2015) 1401912.
8. M. Jorgensen, K. Norrman, and F. C. Krebs, *Solar Energy Materials and Solar Cells*, 92 (2008) 686.
9. B. Ecker, J. Posdorfer, E. von Hauff, and B. Ecker, *Solar Energy Materials and Solar Cells*, 116 (2013) 176.
10. M. Jørgensen, K. Norrman, S. A. Gevorgyan, T.s Tromholt, B. Andreasen, and F. C. Krebs, *Advanced Materials*, 24 (2012) 580.
11. A. W. Hains, C. Ramanan, M. D. Irwin, J. Liu, M. R. Wasielewski, and T. J. Marks, *ACS Applied Materials & Interfaces*, 2 (2010) 175.
12. S. S. Li, K. H. Tu, C. C. Lin, C. W. Chen, and M. Chhowalla, *ACS Nano*, 4 (2010) 3169.

13. J. Liu, Y. Xue, Y. Gao, D. Yu, M. Durstock, and L. Dai, *Advanced Materials*, 24 (2012) 2228.
14. S. Shao, J. Liu, J. Bergqvist, S. Shi, C. Veit, U. Würfel, Z. Xie, and F. Zhang, *Advanced Energy Materials*, 3 (2013) 349.
15. E. L. Ratcliff, J. Meyer, K. X. Steirer, N. R. Armstrong, D. Olson, and A. Kahn, *Organic Electronics*, 13 (2012) 744.
16. Y. Sun, C. J. Takacs, S. R. Cowan, J. H. Seo, X. Gong, A. Roy, and A. J. Heeger, *Advanced Materials*, 23 (2011) 2226.
17. P. Qin, G. Fang, F. Cheng, W. Ke, H. Lei, H. Wang, and X. Zhao, *ACS Applied Materials & Interfaces*, 6 (2014) 2963.
18. Z. Tan, L. Li, F. Wang, Q. Xu, S. Li, G. Sun, X. Tu, X. Hou, J. Hou, and Y. Li, *Advanced Energy Materials*, 4 (2014) 1300884.
19. V. Shrotriya, G. Li, Y. Yao, C. Chu, and Y. Yang, *Applied Physics Letters*, 88 (2006) 073508.
20. H. Pan, L. Zuo, W. Fu, C. Fan, B. Andreasen, X. Jiang, K. Norrman, F. C. Krebs, and H. Chen, *Organic Electronics*, 14 (2013) 797.
21. K. Tennakone, and W. M. Ariyasingha, *Electrochimica Acta*, 25 (1980) 731.
22. B. O'Regan, and D. T. Schwartz, *Chemistry of Materials*, 7 (1995) 1349.
23. B. O'Regan, D. T. Schwartz, S. M. Zakeeruddin, and M. Grätzel, *Advanced Materials*, 12 (2000) 1263.
24. A. Perumal, H. Faber, N. Yaacobi-Gross, P. Pattanasattayavong, C. Burgess, S. Jha, M. A. McLachlan, P. N. Stavrinou, T. D. Anthopoulos, and D. D. C. Bradley, *Advanced Materials*, 27 (2015) 93.

25. P. Pattanasattayavong, G. O. N. Ndjawa, K. Zhao, K. W. Chou, N. Yaacobi-Gross, B. C. O'Regan, A. Amassianb, and T. D. Anthopoulos, *Chemical Communications*, 49 (2013) 4154.
26. P. Pattanasattayavong, N. Yaacobi-Gross, K. Zhao, G. O. N. Ndjawa, J. Li , F. Yan, B. C. O'Regan, A. Amassian, and T. D. Anthopoulos, *Advanced Materials*, 25 (2013) 1504.
27. G. Kumara, A. Konno, G. K. R. Senadeera, P. V. V. Jayaweera, D. D. Silva, and K. Tennakone, *Solar Energy Materials and Solar Cells*, 69 (2001) 195.
28. P. Qin, S. Tanaka, S. Ito, N. Tetreault, K. Manabe, H. Nishino, M. K. Nazeeruddin, and M. Gratzel, *Nature Communications*, 5 (2014) 3834.
29. C. Chappaz-Gillot, S. Berson R. Salazar, B. Lechêne, D. Aldakov, V. Delaye, S. Guillerez, and V. Ivanova, *Solar Energy Materials and Solar Cells*, 120 (2014) 163.
30. S. Ye, W. Sun, Y. Li, W. Yan, H. Peng, Z. Bian, Z. Liu, and C. Huang, *Nano Letters*, 15 (2015) 3723.
31. N. Yaacobi-Gross, N. D. Treat, P. Pattanasattayavong, H. Faber, A. K. Perumal, N. Stingelin, D. D. C. Bradley, P. N. Stavrinou, M. Heeney, and T. D. Anthopoulos, *Advanced Energy Materials*, 5 (2014) 1401529.
32. N. D. Treat, N. Yaacobi-Gross, H. Faber, A. K. Perumal, D. D. C. Bradley, N. Stingelin, and T. D. Anthopoulos, *Applied Physics Letters*, 107 (2015) 013301.
33. M. T. Dang, L. Hirsch, and G. Wantz, *Advanced Materials*, 23 (2011) 3597.
34. S. Beaupré, and M. Leclerc, *Journal of Materials Chemistry A*, 1 (2013) 11097.
35. F. He, and L. Yu, *Journal of Physical Chemistry Letters*, 2 (2011) 3102.
36. L. Ye, S. Zhang, W. Zhao, H. Yao, and J. Hou, *Chemistry of Materials*, 26 (2014) 3603.

37. E. Verploegen, R. Mondal, C. J. Bettinger, S. Sok, M. F. Toney, and Z. Bao, *Advanced Functional Materials*, 20 (2010) 3519.
38. N. Zhou, H. Lin, S. J. Lou, X. Yu, P. Guo, E. F. Manley, S. Loser, P. Hartnett, H. Huang, M. R. Wasielewski, L. X. Chen, R. P. H. Chang, A. Facchetti, and T. J. Marks, *Advanced Energy Materials*, 4 (2014) 1300785.
39. C. D. Wessendorf, G. L. Schulz, A. Mishra, P. Kar, I. Ata, M. Weideler, M. Urdanpilleta, J. Hanisch, E. Mena-Osteritz, M. Lindén, E. Ahlswede, and P. Bäuerle, *Advanced Energy Materials*, 4 (2014) 1400266.
40. J. U. Lee, J. W. Jung, J. W. Job, and W. H. Jo, *Journal of Materials Chemistry*, 22 (2012) 24265.
41. M. Y. Ameen, S. Pradhan, M. R. Suresh, and V.S. Reddy, *Optical Materials*, 39 (2015) 134.
42. L. Lu, T. Zheng, Q. Wu, A. M. Schneider, D. Zhao, and L. Yu, *Chemical Reviews*, 115 (2015) 12666.
43. W. Yan, S. Ye, Y. Li, W. Sun, H. Rao, Z. Liu, Z. Bian, and C. Huang, *Advanced Energy Materials*, 6 (2016) 1600474.
44. L. Cali, S. Kazim, M. Gra'tzel, and S. Ahmad, *Angewandte Chemie International Edition*, 55 (2016) 2.
45. F. Ongul, *Optical Materials*, 50 (2015) 244.
46. N. Chaudhary, J. P. Kesari, R. Chaudhary, and A. Patra, *Optical Materials*, 58 (2016) 116.
47. A. Mishra, T. Rana, A. Looser, M. Stolte, F. Wurthner, P. Bauerle, and G. D. Sharma, *Journal of Materials Chemistry A*, 4 (2016) 17344.
48. N. Chaudhary, R. Chaudhary, J. P. Kesari, A. Patra, and S. Chand, *Journal of Materials Chemistry C*, 3 (2015) 11886.

49. J. E. Jaffe, T. C. Kaspar, T. C. Droubay, T. Varga, M. E. Bowden, and G. J. Exarhos, *Journal of Materials Chemistry C*, 114 (2010) 9111.





# ***Chapter:4***



## **Cost Effective Low Band Gap Polymeric Solar cells using Solution-Processable Copper Iodide (CuI) as Hole Transport Layer**

---

### **4.1 Introduction**

Polymeric solar cells have been gained a significant attention in the last two decades due to their potential advantages like mechanical flexibility, simple fabrication processes, cost effective, light weight and large area fabrication process, which are essential for bulk scale production (1, 2). Till date the power conversion efficiency (PCE) and lifetime of the photovoltaic devices are not adequate for possible commercial applications. Many attempts have been projected to optimization of photovoltaic device to reach the highest possible PCE and lifetime of the device. Among them, introduction of active materials (donor and acceptor materials) and their optimization are the most studied (3-6). In contrast, interfacial layer (hole transport layer; HTL and electron transport layer; ETL) have received scant attention for device fabrication, while interfacial materials are playing a vital role to improve the device performance. Especially, the HTL and their deposition method have significant importance for optimal device performance to reach the highest possible PCE.

Water soluble poly(3,4-ethylenedioxythiophene):poly(styrenesulfonate) (PEDOT:PSS) is the most successfully used HTL in organic solar cells because of its excellent transporting properties, high conductivity, optical transparency in the visible range and suitable work function. While several studies have been confirmed that due to its hygroscopic, protonation and acidic nature often corrode the ITO and affects the long-term stability of the photovoltaic devices (7-10). On the other hand PSS free organic materials like small molecules based (11), graphene-based materials (12,13)

and carbon nanotubes (CNTs) etc. are also used as HTL in organic solar cells, while the photovoltaic performances of these devices are not high as compared to PEDOT:PSS as an HTL. Transition metal oxides with a high work function, namely molybdenum oxide ( $\text{MoO}_x$ ), vanadium oxide ( $\text{V}_2\text{O}_5$ ), nickel oxide ( $\text{NiO}$ ) and tungsten oxide ( $\text{WO}_3$ ) so forth have been successfully used as HTL in organic solar cells to overcome the degradation issue of PEDOT:PSS (14-21). It is worth to mention that thermal deposition of few metal oxides such as  $\text{MoO}_3$  was worked even better as HTL compared to solution-processed deposition.

Recently, solution-processable deposition of metal oxides with a cost-effective method has been attracted significant attention for solar cells applications in general. Despite the significant efforts, however, there remains a clear need for the development of new, robust, inexpensive and solution-processable HTL for cost effective photovoltaic devices and in plastic optoelectronics more generally. Copper thiocyanate ( $\text{CuSCN}$ ) was reported as an efficient solution-processable HTL in BHJ solar cells (22-24). While, poor solubility of  $\text{CuSCN}$  has limits its applications as a solution-processable HTL for solar cells applications to the general public (22-24). Recently, few reports have been appeared in literature for solution processed  $\text{CuI}$  as an HTL for polymeric solar cells (25-27). Bian and coworkers demonstrated solution processable  $\text{CuI}$  as an HTL for poly(3-hexylthiophene):[6,6]-phenyl  $\text{C}_{61}$ -butyric acid methyl ester ( $\text{P3HT:PC}_{61}\text{BM}$ ) (28) based polymeric solar cells and achieved to up to 4.15% PCE (25). Alford and co-worker also reported  $\text{P3HT:PC}_{61}\text{BM}$  based solar cells employing solution-processable  $\text{CuI}$  as an HTL and compared with PEDOT:PSS (26).

Solution-processable  $\text{CuI}$  as an HTL that have replaced PEDOT:PSS for device fabrication based on  $\text{P3HT:PC}_{61}\text{BM}$  has been already reported (25,26). Encouraged by the research of  $\text{CuI}$  over PEDOT:PSS as an HTL, we decided to

explore the solution-processable CuI as an HTL for organic solar cells based on low band gap polymers for photovoltaic performances. In order to examine we have used Poly[N-9'-heptadecanyl-2,7-carbazole-alt-5,5-(4',7'-di-2-thienyl-2',1',3'-benzothiadiazole)] (PCDTBT) (29) and Poly[[4,8-bis[(2-ethylhexyl)oxy]benzo[1,2-b:4,5-b']dithiophene-2,6-diyl][3-fluoro-2-[(2-ethylhexyl) carbonyl] thieno[3,4-b]thiophenediyl]] (PTB7) (30) as two low band gap donor materials blend with phenyl-C<sub>71</sub>-butyric acid methyl ester (PC<sub>71</sub>BM) as an acceptor material based on ITO/CuI/active layer/Al device configuration as shown in Figure 4.1. The highest occupied molecular orbital (HOMO) and lowest unoccupied molecular orbital (LUMO) of PCDTBT, PTB7, PC<sub>71</sub>BM and CuI together with the work function of ITO, PEDOT:PSS and Al are presented in Figure 4.2. The work function of CuI (-5.1 eV) is slightly higher lying compared to PEDOT:PSS (-5.2 eV), which may be suggested CuI is a better hole extraction layer. Moreover, the LUMO level of CuI is about 2.0 eV, which was higher lying than the LUMO of active materials (PCDTBT, PTB7 and PC<sub>71</sub>BM) and as a result easily block the electron transport to anode electrode. Additionally, CuI is a hydrophobic in nature which may provide better compatibility with hydrophobic organic materials like PCDTBT and PTB7, which improve the ordering the organic materials and reduce the contact resistance between the active layer and interfacial layer. The chemical structures of the active materials of PCDTBT, PTB7 and PC<sub>71</sub>BM are presented in Figures 4.3.

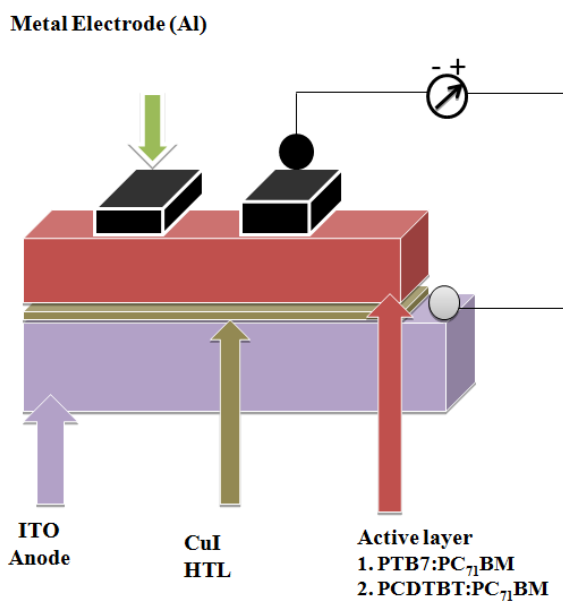


**Figure 4.1** Schematic diagram of the conventional polymeric solar cells in which the CuI layer and active layer are sandwiched between an ITO anode and aluminium cathode.

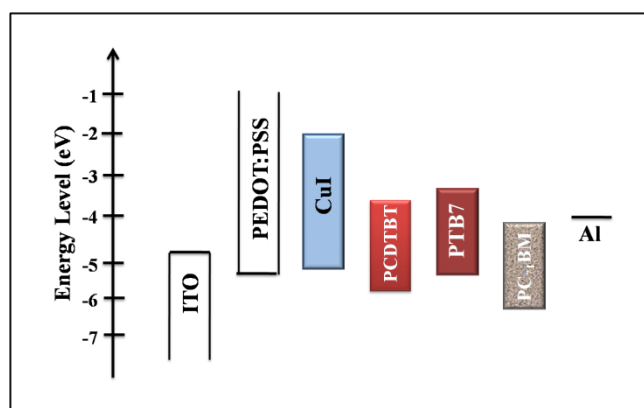


**Figure 4.2** Energy level diagram of the materials used in organic solar cells.

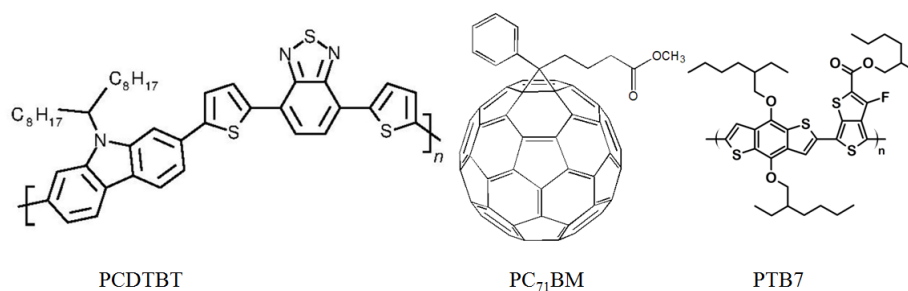
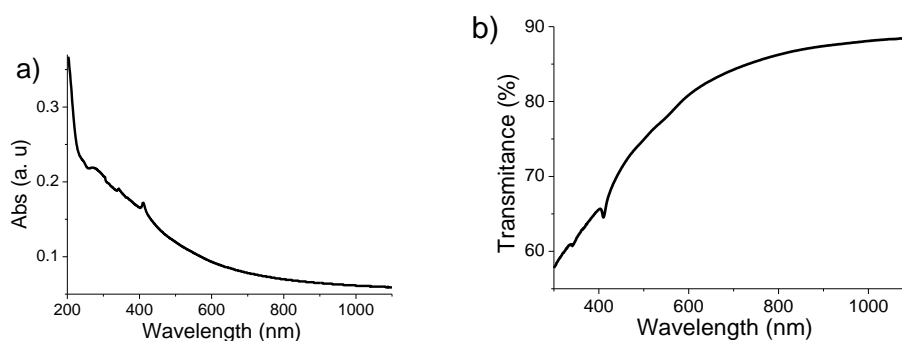


**Figure 4.3** Chemical structures of PCDTBT, PC<sub>71</sub>BM and PTB7.

Here, we demonstrate that CuI as an efficient and solution-processable HTL for low band gap polymeric solar cells. Two different combinations of low band gap polymers (PCDTBT and PTB7) blended with PC<sub>71</sub>BM were used as an active layer for photovoltaic device fabrication. Referential devices based on PEDOT:PSS layer as HTL have been fabricated for PCDTBT and PTB7 respectively. In this present work, the resulted HTLs were characterized by UV-vis-NIR spectroscopy, scanning electron microscope (SEM) and atomic force microscope (AFM) for better understanding to achieve the highest possible efficiency.

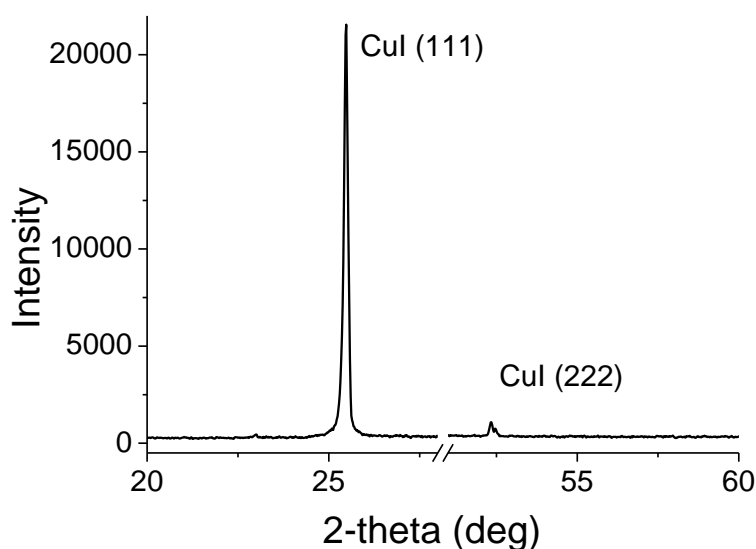
## 4.2 Results and discussion

Figure 4.4 displays the optical spectra of CuI thin films on quartz substrate to investigate the absorption and transmission across the range of solar spectrum (31). CuI film shows absorption in UV region (<450 nm) and very little absorption in the range vis-NIR region (450-1110 nm). In contrast, PEDOT:PSS films exhibit significant absorption in the range vis-NIR region. Accordingly, due to lower parasitic absorption of CuI makes it's an efficient HTL in solar cells for further improvement of PCE compared to PEDOT:PSS. The transmission spectrum reveals that the CuI thin film is highly transparent in the vis-NIR region. Thus CuI thin film exhibits better transparency compared to PEDOT:PSS thin films.



**Figure 4.4** Optical spectra of CuI thin films on quartz substrate, a) absorption and b) transmission.

The X-ray diffraction (XRD) pattern of CuI is shown in Figure 4.5. The CuI exhibits an intense peak at 25.47 ( $2\theta$ ) corresponds to the CuI (111) reflection, which was assigned to  $\gamma$ -phase with zinc blend structure (31). It is worth mentioned here that CuI has three crystalline phases of  $\alpha$ ,  $\beta$  and  $\gamma$ . Among them,  $\gamma$ -phase of CuI exhibits as  $p$ -type semiconductor. The CuI shows another weak peak at 52.35 ( $2\theta$ ) corresponding to CuI (222), which indicates the crystalline nature of the material.



**Figure 4.5** XRD pattern of CuI

To examine the performance of solution-processable CuI as a potential member of HTL for low band gap polymeric solar cells, we have fabricated the device based on ITO/CuI/PCDTBT:PC<sub>71</sub>BM/Al using PCDTBT as a donor polymer with PC<sub>71</sub>BM as an acceptor material. Thin layer of CuI as an HTL was deposited from a solution of acetonitrile (10 mg/mL). Higher and lower concentration of CuI yielded poor performances. Then the active material PCDTBT:PC<sub>71</sub>BM (1.0:4.0 wt%) was deposited on the annealed HTL followed by deposition of 120 nm aluminum layer. The J-V curve in dark and light are presented in Figure 4.6. The area of the active

device is  $5.0 \text{ mm}^2$  and average photovoltaic parameters of 8 devices are presented in Table 4.1. The dark curve shows a characteristic diode behavior. In light, we have found that the resulting devices show average PCE of 3.04% with open circuit voltage ( $V_{oc}$ ), short-circuit current ( $J_{sc}$ ) and fill factor (FF) are 0.63 V,  $11.93 \text{ mA/cm}^2$  and 0.42 respectively. For comparison purpose, we have fabricated the photovoltaic devices by using solution-processable PEDOT:PSS as HTL under similar conditions and found PCE 2.57% with  $J_{sc}$ ,  $V_{oc}$  and FF are  $9.36 \text{ mA/cm}^2$ , 0.72V and 37.9% respectively. It has been prove that photovoltaic devices using solution-processable PEDOT:PSS as an HTL shows slightly lower performance than that of CuI as an HTL under identical conditions as shown in Figure 4.7. The lower performance of the device is mainly due to the lower in FF and  $J_{sc}$  of the device.

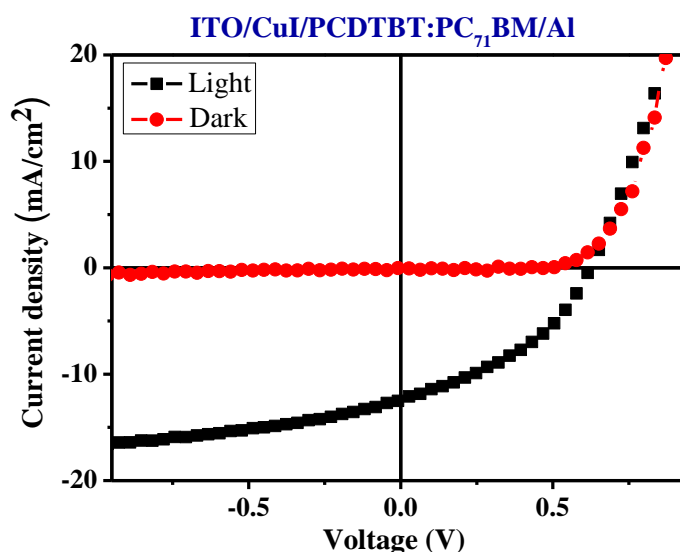


**Figure 4.6** Current density versus voltage ( $J$ - $V$ ) curves of photovoltaic device based PCDTBT:PC<sub>71</sub>BM active layer.

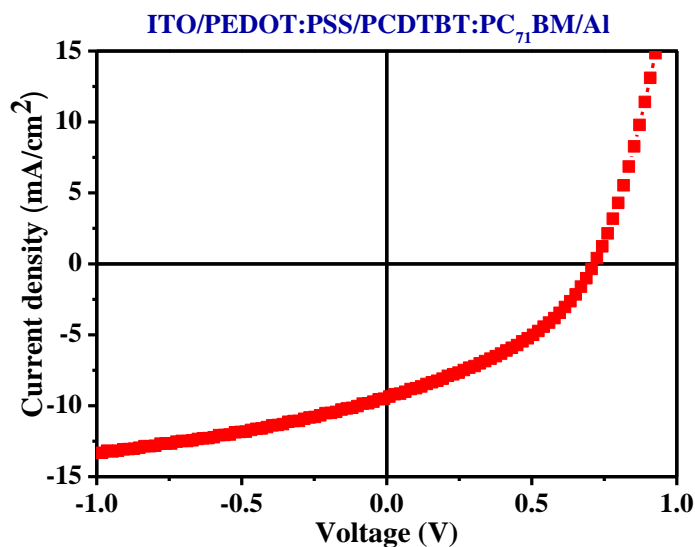


**Figure 4.7** J-V curves for the devices based on the structure of ITO/PEDOT:PSS/PCDTBT:PC<sub>71</sub>BM/Al geometry.

In order to further examine the CuI as an efficient HTL for low band gap polymer, we have considered PTB7 as a donor material blended with PC<sub>71</sub>BM as an acceptor. The CuI as an HTL was deposited from acetonitrile solution (10 mg/mL) on ITO coated glass and annealed. Then the active layer and metal cathode were deposited successively to complete the photovoltaic device with structure of ITO/CuI/PTB7:PC<sub>71</sub>BM/Al. The J-V curves of dark and light are shown in Figure 4.8. The resulting device exhibits PCE of 4.48% with  $V_{oc}$ ,  $J_{sc}$  and FF are 0.63 V, 17.55 mA/cm<sup>2</sup> and 0.40 respectively (Table 4.1). To compare the performance of CuI as an HTL in OPV cells, we have fabricated the reference device using PEDOT:PSS as an HTL under identical conditions. We have fabricated the reference photovoltaic devices based on the structure of ITO/PEDOT:PSS/PTB7:PC<sub>71</sub>BM/Al under similar conditions and found PCE 3.14% with  $J_{sc}$ ,  $V_{oc}$  and FF are 13.25 mA/cm<sup>2</sup>, 0.69 V and 34.4% respectively. The poor performance of the device of about PCE 3.14 % based on PEDOT:PSS is due significant lower FF and  $J_{sc}$  (Figure 4.9). Both the results with low band gap polymeric solar cells based on PCDTBT and PTB7 clearly



demonstrated that solution-processable CuI is even better HTL for photovoltaic applications.

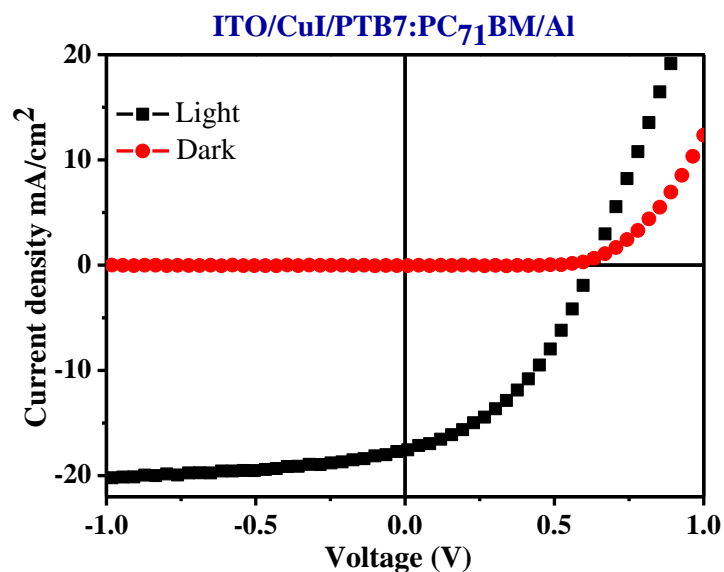


**Figure 4.8** Current density versus voltage ( $J$ - $V$ ) curves of photovoltaic device based PTB7:PC<sub>71</sub>BM active layer.

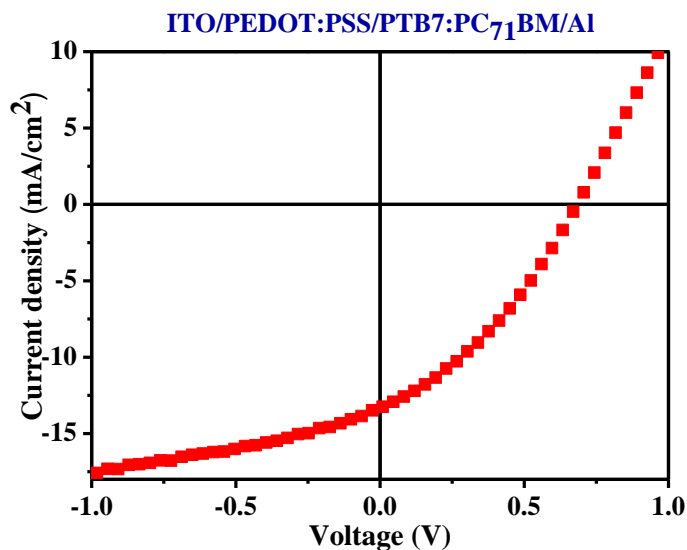


**Figure 4.9**  $J$ - $V$  curves for the devices based on the structure of ITO/PEDOT:PSS/PTB7:PC<sub>71</sub>BM /Al geometry.

**Table 4.1** Solar cells parameters of the devices from the solution-processable CuI as an HTL and donor materials with PC<sub>71</sub>BM of active area 5.0 mm<sup>2</sup> (average of 8 devices).

Donor Materials	HTL	J <sub>sc</sub> (mA/cm <sup>2</sup> )	V <sub>oc</sub> (V)	FF	PCE (%)
PCDTBT	CuI	11.93 (±0.41)	0.63 (±0.01)	0.42 (±0.03)	3.04 (±0.15)
PTB7	CuI	17.55 (±0.84)	0.63 (±0.02)	0.40 (±0.03)	4.48 (±0.21)

Having successful in developing copper iodide (CuI) as an efficient and solution-processable hole transport layer (HTL) using acetonitrile as a deposited solvent in low band gap polymeric solar cells, we decided to explore the use of variety of solvents for deposition of CuI as HTL in low band gap polymeric solar cells in general.

In order to enhance the utilization of CuI as efficient HTL, we used three different alternative solvents compactable with copper iodide for fabrication of organic solar cells.

To demonstrate the performance of bulk heterojunction solar cells based on PCDTBT:PC<sub>71</sub>BM as active material in which PCDTBT a donor polymer with PC<sub>71</sub>BM as an acceptor material to follow the device geometry ITO/CuI/PCDTBT:PC<sub>71</sub>BM/Al. In this experiment, CuI used as a solution-processable HTL dissolved in three solvents (each 10 mg/mL): dimethyl sulfoxide (DMSO), *N,N*-dimethylformamide (DMF) and diisopropyl sulfide. Each solutions of CuI were deposited as thin layer on ITO coated glass substrates by spin coating technique followed by annealing. Afterward active material PCDTBT:PC<sub>71</sub>BM (1:4 wt%) was spin coated on the top of each CuI layer followed by deposition of aluminium layer as

cathode. The J-V curve under light of each device is illustrated in Figure 4.10. The active area of the device is  $5.0 \text{ mm}^2$  ( $2 \text{ mm} \times 2.5 \text{ mm}$ ) and average photovoltaic parameters of 4 devices are presented in Table 4.2. It was observed that the resulting devices exhibit the PCE of 3.04 %, 2.46 % and 3.54 % using CuI dissolved in dimethyl sulfoxide (DMSO), *N,N*-dimethylformamide (DMF) and diisopropyl sulfide respectively. The parameters like open circuit voltage ( $V_{oc}$ ), short-circuit current ( $J_{sc}$ ) and fill factor (FF) are illustrated in Table 4.2.

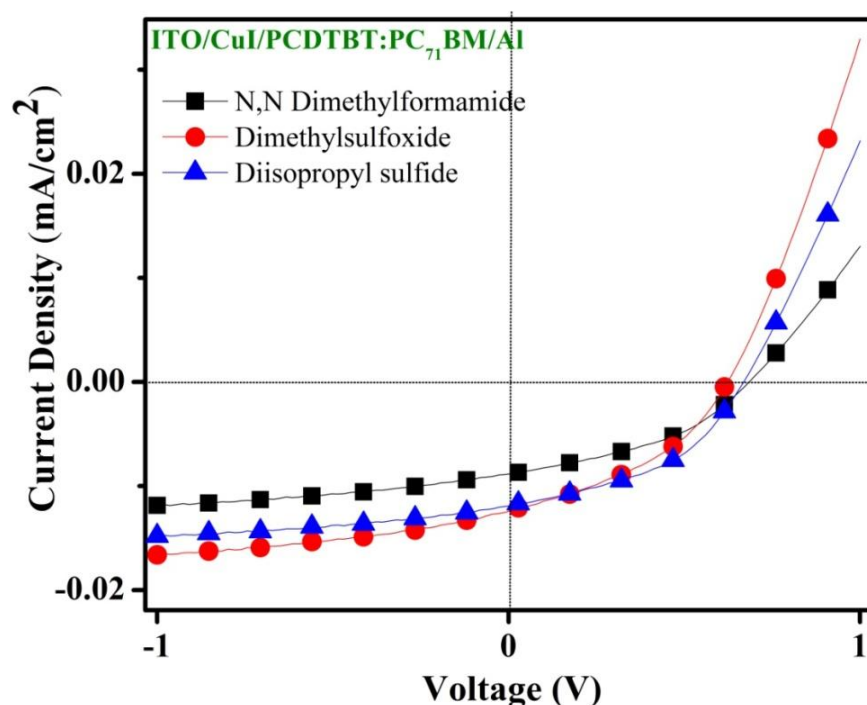


**Figure 4.10** Current density versus voltage (J-V) curves for OPV device performance for ITO/CuI/PCDTBT:PC<sub>71</sub>BM/Al in which CuI (HTL) dissolved in three different solvents.

**Table 4.2** Parameters of the OPV device using CuI as HTL dissolved in 3 different solvents having  $5.0 \text{ mm}^2$  active area using PCDTBT (donor) as low band gap polymeric solar cells.

S. No.	Solvent used for HTL (CuI)	Active Layer (Donor:Acceptor)	$V_{oc}$ (V)	$J_{sc}$ (mA/cm <sup>2</sup> )	FF (%)	PCE (%)
1	Dimethyl sulfoxide	PCDTBT:PC <sub>71</sub> BM	0.63	12.33	39.00	3.04
2	<i>N,N</i> -Dimethylformamide	PCDTBT:PC <sub>71</sub> BM	0.63	10.25	37.18	2.46
3	Diisopropyl sulfide	PCDTBT:PC <sub>71</sub> BM	0.67	11.87	44.5	3.54

In order to further examine the CuI with alternative solvents as an efficient HTL for other low band polymer, we have considered the most successful used PTB7 as a donor material blended with PC<sub>71</sub>BM as an acceptor. CuI dissolved in three different solvents as already mentioned: dimethyl sulfoxide (DMSO), *N,N*-dimethylformamide (DMF) and diisopropyl sulfide were deposited as thin layer on ITO coated glass substrates. After annealing the devices, PTB7:PC<sub>71</sub>BM (1:1.5 wt%) was spin coated on the top of each CuI layer followed by deposition of cathode layer. The J-V curves under light of each device are illustrated in Figure 4.11. It was observed that the resulting devices exhibit the PCE of 4.28%, 2.69% and 4.27% using CuI dissolved in dimethyl sulfoxide (DMSO), *N,N*-dimethylformamide (DMF) and diisopropyl sulfide respectively. Other parameters are illustrated in Table 4.3.

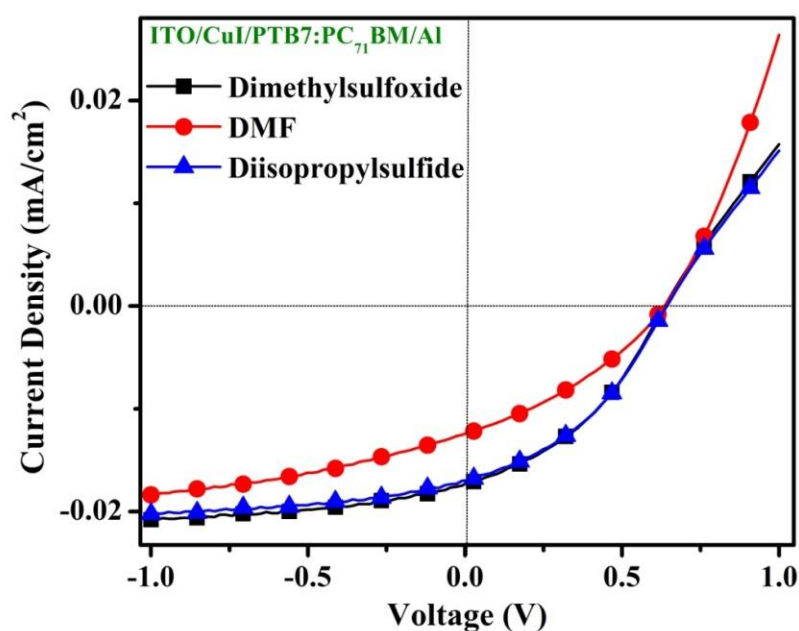


**Figure 4.11** Current density versus voltage ( $J$ - $V$ ) curves for OPV device performance for ITO/CuI/PTB7:PC<sub>71</sub>BM/Al in which CuI (HTL) dissolved in three different solvents.

**Table 4.3** Parameters of the OPV device using CuI as HTL dissolved in 3 different solvents having 5.0 mm<sup>2</sup> active area using PTB7 (donor) as low band gap polymeric solar cells.

S. No.	Solvent used for HTL (CuI)	Active Layer (Donor:Acceptor)	V <sub>oc</sub> (V)	J <sub>sc</sub> (mA/cm <sup>2</sup> )	FF (%)	PCE (%)
1	Dimethyl sulfoxide	PTB7:PC <sub>71</sub> BM	0.65	17.16	38.34	4.28
2	<i>N,N</i> -Dimethylformamide	PTB7:PC <sub>71</sub> BM	0.65	12.33	33.52	2.69
3	Diisopropyl sulfide	PTB7:PC <sub>71</sub> BM	0.65	16.94	38.71	4.27

For better insight of the comparative studies a bar diagram has been presented in Figure 4.12 which clearly indicates the device performance which has been fabricated using acetonitrile, DMSO, DMF and diisopropyl sulfide as a solvent in

CuI (HTL). PCDTBT:PC<sub>71</sub>BM and PTB7:PC<sub>71</sub>BM blend were used as photoactive layer.

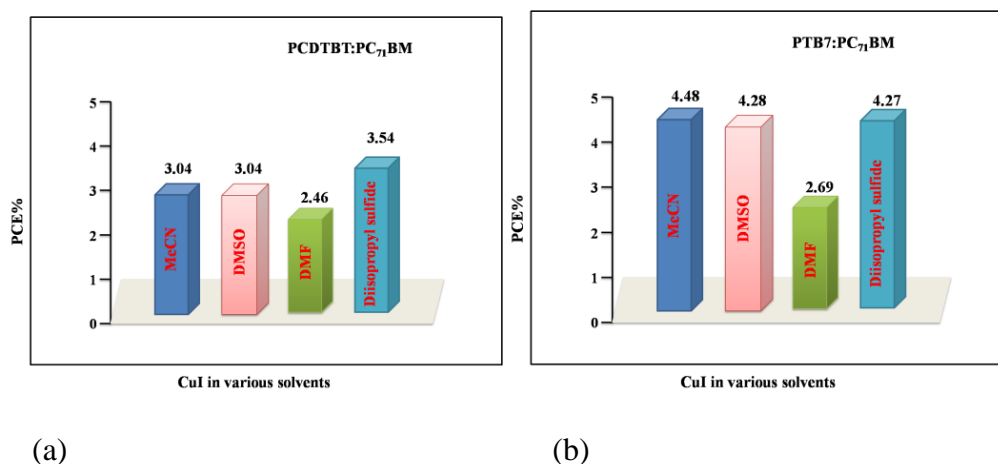


**Figure 4.12** A bar diagram representation of device efficiency of polymer blend (a) PCDTBT:PC<sub>71</sub>BM and (b) PTB7:PC<sub>71</sub>BM in solvents used for the present studies.

To get a better understanding the effect of interface layer on device performance, the morphologies of the CuI layers were characterized by scanning electron microscopy (SEM) and atomic force microscope (AFM). CuI particles form a discontinuous path like CuI islands as shown in SEM image (Figure 4.13). In contrast, PEDOT:PSS film exhibits a smooth surface. The AFM image of CuI film is relatively rough due to growing of CuI particles in acetonitrile as shown in Figure 4.14. It is also noted here that PEDOT:PSS film has been reported as smoother surface.

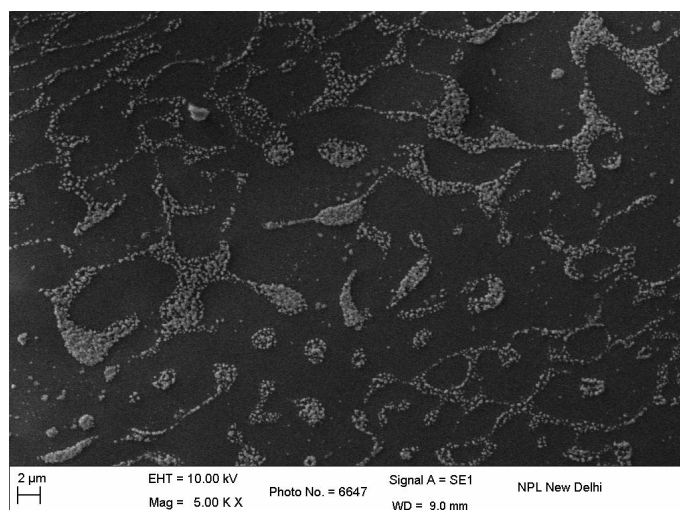


**Figure 4.13** SEM image of CuI thin films on glass substrate.

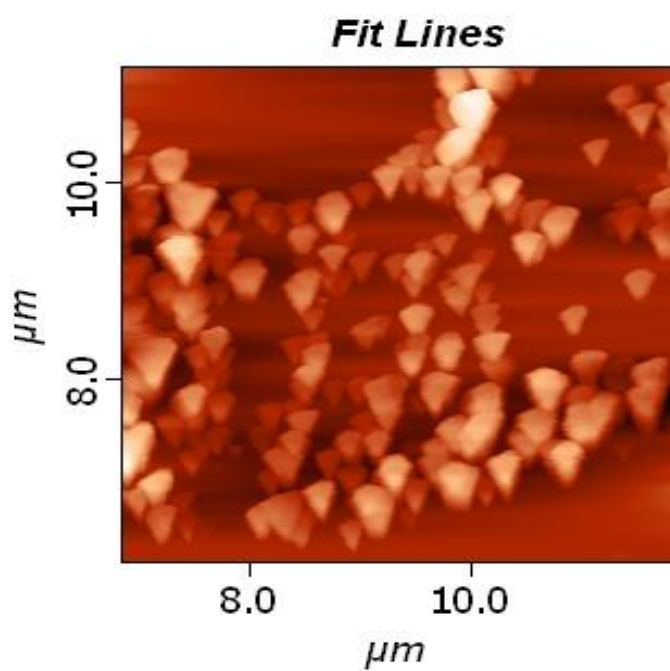


**Figure 4.14** AFM images of CuI films on glass substrate.

### 4.3 Experimental Section

#### 4.3.1 Materials

All chemicals and materials were purchased from sigma-aldrich, and alfa-aesar and used without further purification unless otherwise stated. PCDTBT, PTB7 and PC<sub>71</sub>BM were purchased from 1-material, Canada.

#### 4.3.2 Preparation of CuI thin film as an HTL

10 mg of copper(I) iodide (CuI) was dissolved in 1.0 mL of acetonitrile and the resulting suspension mixture was sonicated for 1hr at room temperature. After sonication the mixture was kept for 10 minutes and the resulting clear solution was used for solution-processable HTL in organic solar cells.

Similarly, we have prepared CuI solution in DMSO, DMF and diisopropyl sulfide by using 10 mg of CuI in 1.0 mL respective solvents as described the procedure for CuI solution in acetonitrile.

#### 4.3.3 Preparation of PEDOT:PSS as an HTL

Around 35 nm thickness PEDOT:PSS was deposited by spin casting. After that the resulting layer was annealed at 120°C for 15 minutes. Then the active layer was deposited.

#### 4.3.4 Preparation of Active Materials

In this study, two different combinations of low band gap polymers (PTB7 and PCDTBT) along with fullerene derivative (PC<sub>71</sub>BM) were used as active layer. PTB7 and PCDTBT acts as the p-type donor polymer whereas PC<sub>71</sub>BM as the n-type acceptor in the active layer.

PCDTBT:PC<sub>71</sub>BM: The composition ratio of PCDTBT:PC<sub>71</sub>BM is 1:4 that dissolved in a mixture of chlorobenzene and dichlorobenzene (1:3 ratio) in a concentration of 35 mg/mL.



PTB7:PC<sub>71</sub>BM: The compositions ratio of PTB7:PC<sub>71</sub>BM is 1:1.5 that dissolved in a mixture of chlorobenzene and 1,8-diiodoctane (97:3 vol%) in a concentration of 25 mg/ml.

#### 4.3.5 Device Fabrication

The fabrication of polymeric solar cells was done on ITO coated glass slides based on ITO/HTL/active layer/Al. First, etching of ITO slides having a suitable pattern was done by using laser scribing system. Then the slides were cleaned using soap solution followed by several rinses with deionized water. The substrates were further cleaned in boiling acetone followed by trichloroethylene and isopropanol. After annealing the slides, a thin film of CuI (40 nm) layer was deposited by spin coating over it at 3500 rpm for 60 seconds (concentration used: 10 mg CuI in 1.0 mL acetonitrile). The resulting substrates were annealed at 100 °C for 15 minutes followed by dried at room temperature for 1 h. For reference devices 35 nm thickness of PEDOT:PSS as an HTL layer was used for solar cells fabrication. Active materials (PCDTBT:PC<sub>71</sub>BM and PTB7:PC<sub>71</sub>BM) were used and spin coated on top of CuI layer at 1000 rpm for 90 seconds. Then the substrates were baked using a hotplate at 70 °C for 10 minutes in the glove box. Finally, the devices were completed via the deposition of the aluminum layer (120 nm) as cathode within a vacuum chamber at pressure  $8 \times 10^{-6}$  mbar.

Correspondingly, we have also deposited thin film of CuI layer (dissolved in three different solvents: DMSO, DMF and diisopropyl sulfide using 10 mg of CuI in 1.0 mL respective solvents) by spin coating technique at 3500 rpm for 60 seconds. The resulting substrates were annealed at 100 °C for 15 minutes followed by dried at room temperature for 1 h. Each cell follows the same device geometry: ITO/HTL/active layer/Al. Further fabrication process was same as above.

#### 4.3.6 Device Characterization

All the device measurements were performed in ambient conditions without a protective atmosphere. The current-voltage (J-V) characteristics and PCEs were measured with a computer controlled Keithley 2400 source meter. To measure the current density under illumination, the devices were illuminated from the transparent ITO electrode side using solar simulator with an air mass 1.5G (AM 1.5G) (100 mW/cm<sup>2</sup>). UV/Vis spectra were obtained on UV-1800, Shimadzu spectrophotometer (spectral resolution 1.0 nm). AFM and SEM images of CuI films were obtained on model number NT-MDT Solver Pro and Zeiss EVO MA-10, variable pressure. XRD was performed using Cu K $\alpha$  radiation with  $\lambda = 0.15405929$  at Rigaku Miniflex-II.

#### 4.4 Conclusion

In conclusion, we have demonstrated the efficient polymeric solar cells based on the inexpensive and solution-processable CuI as an HTL. The use of CuI improves light absorption within the active materials and achieved efficiency up to 3.04% and 4.48% PCEs for active materials of PCDTBT: PC<sub>71</sub>BM and PTB7: PC<sub>71</sub>BM respectively. These results are relatively better when compared to the devices fabricated using solution processed PEDOT:PSS as HTLs under similar conditions and is due to the improvement of the J<sub>sc</sub> and FF. In summary, we have provided further examples of solution-processable CuI as a good and inexpensive HTL over PEDOT:PSS for low band gap polymeric solar cells. This study clearly demonstrates that due to non-acidic nature of CuI there is further opportunity to optimize the solution-processable CuI as an HTL to improve the PCE and lifetime of the device.

In order to enhance the utilization of CuI as efficient HTL, we used three different alternative solvents compactable with copper iodide for fabrication of organic solar cells. CuI used as a solution-processable HTL dissolved in three solvents (each 10 mg/mL): dimethyl sulfoxide (DMSO), *N,N*-dimethylformamide (DMF) and diisopropyl sulfide. We have successfully fabricated organic solar cells based on low band gap polymers and achieve good performance.

**References:**

1. Polymer photovoltaics: Materials, Physics, and Device Engineering, (Eds.), F. Huang, and H. L. Yip, Y. Cao, RSC Polymer Chemistry Series SC Polymer Chemistry Series, 2015.
2. Organic Photovoltaics: Materials, Device Physics, and Manufacturing Technologies, (2<sup>nd</sup> Eds.), C. Brabec, U. Scherf and V. Dyakonov, Wiley-VCH Verlag GmbH & Co. KGaA, 2014.
3. Y-J. Cheng, S-H. Yang, and C-S. Hsu, Chemical Reviews, 109 (2009) 5868.
4. P. M. Beaujuge, and J. M. J. Fréchet, Journal of the American Chemical Society, 133 (2011) 20009.
5. H. Dong, H. Zhu, Q. Meng, X. Gongb, and W. Hu, Chemical Society Reviews, 41 (2012) 1754.
6. L. Ye, S. Zhang, L. Huo, M. Zhang, and J. Hou, Accounts of Chemical Research, 47 (2014) 1595.
7. B. Roth, G. A. d. R. Benatto, M. Corazza, R. R. Søndergaard, S. A. Gevorgyan, M. Jørgensen, and F. C. Krebs, Advanced Energy Materials, 5 (2015) 201401912.
8. M. Jorgensen, K. Norrman, and F. C. Krebs, Solar Energy Materials and Solar Cells, 92 (2008) 686.
9. B. Ecker, J. Posdorfer, E. von Hauff, and B. Ecker, Solar Energy Materials and Solar Cells, 116 (2013) 176.
10. M. Jørgensen, K. Norrman, S. A. Gevorgyan, T.S. Tromholt, B. Andreasen, and F. C. Krebs, Advanced Materials, 24 (2012) 580.
11. A. W. Hains, C. Ramanan, M. D. Irwin, J. Liu, M. R. Wasielewski, and T. J. Marks, ACS Applied Materials & Interfaces, 2 (2010) 175.

12. S-S. Li, K-H. Tu, C-C. Lin, C-W. Chen, and M. Chhowalla, *ACS Nano*, 4 (2010) 3169.
13. J. Liu, Y. Xue, Y. Gao, D. Yu, M. Durstock, and L. Dai, *Advanced Materials*, 24 (2012) 2228.
14. M. D. Irwin, D. B. Buchholz, A. W. Hains, R. P. H. Chang, and T. J. Marks, *Proceedings of the National Academy of Sciences*, 105 (2008) 2783.
15. R. Steim, F. R. Kogler, and C. J. Brabec, *Journal of Materials Chemistry*, 20 (2010) 2499.
16. S. Shao, J. Liu, J. Bergqvist, S. Shi, C. Veit, U. Würfel, Z. Xie, and F. Zhang, *Advanced Energy Materials*, 3 (2013) 349.
17. E. L. Ratcliff, J. Meyer, K. X. Steirer, N. R. Armstrong, D. Olson, and A. Kahn, *Organic Electronics*, 13 (2012) 744.
18. Y. Sun, C. J. Takacs, S. R. Cowan, J. H. Seo, X. Gong, A. Roy, and A. J. Heeger, *Advanced Materials*, 23 (2011) 2226.
19. P. Qin, G. Fang, F. Cheng, W. Ke, H. Lei, H. Wang, and X. Zhao, *ACS Applied Materials & Interfaces*, 6 (2014) 2963.
20. (a) Z. Tan, L. Li, F. Wang, Q. Xu, S. Li, G. Sun, X. Tu, X. Hou, J. Hou, and Y. Li, *Advanced Energy Materials*, 4 (2014) 1300884 (b) V. Shrotriya, G. Li, Y. Yao, C. Chu, and Y. Yang, *Applied Physics Letters*, 88 (2006) 073508.
21. H. Pan, L. Zuo, W. Fu, C. Fan, B. Andreasen, X. Jiang, K. Norrman, F. C. Krebs, and H. Chen, *Organic Electronics*, 14 (2013) 797.
22. N. Yaacobi-Gross, N. D. Treat, P. Pattanasattayavong, H. Faber, A. K. Perumal, N. Stingelin, D. D. C. Bradley, P. N. Stavrinou, M. Heeney, and T. D. Anthopoulos, *Advanced Energy Materials*, 5 (2014) 1401529.

23. N. D. Treat, N. Yaacobi-Gross, H. Faber, A. K. Perumal, D. D. C. Bradley, N. Stingelin, and T. D. Anthopoulos, *Applied Physics Letters*, 107 (2015) 013301.
24. N. Chaudhary, R. Chaudhary, J. P. Kesari, A. Patra, and S. Chand, *Journal of Materials Chemistry C*, 3 (2015) 11886.
25. W. Sun, H. Peng, Y. Li, W. Yan, Z. Liu, Z. Bian, and C. Huang, *Journal of Materials Chemistry C*, 118 (2014) 16806.
26. S. Das, J-Y. Choi, and T.L. Alford, *Solar Energy Materials and Solar Cells*, 133 (2015) 255.
27. Y. Peng, N. Yaacobi-Gross, A. K. Perumal, H. A. Faber, G. Vourlias, P. A. Patsalas, D. D. C. Bradley, Z. He, and T. D. Anthopoulos, *Applied Physics Letters*, 106 (2015) 243302.
28. M. T. Dang, L. Hirsch, and G. Wantz, *Advanced Materials*, 23 (2011) 3597.
29. S. Beaupré, and M. Leclerc, *Journal of Materials Chemistry A*, 1 (2013) 11097.
30. (a) F. He, and L. Yu, *Journal of Physical Chemistry Letters*, 2 (2011) 3102. (b) L. Ye, S. Zhang, W. Zhao, H. Yao, and J. Hou, *Chemistry of Materials* 26 (2014) 3603.
31. M. Grundmann, F-L. Schein, M. Lorenz, T. Böntgen, J. Lenzner, and H. V. Wenckstern, *Phys. Status Solidi A*, 210 (2013) 1671.



# ***Chapter:5***

# Effect of Composition Ratio of P3HT:PC<sub>61</sub>BM in Organic Solar Cells: Optical and Morphological Properties

---

## 5.1 Introduction

Organic solar cells research based on solution-processable bulk heterojunction (BHJ) (1) has attracted significant scientific and commercial interest in the last decade due to rapid increase in the power conversion efficiency (PCE) for renewable energy source. There are tremendous number of research have been reported in the area of organic solar cells (2-8). Among them poly(3-hexylthiophene) (P3HT) and phenyl-C<sub>61</sub>-butyric acid methyl ester (PC<sub>61</sub>BM) are most studied donor and acceptor materials respectively for solar cells and wide range of PCE (up to ~ 5%) and stability have been reported (9-13). Surprisingly, still lower PCE < 0.5%, as well as higher PCE > 4% for P3HT:PC<sub>61</sub>BM active layer in BHJ geometry have been reported (9). The active layer is typically optimized by thickness (14), annealing temperature (15), morphology (16), additive (17-20), energy levels, miscibility, composition ratio (21-22), and compatibly with innovative idea (23) to reach maximum possible PCE and stability for organic solar cells (24) to reach maximum possible PCE and stability for organic solar cells (21,22,24). As for example the composition ratio of polymer (donor material) and fullerene (acceptor material) are significantly differ for low band gap and high band gap polymers to reach the highest PCE. The composition ratio of donor and acceptor also depends on solvent, hole transport layer, device geometry and many others (9, 21, 22, 24).



Herein, we demonstrate the effect of composition ratio of most studied P3HT as a donor material and PC<sub>61</sub>BM as an acceptor material in conventional BHJ solar cell for highest possible PCE in ambient conditions. We have used different composition ratios of P3HT:PC<sub>61</sub>BM materials in active layer to fabricate the solar cells with simple geometry of ITO/PEDOT:PSS/P3HT:PC<sub>61</sub>BM/Al. We also present efficient characterization, optical properties and morphology of the active layers and made a correlation among them.

## 5.2 Results and discussion

### 5.2.1 Photovoltaic properties

To examine the photovoltaic properties for different composition ratios of P3HT:PC<sub>61</sub>BM in active layer was investigated in BHJ solar cells to reach the highest possible PCE in ambient conditions. In this study ten different composition ratios of P3HT:PC<sub>61</sub>BM were used for device fabrication to optimize the composition ratio in active layer with device structure of ITO/PEDOT:PSS/P3HT:PC<sub>61</sub>BM/Al as presented in Figure 5.1. The energy level diagram is shown in Figure 5.2. The thickness of the hole transport layer, active layer and Al are 60 nm, 80 nm and 120 nm respectively. These thickness are optimized for highest PCE.

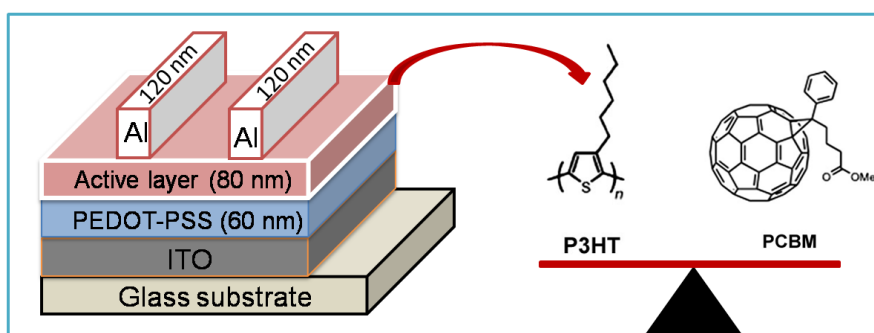


**Figure 5.1** Conventional structure of BHJ solar cells and chemical structures of P3HT and PC<sub>61</sub>BM.

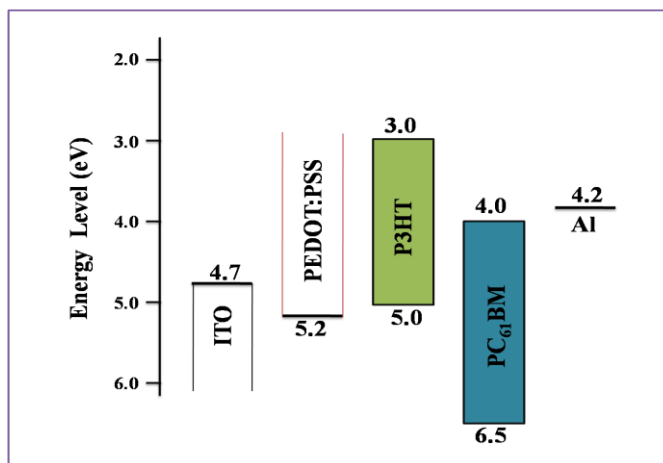


**Figure 5.2** Electronic energy levels of the materials used in organic solar cells.

Photovoltaic results using these 10 different composition ratios of P3HT:PC<sub>61</sub>BM under AM 1.5 G illumination with 100 mW/cm<sup>2</sup> are presented in Figure 5.3 and 5.4 (Table 5.1 and 5.2). The devices results are shown in both Tables (5.1 and 5.2) clearly indicated that 1.0:0.8 weight ratio of P3HT:PC<sub>61</sub>BM has achieved highest PCE of ~1.62% with open circuit voltage ( $V_{oc}$ ), short-circuit current ( $J_{sc}$ ) and fill factor (FF) are 4.91 V, 7.46 mA/cm<sup>2</sup> and 0.44 respectively (Table 5.1). P3HT:PC<sub>61</sub>BM composition ratios range from 1.0:0.4 to 1.0:1.2 in active layer show relatively good efficiency (Table 5.1 and 5.2). The total PCE difference is 0.72% has been observed between the two devices were fabricated using P3HT:PC<sub>61</sub>BM composition ratios of 1.0:0.8 and 1.0:0.4 respectively and PCE difference is 0.43% when P3HT:PC<sub>61</sub>BM composition ratios are 1.0:0.8 and 1.0:1.2 respectively. While further decrease or increase the composition ratio of P3HT:PC<sub>61</sub>BM in active layer the resulted devices show very poor PCE (Table 5.1 and 5.2).

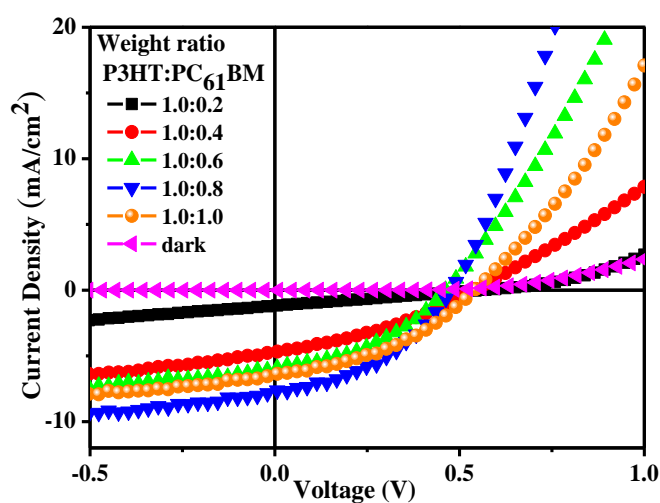


**Figure 5.3** Current density vs voltage ( $J$ - $V$ ) curves using  $P3HT:PC_{61}BM$  having composition ratios (1.0:0.2; 1.0:0.4; 1.0:0.6; 1.0:0.8; 1.0:1.0) measured under  $100 \text{ mW cm}^{-2}$  AM 1.5 G illumination with dark curve.

**Table 5.1** BHJ solar cells parameters using  $P3HT:PC_{61}BM$  with different weight ratio ((1.0:0.2; 1.0:0.4; 1.0:0.6; 1.0:0.8; 1.0:1.0) in chlorobenzene with devices structure ITO/PEDOT:PSS/ $P3HT:PC_{61}BM$ /Al.

S. No.	$P3HT:PC_{61}BM$ Composition ratio	$V_{oc}$ (V)	$J_{sc}$ ( $\text{mA/cm}^2$ )	FF (%)	PCE* (%)
1	1.0:0.2	0.57	1.21	0.25	0.17
2	1.0:0.4	0.54	4.46	0.37	0.90
3	1.0:0.6	0.48	6.00	0.40	1.16
4	1.0:0.8	0.49	7.46	0.44	1.62
5	1.0:1.0	0.54	6.13	0.43	1.43

\*All the devices measurements were performed in ambient condition without a protective atmosphere and active area is  $6.0 \text{ mm}^2$ .

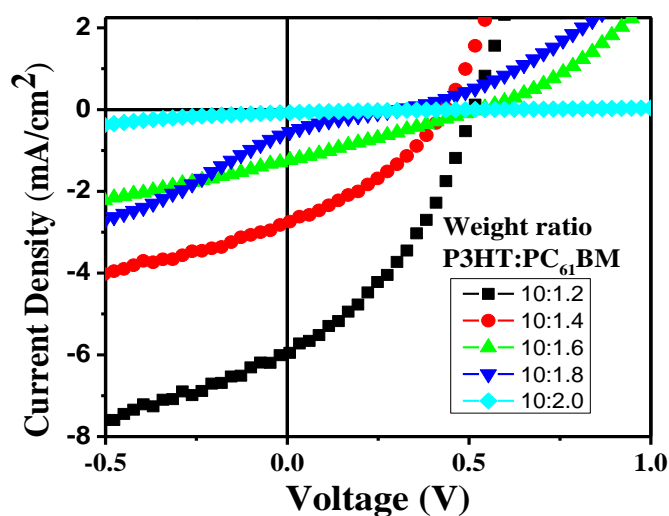


**Figure 5.4** Current density vs voltage ( $J$ - $V$ ) curves using  $P3HT:PC_{61}BM$  composition ratios (1.0:1.2; 1.0:1.4; 1.0:1.6; 1.0:1.8; 1.0:2.0) measured under  $100 \text{ mW cm}^{-1}$  AM 1.5 G illumination.

**Table 5.2** BHJ solar cells parameters using  $P3HT:PC_{61}BM$  with different weight ratio ((1.0:1.2; 1.0:1.4; 1.0:1.6; 1.0:1.8; 1.0:2.0) in chlorobenzene with devices structure ITO/PEDOT:PSS/ $P3HT:PC_{61}BM$ /Al.

S. No.	$P3HT:PC_{61}BM$ Composition ratio	$V_{oc}$ (V)	$J_{sc}$ ( $\text{mA}/\text{cm}^2$ )	FF (%)	PCE* (%)
1	1.0:1.2	0.52	5.80	0.40	1.19
2	1.0:1.4	0.44	2.61	0.37	0.43
3	1.0:1.6	0.53	1.19	0.28	0.18
4	1.0:1.8	0.32	0.55	0.20	0.034
5	1.0:2.0	0.50	0.07	0.20	0.007

\*All the devices measurements were performed in ambient condition without a protective atmosphere and active area is  $6.0 \text{ mm}^2$ .

The systematic studies of photovoltaic performances with different composition ratios of P3HT:PC<sub>61</sub>BM clearly demonstrated that composition ratio has significant effect on  $J_{sc}$  compared to  $V_{oc}$  and FF (Figure 5.5). It is worth mentioned here that significant changes in  $J_{sc}$  has been observed for the devices having composition ratio from 1.0:0.4 to 1.0:1.2 (Table 5.1 and 5.2), while minor changes for FF and  $V_{oc}$  were observed. The trends are more prominent, when devices were fabricated with further decrease or increase of PC<sub>61</sub>BM:P3HT ratio in active layer (Table 5.1 and 5.2)

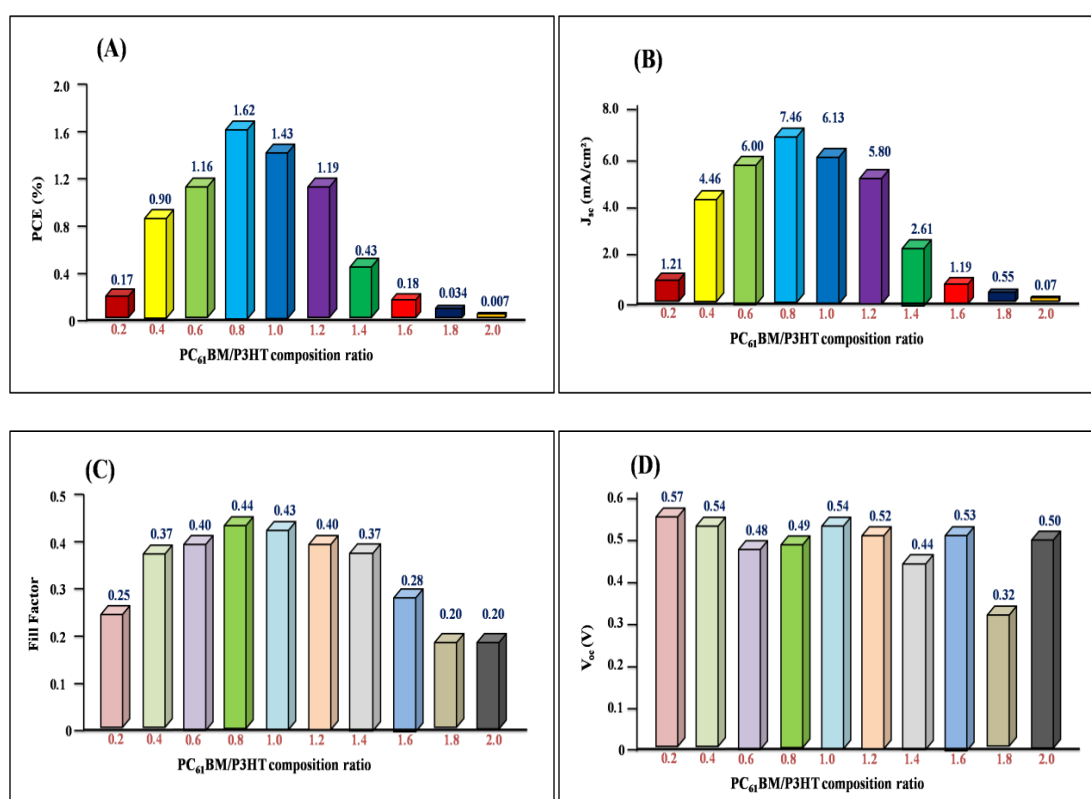


**Figure 5.5** Bar diagram showing OPV cell parameters, PCE,  $J_{sc}$ , FF, and  $V_{oc}$  vs the PC<sub>61</sub>BM:P3HT composition ratio used for device fabrication. The  $J_{sc}$  has strong correlation with composition ratio resulting in higher PCE with 1.0:0.8 composition ratio of P3HT:PC<sub>61</sub>BM.

### 5.2.2 Absorption and emission spectra

We have investigated the effect of  $J_{sc}$  from the perspectives of optical properties in different composition ratios. As shown in Figure 5.6 a, the measured optical absorption spectra for best five different composition ratios of P3HT:PC<sub>61</sub>BM in chlorobenzene are comparable. For comparison purpose absorption spectra for P3HT, PC<sub>61</sub>BM and other five different composition ratios in chlorobenzene are presented in Figures 5.6 b-c. Two major peaks at 330 and 455 nm originated from PC<sub>61</sub>BM and P3HT respectively, have been observed in absorption spectra of these composition ratios. There is no bathochromic shift among 10 different composition ratios of P3HT:PC<sub>61</sub>BM, while hyper chromic shifts have been observed. As a result intensity of the two peaks at 330 and 455 nm changes due to composition variation of P3HT and PC<sub>61</sub>BM. The solid state film absorption spectra of different composition ratios are presented in Figure 5.6 d. It is notable that significant red shift has been observed in solid state absorption spectra as compared to absorption spectra in solution. Thus the amount of photon absorption by active layer should be significantly different and 1.0:0.8 composition ratio of P3HT:PC<sub>61</sub>BM may be absorbed the highest possible photons among them. Therefore, significant variation of  $J_{sc}$  may be arising from amount of photon absorption by active layers and higher  $J_{sc}$  should be observed from strong absorption of 1.0:0.8 composition ratio of P3HT:PC<sub>61</sub>BM active layer used in this study. The comparative photoluminescence (PL) spectra of various composition ratio of P3HT:PC<sub>61</sub>BM were studied to investigate the quenching effect (Figure 5.7 a-b). The PL spectra of the best five composition ratios (P3HT:PC<sub>61</sub>BM= 1.0:0.4; 1.0:0.6; 1.0:0.8; 1.0:1.0 and 1.0:1.2) (Figure 5.7 a) are similar to each other and no significant quenching difference among them have been found (Figure 5.7 a).

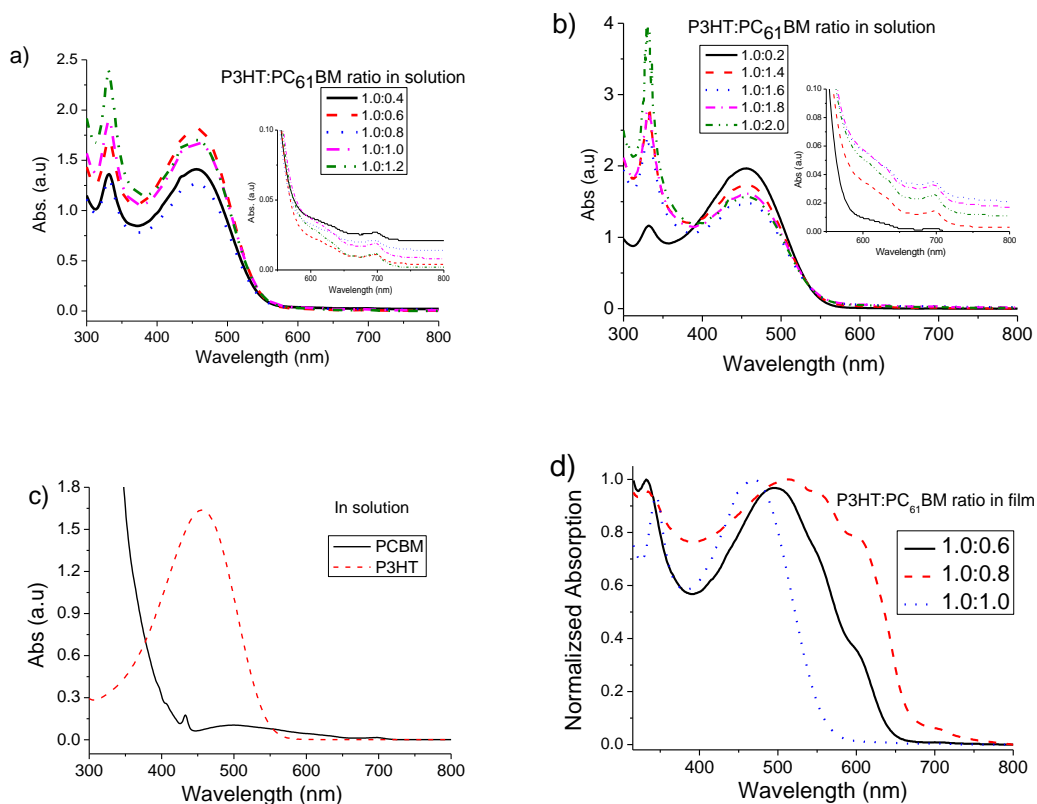


**Figure 5.6** UV-vis absorption spectra of different composition ratio of P3HT:PC<sub>61</sub>BM mixture, P3HT and PCBM. (a-c) in chlorobenzene and (d) in film.

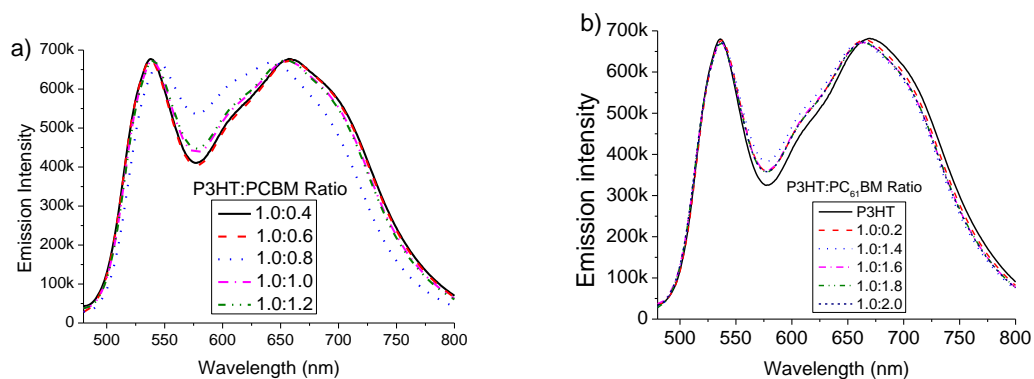


**Figure 5.7** Emission spectra of different weight ratio P3HT:PC<sub>61</sub>BM mixture in chlorobenzene.

### 5.2.3 Morphology

To elucidate the role of morphology of photoactive layer we have investigated surface morphology and roughness of P3HT:PC<sub>61</sub>BM layer using atomic force microscope (AFM). The blend film was spin-coated from the solution of P3HT:PC<sub>61</sub>BM (used composition ratio 1.0:0.8) in chlorobenzene. AFM image exhibits the smooth and a homogeneous surface of the film induces better contact with the cathode (Figure 5.8). No large phase separation, domain and aggregation in the film surface were observed, which is favorable for efficient exciton dissociation, leading to relatively high J<sub>sc</sub>. The presence of nanoscale phase separation in the film morphology is leading to the highest J<sub>sc</sub>, FF, and PCE. Morphology of the PEDOT:PSS film as HTL was also studied by AFM (Figure 5.9). Like the photoactive layer, the film shows relatively smooth surface and no large phase separation which improves the contact and hole collection. This characteristic for both photoactive and HTL could facilitate the diffusion, separation of excitons and charge transport, that improve J<sub>sc</sub>, FF, and PCE.



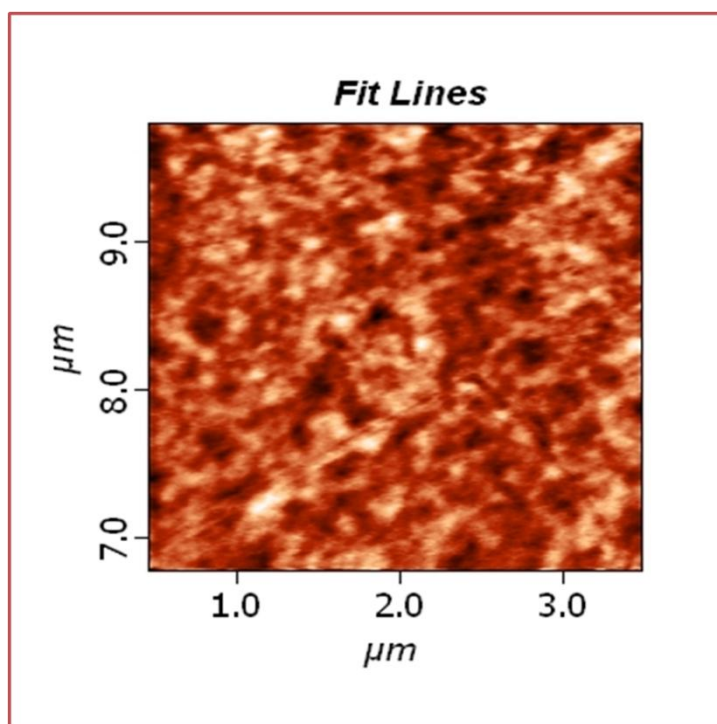


**Figure 5.8** 2D AFM image of a spin coated of P3HT:PC<sub>61</sub>BM (composition ratio 1.0:0.8) on glass.

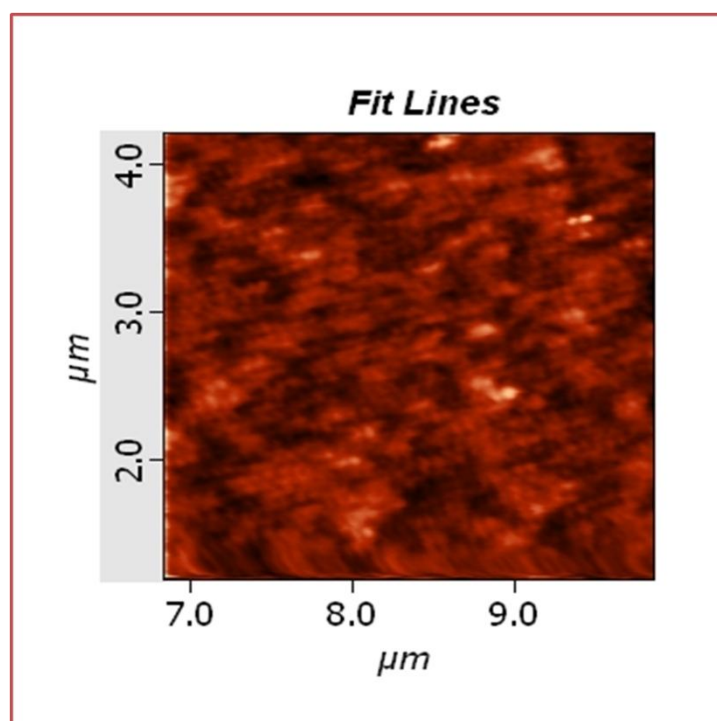


**Figure 5.9** 2D AFM image of a spin coated of PEDOT:PSS on glass.

### 5.3 Experimental

All chemicals and materials were purchased from sigma-aldrich and used without further purification unless otherwise stated. P3HT ( $M_n \sim 54,000$  and  $PDI < 2.5$ ) and PEDOT:PSS were purchased from sigma-aldrich and PC<sub>61</sub>BM was purchased from nano-C.

#### 5.3.1 Device Fabrication

The organic photovoltaic devices with geometry of glass/ITO/PEDOT:PSS/P3HT:PC<sub>61</sub>BM/Al were fabricated on ITO coated glass substrates. Prior to use, the substrates were cleaned with soap solution followed by deionized water. Then the substrates were reflux in acetone followed by trichloroethane and isopropanol respectively. After drying the substrates, a thin film of PEDOT:PSS (60 nm) layer was spin coated at 2000 rpm for 2 minutes. The resulted thin films were annealed at 120°C for 10 minutes. Active materials P3HT and PC<sub>61</sub>BM were dissolved in chlorobenzene with a concentration of 20 mg/mL. Ten different composition ratios of P3HT and PC<sub>61</sub>BM (P3HT:PC<sub>61</sub>BM ratios are 1.0:0.2, 1.0:0.4, 1.0:0.6, 1.0:0.8, 1.0:1.0, 1.0:1.2, 1.0:1.4, 1.0:1.6, 1.0:1.8, 1.0:2.0 by weight) were used for active layers deposition. The active layers were spin coated on top of the PEDOT:PSS layer using 2000 rpm for 2 minutes and resulting substrates were annealed at 110 °C for 20 minutes. Finally the devices were completed by deposition of 120 nm aluminium layer at a pressure of  $8 \times 10^{-6}$  mbar.

#### 5.3.2 Device Characterization

All the device measurements were performed in ambient condition without a protective atmosphere. The current-voltage (J-V) characteristics and PCE were measured with a computer controlled keithley 2400 source meter. To measure the

current density under illumination, the devices were illuminated from the transparent ITO electrode side using solar simulator with an air mass 1.5G (AM 1.5G) (100 mW/cm<sup>2</sup>). UV/Vis spectra were obtained on UV-1800, shimadzu spectrophotometer (spectral resolution 1.0 nm) in chlorobenzene, fluorescence spectra were recorded on a fluorolog fluorimeter in a 1 cm quartz cuvette and atomic force microscope (AFM) images were obtained on model number NT-MDT Solver Pro.

#### 5.4 Conclusions

We have investigated the effect of composition ratio of P3HT:PC<sub>61</sub>BM as donor and acceptor materials for conventional BHJ solar cells in ambient conditions. We have observed that 1.0:0.8 composition ratio for P3HT:PC<sub>61</sub>BM has achieved highest PCE. The P3HT:PC<sub>61</sub>BM composition ratios range from 1.0:0.4 to 1.0:1.2 show relatively good PCE while further decrease or increase in the composition ratio of P3HT:PC<sub>61</sub>BM resulted devices show very poor PCE. Thus composition ratio of P3HT:PC<sub>61</sub>BM has significant effect on  $J_{sc}$ , while a small on  $V_{oc}$  and FF of the optimized devices.

**References:**

1. G. Yu, J. Gao, J. C. Hummelen, F. Wudl, and A. J. Heeger, *Science*, 270 (1995) 270.
2. Y. J. Cheng, S. H. Yang, and C. S. Hsu, *Chemical Reviews*, 109 (2009) 5868.
3. H. Dong, H. Zhu, Q. Meng, X. Gong, and W. Hu, *Chemical Society Reviews*, 41 (2012) 1754.
4. X. Zhan, and D. Zhu, *Polymer Chemistry*, 1 (2010) 409.
5. P-L. T. Boudreault, A. Najari, and M. Leclerc, *Chemistry of Materials*, 23 (2011) 457.
6. H. J. Son, F. He, B. Carsten, and L. Yu, *Journal of Materials Chemistry*, 21 (2011) 18934.
7. P. M. Beaujuge, and J. M. J. Fréchet, *Journal of the American Chemical Society*, 133 (2011) 20009.
8. Y. Li, *Accounts of Chemical Research*, 45 (2012) 723.
9. M.T. Dang, L. Hirsch, and G. Wantz, *Advanced Materials*, 23 (2011) 3597.
10. (a) S. H. Lee, D. H. Kim, J. H. Kim, G. S. Lee, and J. G. Park, *Journal of Physical Chemistry C*, 113 (2009) 21915; (b) S. H. Lee, J. H. Kim, T. H. Shim, and J. G Park, *Electronic Materials Letters*, 5 (2009) 47.
11. M. R. Reyes, K. Kim, and D. L. Carroll, *Applied Physics Letters*, 87 (2005) 83506.
12. G. Li, V. Shrotriya, J. Huang, Y. Yao, T. Moriarty, K. Emery, and Y. Yang, *Nature Materials*, 4 (2005) 854.
13. (a) A. J. Moulé, and K. Meerholz, *Advanced Materials*, 20 (2008) 240; (b) W. Ma, C. Yong, X. Gong, K. Lee, and A. J. Heeger, *Advanced Functional*

- Materials, 15 (2005) 1617; c) C. H. Woo, B. C. Thompson, B. J. Kim, M. F. Toney, and J. M. J. Fréchet, *Journal of American Chemical Society*, 130 (2008) 16324.
14. D. H. Apaydın, D. E. Yıldız, A. Cirpan, and L. Toppare, *Solar Energy Materials and Solar Cells*, 113 (2013) 100.
  15. Y. Kim, S. A. Choulis, J. Nelson, D. D. C. Bradley, S. Cook, and J. R. Durrant, *Applied Physics Letters*, 86 (2005) 063502.
  16. Y. Huang, E. J. Kramer, A. J. Heeger, and G. C. Bazan, *Chemical Reviews*, 114 (2014) 7006.
  17. J. K. Lee, W. L. Ma, C. J. Brabec, J. Yuen, J. S. Moon, J. Y. Kim, K. Lee, G. C. Bazan, and A. J. Heeger, *Journal of American Chemical Society*, 130 (2008) 3619.
  18. H. C. Liao, C. C. Ho, C. Y. Chang, M. H. Jao, S. B. Darling, and W. F. Su, *Materials Today*, 16 (2013) 326.
  19. L. A. Perez, J. T. Rogers, M. A. Brady, Y. Sun, G. C. Welch, K. Schmidt, M. F. Toney, H. Jinnai, A. J. Heeger, M. L. Chabinyc, G. C. Bazan, and E. J. Kramer, *Chemistry of Materials*, 26 (2014) 6531.
  20. S. S. Sharma, G. D. Sharma, and J. A. Mukroyannidis, *Solar Energy Materials and Solar Cells*, 95 (2011) 1219.
  21. M. Sanyal, B. Schmidt-Hansberg, M. F. G. Klein, C. Munuera, A. Vorobiev, A. Colsmann, P. Scharfer, U. Lemmer, W. Schabel, H. Dosch, and E. Barrena, *Macromolecules*, 44 (2011) 3795.
  22. S. S. van Bavel, M. Barenklau, G. de With, H. Hoppe, and J. Loos, *Advanced Functional Materials*, 20 (2010) 1458.

23. D. M. González, V. Körstgens, Y. Yao, L. Song, G. Santoro, S. V. Roth, and P. Müller-Buschbaum, *Advanced Energy Materials*, 5 (2015) 1401770.
24. Y. C. Hung, C. Y. Chao, C. A. Dai, W. F. Su, and S. T. Lin, *The Journal of Physical Chemistry B*, 117 (2013) 690.



# ***Chapter:6***



### Conclusions and Scope of Future Work

---

#### 6.1 Conclusions

- ❖ We have successfully demonstrated, solution-processable CuSCN (diisopropyl sulfide as a deposited solvent) as HTL in conventional BHJ solar cells. The active materials PCDTBT:PC<sub>71</sub>BM and PTB7:PC<sub>71</sub>BM were used for device fabrication and thereby leads up to 5.94 % and 4.60 % PCEs for these active layers respectively. The effect of annealing temperature was also optimized on device fabrication. Annealing temperature for the CuSCN as HTLs in organic solar cells has significant effect on PCE specifically the FF and J<sub>sc</sub>.
- ❖ Further, we have demonstrated an eco-friendly solution-processable deposition of CuSCN using DMSO solvent as HTL in efficient organic solar cells. The photovoltaic devices were fabricated with the device structure of ITO/CuSCN/active layer/Al and PCE up to 4.20 % has been achieved with relatively higher FF as compared to reported in previously published literature.
- ❖ In parallel with the above work, investigations were also directed towards development of alternative and universal solvents for CuSCN for fabrication of low band gap polymeric solar cells. In this connection, we used five different alternative solvents compactable with CuSCN for fabrication of organic solar cells: *N,N*-dimethylformamide, dioxane, acetonitrile, ethylene glycol, propylene carbonate using same device structure as above.

- ❖ We have also successfully demonstrated inexpensive and solution-processable CuI (acetonitrile as a deposited solvent) as an HTL in low band polymeric solar cells. The PCEs has been achieved up to 3.04% and 4.48% PCEs for active materials of PCDTBT:PC<sub>71</sub>BM and PTB7:PC<sub>71</sub>BM respectively. These results are relatively better when compared to the devices fabricated using solution processed PEDOT:PSS as HTLs under similar conditions.
- ❖ In order to enhance the utilization of CuI as efficient HTL, we used three different alternative solvents compactable with copper iodide for fabrication of organic solar cells. CuI used as a solution-processable HTL dissolved in three solvents (each 10 mg/mL): dimethyl sulfoxide (DMSO), *N,N*-dimethylformamide (DMF) and diisopropyl sulfide. We have successfully fabricated organic solar cells based on low band gap polymers and achieved good performance.
- ❖ We have investigated the effect of composition ratio of P3HT:PC<sub>61</sub>BM as donor and acceptor materials for conventional BHJ solar cells in ambient condition and observed that 1.0:0.8 composition ratio for P3HT:PC<sub>61</sub>BM has achieved highest PCE. The P3HT:PC<sub>61</sub>BM composition ratios range from 1.0:0.4 to 1.0:1.2 show relatively good PCE while further decrease or increase the composition ratio of P3HT:PC<sub>61</sub>BM the resulted devices show very poor PCE.

## 6.2 Scope of Future Work

- ❖ This study clearly demonstrates that due to non-acidic nature of CuI and CuSCN may be used as a potential candidate as HTLs to improve the PCE for low band gap polymeric solar cells.
- ❖ Further study on lifetime of these devices could be perform for possible commercial applications in future.
- ❖ Further study may be perform to examine the effectiveness of these CuSCN and CuI as HTM in device application such as perovskite solar cells etc.
- ❖ Solution processable HTM such as CuSCN and CuI based study has a potential for efficient and inexpensive approach for the development of stable, large area and cost effective organic photovoltaic devices for off-grid application.



## **Curriculum Vitae**



### **PERSONAL INFORMATION**

Name : **NEERAJ CHAUDHARY**  
Residential Address : D-68, Ganga Vihar, Delhi-110094  
Official Address : CSIR-National Physical Laboratory, New Delhi-110012  
Telephone : +91-98100-13029  
E-mail : [neerajnpl@gmail.com](mailto:neerajnpl@gmail.com) (Personal)  
[chaudharyn@nplindia.org](mailto:chaudharyn@nplindia.org) (Official)  
Nationality : Indian  
Date of birth : 13-10-1981  
Gender : Male

### **EDUCATIONAL QUALIFICATIONS AND EXPERIENCE**

Qualification : 1. M.S. (Manufacturing Management) from BITS, Pilani.  
2. B.Tech (Mechanical Engineering) from IASE University, Rajasthan.  
3. Diploma in Mechanical Engineering from Pusa Polytechnic, New Delhi.  
Experience : Technical Officer in CSIR-NPL, New Delhi-110012, from 29/08/2007 onward (10 Years approx.)  
Job Profile : Working as Technical Officer into time targeting and Technology-Oriented project in area of Organic Photovoltaic devices for efficient R&D work.

**Neeraj Chaudhary**

